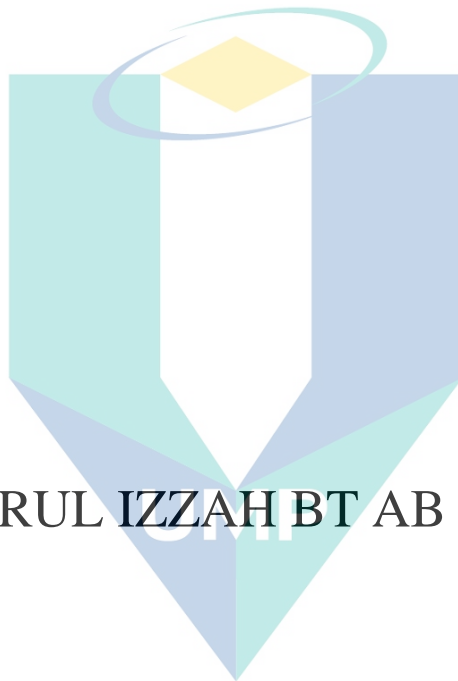


CRASH PERFORMANCE OF  
POLYURETHANE FOAM-FILLED  
ALUMINIUM COLUMN



NURUL IZZAH BT AB RAHIM

اونيورسيتي ملايسيا قهغ

UNIVERSITI MALAYSIA PAHANG

MASTER OF SCIENCE

UNIVERSITI MALAYSIA PAHANG

UNIVERSITI MALAYSIA PAHANG

**DECLARATION OF THESIS AND COPYRIGHT**

Author's Full Name : NURUL IZZAH BT AB RAHIM

Date of Birth : 13 MAY 1978

Title : CRASH PERFORMANCE OF POLYURETHANE FOAM-  
FILLED ALUMINIUM COLUMN

Academic Session : SEMESTER 1 2020/2021

I declare that this thesis is classified as:

- CONFIDENTIAL (Contains confidential information under the Official Secret Act 1997)\*
- RESTRICTED (Contains restricted information as specified by the organization where research was done)\*
- OPEN ACCESS I agree that my thesis to be published as online open access (Full Text)

I acknowledge that Universiti Malaysia Pahang reserves the following rights:

1. The Thesis is the Property of Universiti Malaysia Pahang
2. The Library of Universiti Malaysia Pahang has the right to make copies of the thesis for the purpose of research only.
3. The Library has the right to make copies of the thesis for academic exchange.

Certified by:

\_\_\_\_\_  
(Student's Signature)

780513-03-6018

\_\_\_\_\_  
New IC/Passport Number

Date:

\_\_\_\_\_  
(Supervisor's Signature)

Dr. Salwani bt Mohd Salleh

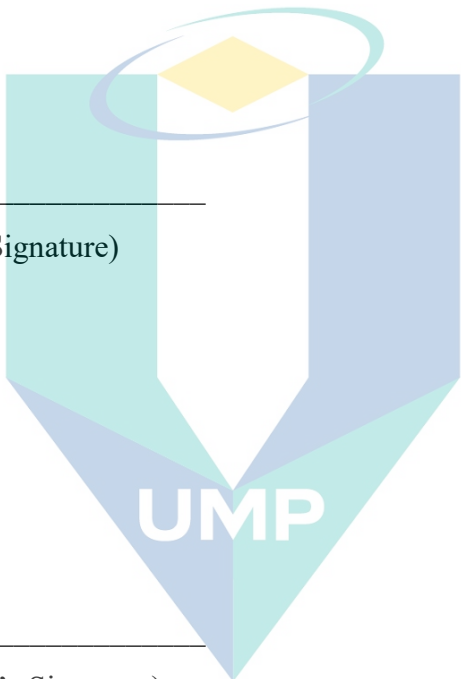
\_\_\_\_\_  
Name of Supervisor

Date:

NOTE : \* If the thesis is CONFIDENTIAL or RESTRICTED, please attach a thesis declaration letter.

## SUPERVISOR'S DECLARATION

We hereby declare that We have checked this thesis and in our opinion, this thesis is adequate in terms of scope and quality for the award of the degree of Master of Science.



---

(Supervisor's Signature)

Full Name :  
Position :  
Date :

---

(Co-supervisor's Signature)

Full Name :  
Position :  
Date :

اونیورسیتی ملیسیا پاهنگ

# UNIVERSITI MALAYSIA PAHANG

## STUDENT'S DECLARATION

I hereby declare that the work in this thesis is based on my original work except for quotations and citations which have been duly acknowledged. I also declare that it has not been previously or concurrently submitted for any other degree at Universiti Malaysia Pahang or any other institutions.

---

(Student's Signature)

Full Name : NURUL IZZAH BT AB RAHIM

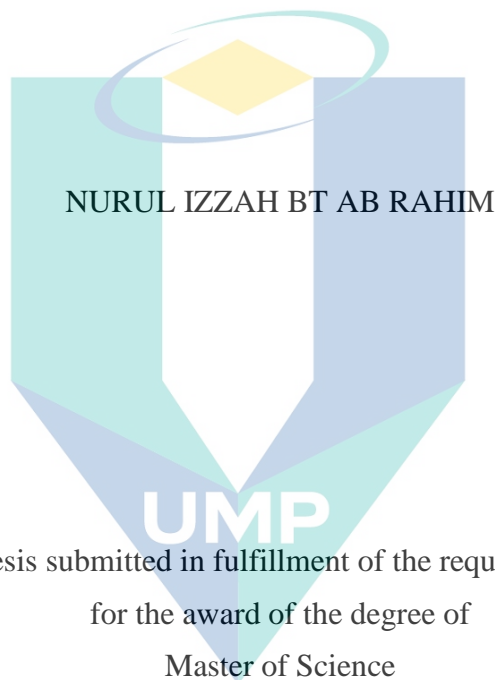
ID Number : MMM17019

Date :

اونيورسيتي ملايسيا قهغ

UNIVERSITI MALAYSIA PAHANG

CRASH PERFORMANCE OF POLYURETHANE FOAM-FILLED ALUMINIUM  
COLUMN



اونيورسيتي مليسيا قهغ

UNIVERSITY OF MECHANICAL AND AUTOMOTIVE ENGINEERING TECHNOLOGY  
UNIVERSITI MALAYSIA PAHANG

DECEMBER 2020

## ACKNOWLEDGEMENTS

First, I would like to sincere thanks and appreciation to my primary supervisor, Dr Salwani Mohd Salleh for supervising me as her master student. I really value her advice, support, encouragement, respect, comments and most importantly her patience throughout the years that I have been working with her. My special thanks to Associate Professor Dr Syarifah Nur Aqida, Dr Mohd Ruzaimi Mat Rejab, Dr Nasrul Azuan Alang and Associate Professor Dr Amir Radzi Abd Ghani (UiTM) for their feedback, knowledge and motivations throughout this journey.

My sincere gratitude to members of Faculty of Mechanical and Automotive Engineering Technology, including En. Zulkarnain, En. Asmizam and En. Sazali for their kindly assistance with the experimental preparation and testing. My appreciation is also due to all the staffs and friends in the university that I have been associating directly or indirectly during my study at Universiti Malaysia Pahang.

I am delighted to the love and support of my family and my parents over the past years. Also, to my lovely son and daughters, Muhammad Nur Iskandar, Nur Irdina Syazwani and Nur Insyirah Safiyyah for giving me the tears and joys all these years. A special dedication to my lovely husband, Sufian b Abd Lajak for his love, support, understanding and patience throughout the ups and downs in finishing this study.

And finally, I would like to acknowledge the support of Universiti Malaysia Pahang under internal grant RDU180316, PGRS190337 and the Ministry of Higher Education, Malaysia under Fundamental Research Grant Scheme, FRGS/1/2016/TK03/UMP/02/22 for sponsoring my study.

اونيورسيتي مليسيا قهغ

UNIVERSITI MALAYSIA PAHANG

## ABSTRAK

Rekabentuk penyerap tenaga impak yang ideal perlu menghasilkan daya puncak awal yang minimum tetapi kapasiti tenaga serapan dan tenaga serapan tentu yang maksimum. Penggunaan tiub berdinding nipis sebagai penyerap tenaga di bawah beban paksi menghasilkan mampatan progresif terkawal yang merupakan mekanisme yang dikehendaki semasa proses pemampatan. Walaubagaimanapun, tiub berdinding nipis yang konvensional menghasilkan daya puncak awal dan graf turun naik yang tidak stabil semasa proses mampatan. Rekabentuk aluminium yang diisi busa secara penuh telah berjaya memberi kestabilan kepada tiub berdinding nipis dan meningkatkan tenaga serapan tentu namun daya puncak awal juga meningkat. Kajian ini dijalankan untuk meningkatkan prestasi struktur penyerap tenaga dengan menggunakan struktur yang diisi dengan busa secara separa dengan beberapa variasi panjang busa. Keseluruhan prestasi spesimen telah disiasat melalui eksperimen. Tujuan kajian ini adalah untuk mengurangkan daya puncak awal dan mengoptimumkan tenaga serapan tentu. Rekabentuk yang diisi separa busa ini menggunakan 3 variasi panjang busa yang berbeza iaitu 195 mm, 190 mm dan 185 mm yang mengisi ruang aluminium berbentuk segi empat. Hasil eksperimen menunjukkan bahawa pengurangan panjang busa telah mempengaruhi keupayaan penyerapan tenaga dan daya puncak awal struktur. Di bawah ujian separa statik, pengurangan panjang busa kepada 195 mm telah menurunkan daya puncak awal hingga 23% dengan hanya menurunkan 1% pada tenaga serapan tentu berbanding spesimen yang diisi busa secara penuh (A1.4P200) bagi specimen berketebalan 1.4 mm. Untuk spesimen berketebalan 2.0 mm pula, daya puncak awal dan tenaga serapan tentu masing-masing menurun sebanyak 3% dan 24% bagi specimen yang mempunyai panjang busa 195 mm berbanding spesimen yang diisi busa secara penuh (A2.0P200). Manakala dalam ujian impak, specimen berketebalan 1.4 mm dengan panjang busa 190 mm menunjukkan prestasi terbaik dengan mengurangkan daya puncak awal sebanyak 31% sementara hanya mengurangkan 6% dari tenaga serapan tentu. Untuk spesimen ketebalan 2 mm, daya puncak awal berkurang dengan pengurangan panjang busa tetapi tenaga serapan tentu tetap untuk semua spesimen. Reka bentuk baru terbukti dapat mengurangkan daya puncak awal dan mengoptimumkan tenaga serapan tentu. Seterusnya, kaedah pengoptimuman menggunakan kaedah gerak balas permukaan menunjukkan bahawa untuk ujian separa statik, penyelesaian terbaik yang diperoleh dengan panjang busa 195 mm dengan ketebalan 1.74 mm yang menghasilkan nilai daya puncak awal sebanyak 70 kN dan tenaga serapan tentu pada nilai 1.7 kJ/kg sementara untuk ujian impak penyelesaian terbaik yang diperoleh dengan panjang busa 195 mm dengan ketebalan 1.46 mm yang menghasilkan nilai daya puncak awal 103 kN dan tenaga serapan tentu 1.5 kJ/kg.



## ABSTRACT

For an ideal impact energy absorber, the initial peak force (IPF) should be minimized but energy absorption (EA) and specific energy absorption (SEA) should be maximized. Application of the thin-walled tube as energy absorber under axial loading condition produces controlled progressive collapse during the crushing process which is a desirable collapse mechanism. However, the conventional thin-walled tubes produce high initial peak force and fluctuations during the crushing process. The existing foam-filled design has been succeeded in stabilising the fluctuation and increase the SEA but the initial peak force is increased simultaneously. The aim of this study is to decrease the initial peak force and optimise the specific energy absorption. This study has been carried out to improve the performance of energy-absorbing structure by using a partially foam-filled structure with a few variations in foam length. The entire crushing performance of the specimen has been investigated by experiment. This proposed partially foam-filled structure design using 3 different length of foam which is 195 mm, 190 mm and 185 mm that filled in the square aluminium column. The experimental results showed that the reduction of foam length has affected the initial peak force of the structure and energy absorption capacity. Under quasi-static test, reduction in foam length to 195 mm has decreased the IPF to 23% by decreasing only 1% in SEA compared to full-filled (A1.4P200) specimen for 1.4 mm thickness structure. For specimen with 2.0 mm thickness, the IPF and SEA were decreased by 3% and 24% respectively compared to full-filled (A2.0P200) specimen. While under impact test, specimen with 1.4 mm thickness and length of foam 190 mm shown the best performance by reducing the IPF by 31% while reduced only 6% of the SEA. For 2 mm thickness specimen, the IPF was reducing with the reduction in length of foam but the SEA was constant for all specimen. The new design which using the partly foam-filled, is proved to reduce the IPF and optimise the SEA of the structure. Finally, the optimization method using response surface method has shown that for the quasi-static test, the best solution gained by the length of foam of 195 mm with the thickness of 1.74 mm that produces the value for IPF of 70 kN and SEA of 1.7 kJ/kg while for impact test the best solution gained by length of foam of 195 mm with the thickness of 1.46 mm that produce the value of IPF for 103 kN and SEA of 1.5 kJ/kg.

اونيور سيني مليسيا فھق

UNIVERSITI MALAYSIA PAHANG



## TABLE OF CONTENT

<b>DECLARATION</b>	
<b>TITLE PAGE</b>	
<b>ACKNOWLEDGEMENTS</b>	<b>ii</b>
<b>ABSTRAK</b>	<b>iii</b>
<b>ABSTRACT</b>	<b>iv</b>
<b>TABLE OF CONTENT</b>	<b>v</b>
<b>LIST OF TABLES</b>	<b>ix</b>
<b>LIST OF FIGURES</b>	<b>x</b>
<b>LIST OF SYMBOLS</b>	<b>xiii</b>
<b>LIST OF ABBREVIATIONS</b>	<b>xiv</b>
<b>CHAPTER 1 INTRODUCTION</b>	<b>1</b>
1.1 Research background	1
1.2 Problem statement	4
1.3 Research Objectives	5
1.4 Scope	5
1.5 Thesis Outline	6
<b>CHAPTER 2 LITERATURE REVIEW</b>	<b>7</b>
2.1 Introduction	7
2.2 Vehicle impact	7
2.3 Application of Foam-filled Structures	9
2.3.1 Lightweight construction	9

2.3.2	Thermal insulation	10
2.3.3	Acoustic management	10
2.3.4	Energy absorbers	10
2.4	Energy absorber design	11
2.4.1	Hollow Thin-walled Structure	11
2.4.2	Foam-filled Thin-walled Structure	12
2.4.3	Polymeric foam	13
2.4.4	Aluminium foam-filled column	18
2.4.5	Honeycomb filler	20
2.4.6	Multi-cell column	25
2.4.7	Corrugated column	27
2.4.8	Functionally Graded Thickness Column	30
2.4.9	Composite Thin-Walled Structure	31
2.4.10	Triggering mechanism	34
2.5	Impact parameter	36
2.5.1	Conservation of energy	36
2.5.2	Crashworthiness parameter	37
2.6	Principle of conservation of momentum	39
2.7	Crash Optimization	39
2.7.1	Optimization method	39
2.7.2	Optimisation design for crashworthiness	41
2.7.3	Optimisation Algorithm	42
2.7.4	Multi objective optimisation for structure	43
2.7.5	Response Surface Methodology (RSM)	43

<b>CHAPTER 3 METHODOLOGY</b>	<b>45</b>
3.1 Introduction	45
3.2 Design of Experiment (DOE)	47
3.3 Specimen preparation	48
3.3.1 Preparation of aluminium alloy square column	48
3.3.2 Product acceptance/ material assurance process for aluminium	49
3.3.3 Preparation of polyurethane foam (PU foam)	50
3.3.4 Product acceptance/ material assurance process for PU foam	51
3.3.5 Compression test of polyurethane (PU) foam	52
3.4 Mechanical Testing	53
3.4.1 Quasi-static compressive test	53
3.4.2 Low velocity impact test	54
3.5 Optimization	55
3.6 Verification of optimization results	56
3.7 Conclusion	56
<b>CHAPTER 4 RESULTS AND DISCUSSION</b>	<b>57</b>
4.1 Introduction	57
4.2 Mechanical Properties of Materials	57
4.2.1 Stress and strain of the aluminium alloy	57
4.2.2 Density of the rigid polyurethane (PU) foam	59
4.2.3 Stress and strain curve of polyurethane (PU) foam	60
4.3 Quasi Static Test	62
4.3.1 Crushing behaviour of specimen with 1.4 mm thickness	62
4.3.2 Crushing behaviour of specimen with 2.0 mm thickness	65

4.3.3	Effect of length of foam to crushing response of specimen with 1.4 mm thickness	67
4.3.4	Effect of length of foam to crushing response of specimen with 2.0 mm thickness	71
4.3.5	Effect of wall thickness to crushing response of specimen	74
4.4	Low velocity impact test	76
4.4.1	Effect of length of foam to crushing response of specimen with 1.4 mm thickness under impact test	77
4.4.2	Effect of length of foam to crushing response of specimen with 2.0 mm thickness	79
4.4.3	Effect of wall thickness to crushing response of specimen	81
4.5	Optimization	84
4.5.1	Optimization methodology	84
4.5.2	Historical data Design	85
4.5.3	Response surface model	85
4.5.4	Analysis of variance (ANOVA)	86
4.5.5	Validation of the Response Surface models	90
4.5.6	Optimization results	93
4.5.7	Verification of optimization results	97
<b>CHAPTER 5 CONCLUSION</b>		<b>100</b>
5.1	Introduction	100
5.2	Conclusion	100
5.3	Suggestion for future work	101
<b>REFERENCES</b>		<b>102</b>

## LIST OF TABLES

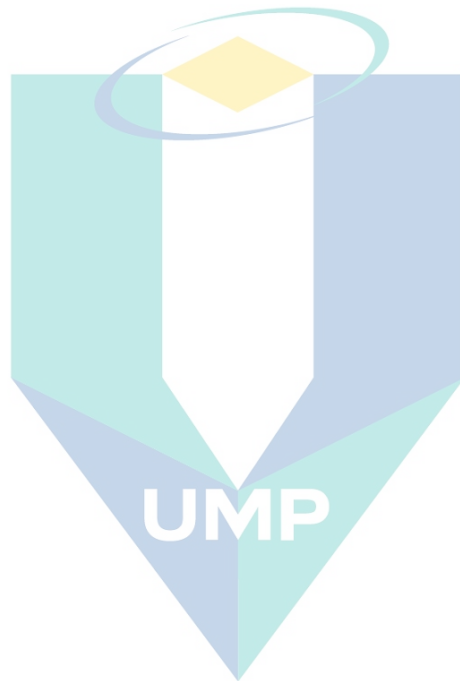
Table 2.1	Optimisation design of crashworthiness for energy absorbers	42
Table 3.1	Design of experiment.	47
Table 4.1	Material Properties of Aluminium 6063-T5.	59
Table 4.2	Calculation for foam density.	60
Table 4.3	Material properties of polyurethane.	62
Table 4.4	Specimen notification.	62
Table 4.5	Summary of collapse mode for the specimen all specimen	67
Table 4.6	Energy absorption indices derived from the force-displacement traces for 1.4mm thickness specimen.	69
Table 4.7	Energy absorption indices derived from the force-displacement traces for 2.0 mm thickness specimen.	72
Table 4.8	Crashworthiness parameter derived for impact test results for 1.4 mm thickness specimen.	78
Table 4.9	Crashworthiness parameter derived for impact test results for 2.0 mm thickness specimen under impact test.	80
Table 4.10	Experimental data inserted in design expert software for 1.4 mm specimen.	85
Table 4.11	Experimental data inserted in design expert software for 2.0 mm specimen.	85
Table 4.12	Analysis of variance (ANOVA) table for quasi static test.	87
Table 4.13	Analysis of variance (ANOVA) table for impact test.	88
Table 4.14	Design solution given by Design Expert software for quasi-static test.	93
Table 4.15	Design solution given by Design Expert software for impact test	95
Table 4.16	Simulated value of IPF and SEA for quasi-static test	98
Table 4.17	Comparison of data in simulation and optimization for the value of IPF and SEA under quasi-static test	98
Table 4.18	Simulation data for IPF and SEA value under impact test	99
Table 4.19	Comparison of data in simulation and optimization for the value of IPF and SEA under impact test	99

## LIST OF FIGURES

Figure 1.1	Number of road crashes from 2010-2017	1
Figure 1.2	Crash box that is attached to front end of a car	3
Figure 2.1	PU foam prepared for testing	14
Figure 2.2	Comparison of solid and polymeric foam by energy absorption under the graph at constant load.	15
Figure 2.3	Aluminium foam inserted in the aluminium tube	18
Figure 2.4	Aluminium honeycomb in (a) hexagonal cells can enhance the energy absorption of a structures (b) triangular and (c) square honeycomb	21
Figure 2.5	Circular multi-cell tubes	27
Figure 2.6	A foam-filled double corrugated tubes	28
Figure 2.7	Configuration of the TCSS tube	30
Figure 2.8	Configuration of the SSG and DSG tubes	31
Figure 2.9	(a) Foam-filled flax/epoxy tube (b) empty flax/epoxy tube	33
Figure 2.10	Types of trigger mechanism that can be applied	35
Figure 2.11	IPF in force-displacement curve	38
Figure 2.12	The operation of analysis models	40
Figure 3.1	Methodology flow chart.	46
Figure 3.2	Aluminium column.	49
Figure 3.3	Dimension of sub size specimen for tensile test.	49
Figure 3.4	(a)Tachometer that has been used to define the speed of the hand mixer (b) the tachometer was directed to the rotating blades.	51
Figure 3.5	Schematic diagram of PU in cubic shapes prepared for testing.	53
Figure 3.6	Specimen was placed between two platens.	54
Figure 3.7	Instron Dynatup impact tester	54
Figure 4.1	Engineering stress vs engineering strain graph for AA6063-T5 for 1.4 mm thickness.	58
Figure 4.2	Engineering stress vs engineering strain graph for AA6063-T5 for 2.0 mm thickness.	58
Figure 4.3	(a) Cross-section of PU foam. (b) sketching of the cross-section	59
Figure 4.4	Compression of PU foam (a) initial setup(b) after 70% compression.	60
Figure 4.5	Stress-strain curve for the tested PU foam.	61
Figure 4.6	Axial progressive deformation mode of square tubes: (a) extensional mode (b) inextensional mode (c) asymmetric mixed mode	63

Figure 4.7	Deformation of A1.4P0 (a) initial crush (b) after 70% crush.	63
Figure 4.8	Deformation of A1.4P185 (a) initial crush (b) after 70% crush.	64
Figure 4.9	Deformation of A1.4P195 (a) initial crush (b) after 70% crush.	65
Figure 4.10	Deformation of A2.0P0 (a) initial crush (b) after 70% crush.	66
Figure 4.11	Deformation of A2.0P200 (a) initial crush (b) after 70% crush.	66
Figure 4.12	Force-displacement traces for P0 (empty column), P185, P190, P195 and P200 (full column) for specimen thickness 1.4 mm.	68
Figure 4.13	Value of SEA and IPF compared to A1.4P200 for 1.4 mm thickness specimen.	70
Figure 4.14	Force-displacement traces for P0 (empty column), P185, P190, P195 and P200 (full column) for specimen thickness 2.0 mm.	71
Figure 4.15	Value of SEA and IPF compared to P200 for 2.0mm thickness specimen.	73
Figure 4.16	Energy absorption gained by 1.4 mm and 2.0 mm thickness specimen.	74
Figure 4.17	Initial peak force achieved by 1.4 mm and 2.0 mm thickness specimen.	75
Figure 4.18	Specific energy absorption gained by 1.4 mm and 2.0 mm thickness specimen.	76
Figure 4.19	Force-displacement traces for A1.4P0, A1.4P185, A1.4P190, A1.4P195 and A1.4P200 under dynamic loading condition.	77
Figure 4.20	Value of SEA and IPF compared to A1.4P200 for 1.4 mm thickness specimen under impact test.	78
Figure 4.21	Force-displacement traces for A2.0P185, A2.0P190, A2.0P195 and A2.0P200 under impact test for thickness 2.0 mm specimen.	79
Figure 4.22	Reduction of SEA and IPF compared to P200 for 2mm thickness specimen under impact test.	81
Figure 4.23	Energy absorption gained by 1.4 mm and 2.0 mm thickness specimen.	82
Figure 4.24	Initial peak force achieved by 1.4 mm and 2.0 mm thickness specimen.	83
Figure 4.25	Specific energy absorption obtained by 1.4 mm and 2.0 mm thickness specimen.	84
Figure 4.26	Predicted versus experimental graph (a) Energy Absorption response (quasi-static), (b) Initial Peak Force response (quasi-static), (c) Specific Energy Absorption response (quasi-static)	91
Figure 4.27	Predicted versus experimental graph (a) Energy Absorption response (impact), (b) Initial Peak Force response (impact) (c) Specific Energy Absorption response (impact).	92
Figure 4.28	Effect of L and t to (a) EA (b) IPF (c) SEA for quasi-static test.	94
Figure 4.29	Effect of L and t to (a) EA (b) IPF (c) SEA for impact test	96



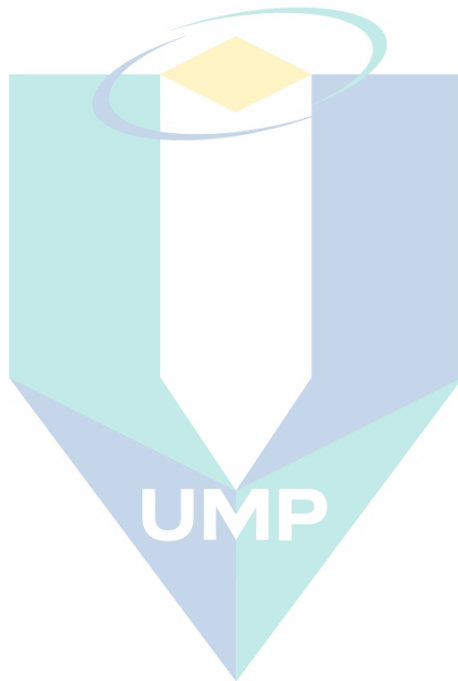


اونيورسيتي ملايسيا قهغ

UNIVERSITI MALAYSIA PAHANG

## LIST OF SYMBOLS

$E_c$	Compression modulus
$S$	Slope of the linear phase
$A$	Cross-section area
$t$	Thickness



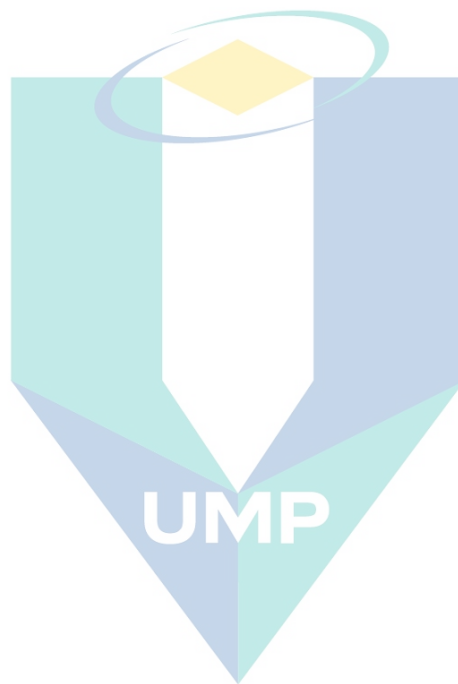
اونيورسيتي ملايسيا قهغ

UNIVERSITI MALAYSIA PAHANG

## LIST OF ABBREVIATIONS

ECE-R42	United Nations Economic Commission for Europe Regulation
CFR	Code of Federal Regulations
EA	Energy absorption
SEA	Specific energy absorption
IPF	Initial peak force
RSM	Response surface methodology
EuroNCAP	European New Car Assessment Programme
RCAR	Research Council for Automobile Repairs
CMVSS	Canadian Motor Vehicle Safety Standards
AZT	Allianz Zentrum fur Technik
PU	Polyurethane
MCF	Mean crushing force
PCF	Peak crushing force
CFE	Crushing force efficiency
EA	Energy absorption
SEA	Specific energy absorption
IPF	Initial peak force
CFRP	Carbon fiber reinforced polymer
CNC	Computer numerical control
CAE	Computer Aided Engineering
HFST	Honeycomb-filled square tube
HFCT	Honeycomb-filled square tube
UGAH	Unidirectional-graded auxetic honeycomb
BGAH	Bidirectional-graded auxetic honeycomb
BHTNS	Bionic honeycomb tubular nested structure
FGF	Functionally graded foam
FGFTAGP	Functionally graded foam tapered with ascending grading pattern
FGFTDGP	Functionally graded foam tapered with descending grading pattern
CTT	Corrugated tapered tubes
SSLC	Sandwich sinusoidal lateral corrugated
TCSS	Truncated conical sandwich shell with corrugated cores

SSG	Single surface gradient
DSG	Double surface gradient
GFRP	Glass fiber reinforced polymer
RBF	Radial basis function
KRG	Kriging
SVR	Support vector regression
PRS	Polynomial response surface



اونيورسيتي ملايسيا قهغ

UNIVERSITI MALAYSIA PAHANG

# CHAPTER 1

## INTRODUCTION

### 1.1 Research background

Development in human technology has increased the needs of automobile in human life. Financial assistance provided by the banks has contributed to affordability of car ownership. Increase in number of vehicles on the road has contributed to the increase of road accidents every year. Figure 1.1 is adapted from statistic's book by Jabatan Keselamatan Jalan Raya Malaysia (JKJR).

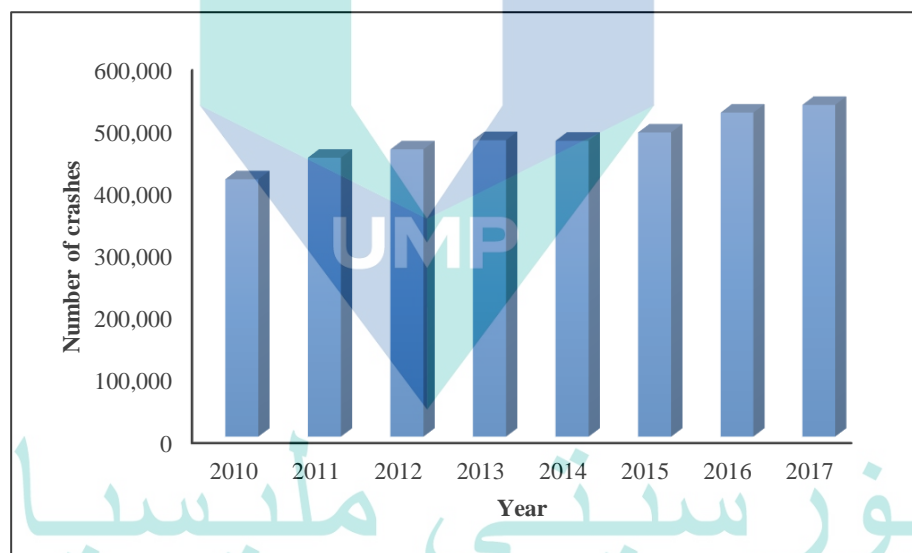


Figure 1.1 Number of road crashes from 2010-2017

Source : Buku statistik kemalangan jalan raya tahun 2018, (2019)

Figure 1.1 shows that the number of road crash is increased from 414,421 in 2010 to 533,875 in 2017. In all types of crash accidents, frontal crashes cover about 30 % of the total number of accidents (Shen et al., 2012). Therefore, recent designs of automobile have considered the entire possible factor to ensure better passenger protection by improving passive safety performance. Passive safety refers to the automotive components that help to reduce the effect of collision while active safety emphasis on the

technology in preventing the accident from occurs. Passive safety load cases were divided into two which is high speed crashes and low speed crash. High speed crashes mainly focused on front, side and rear impacts, occupant and pedestrian safety while low speed crashes more to insurance classification purposes. Some national and international standards regulate performance of the low impact test depends on in which country the vehicle is commercialized for example (United Nations Economic Commission for Europe Regulation 42) ECE-R42 in Europe and (Code of Federal Regulations for transportation in bumper standard) 49 CFR 581 in United States. Low speed impact is important because instead of being a legislation demands, the insurance classification's test has become a prerequisite. In Europe, the crash reparability test with 15 km/h speed has been implemented for insurance rating (Enderich, 2007)

The vehicle body design is divided into three areas which is front energy absorption areas, middle energy absorption areas and rear energy absorption areas (Shen et al., 2012). The front energy absorption area consists of front bumper beam, bumper beam buffer block, engine hood front end and crash box. This part is designed with a crumple zone which will be damaged in controlled manner so that impact of the collision will minimize injury of the passenger during frontal crash. Passenger in moving vehicle has certain amount of kinetic energy. During a collision, vehicle will decelerate and finally stop. According the conservation of energy, the kinetic energy should be transformed in slow motion to increase the passenger's safety (Nakazawa et al.,).

Crash box is one of the energy absorbing structures that attached between chassis and bumper beam. Figure 1.2 shows the structure of crash box on a car. The crash box is used to minimize the side member damage during a collision (N. N. Hussain, 2015). Ability of the crash box to absorb maximum energy from the impact is important to ensure the safety of the passenger in the vehicle. Crash box is estimated to be collapsed by absorbing the maximum crash energy prior to the other vehicle members. Crashworthiness of the energy absorbing structures is an important matter that has been discussed by many researchers (Onsalung et al., 2014)

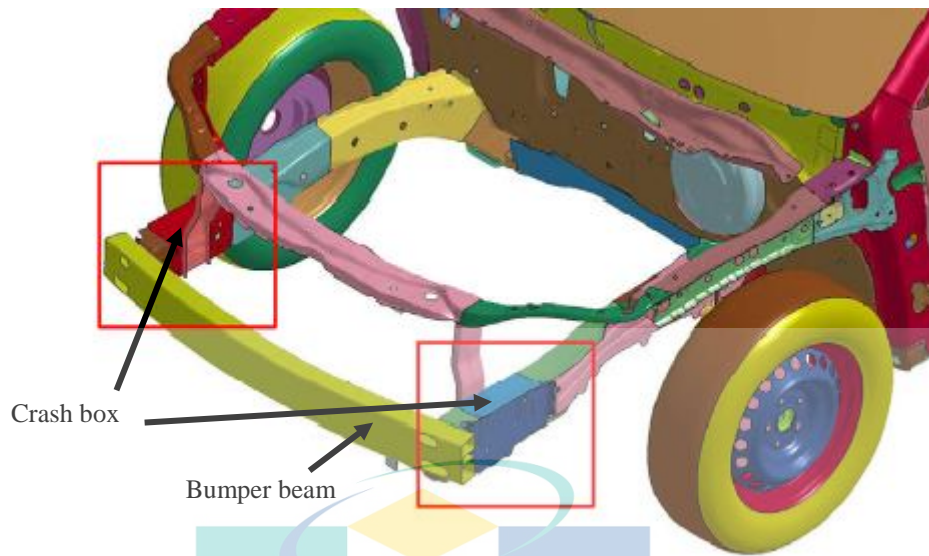


Figure 1.2 Crash box that is attached to front end of a car

Source : Marzougui et al. (2016)

The application and development of materials for structural is changing rapidly. One of the most important considerations in structural studies is to minimise the weight of the structure without sacrificing the strength. Therefore, this engineering needs has led the researchers to design and manufacture lightweight structures that can offer a higher strength and absorb more energy under various loading conditions.

Design of the crash box is limited due to environmental constraint such as reduction of weight of the vehicle to increase the performance as well as minimizing the fuel consumption. The new regulations of fuel economy and gas emissions require design of the crash box have to satisfy both reduction of body weight and improvement of crashworthiness. In crashworthiness, parameter such as initial peak force (IPF), energy absorption (EA) or specific energy absorption (SEA) and crush force efficiency commonly investigated (Kiliçaslan, 2015).

Foam-filled thin-walled tubes were introduced to enhanced the energy absorption while maintaining the mass of the vehicle. This is because the foam helps to support some energy which enhanced the energy absorption (Onsalung et al., 2014). There are several types of foams that used by the researchers such as polyurethane (Subramaniyan, Mahzan, Ghazali, Ahmad Zaidi, & Prabagaransd, 2013), polystyrene (Toksoy & Güden, 2005), aluminium foam (Goel, 2015), aluminium honeycomb (Hussein, Ruan, Lu,



Guillow, & Yoon, 2017) and polyethylene (Costas, Morin, Langseth, Romera, & Díaz, 2016). Energy absorption and peak force of the thin-walled tubes were affected by density and length of foam (M Altin, Acar, & Güler, 2018)

A few method has been introduced to minimize the initial peak force such as origami pattern columns (J. Song, Chen, & Lu, 2012), columns with different shapes of holes (Estrada et al., 2017) and creation of trigger mechanism on the column (N. N. Hussain, Regalla, & Rao, 2017). In this study, an experimental investigation of different length of foam is introduced to minimize the initial peak force and at the same time maximize the energy absorption of the crash box.

Initial peak force refers to the maximum force obtained by a structure during the crushing process. Initial peak force occurs when the force reaches maximum level during crushing when the energy absorber is deformed (N. N. Hussain et al., 2017). In energy absorption devices, peak force is one of the important parameters to be considered because at low velocity impact, it is desirable to avoid permanent deformation of the expensive part and to ensure that the impact from the collision did not transmitted to the passenger.

This study focused on optimization of foam-filled columns with respect to thickness of the tube and length of foam to reduce initial peak force. Foam-filled tubes with 5 different configuration of foam length and two different thickness of tube is proposed in order to reduce initial peak force compared to the full-filled tubes. Quasi-static and impact test were conducted for all the specimen. The experimental data were optimized using response surface model to achieve maximum energy absorption with minimum initial peak force.

## 1.2 Problem statement

During collision, energy absorption of the crash box should be optimum to ensure safety of the passenger. Specific energy absorption and initial peak force is the important criterion that vital for passenger safety. To avoid injury to the passenger inside the car during collision, the crash box should have exhibit maximum energy absorption but low initial peak force. Existing research showed that the value of initial peak is directly proportional with the energy absorption (Jailani & Othman, 2014) while some research

only reported on the energy absorption (EA) and specific energy absorption (SEA) but not emphasize on the initial peak during crushing process (Nianfei Gan et al., 2016)

Foam-filled structures were introduced to optimised the specific energy absorption. But the application of the foam-filled structures led to the higher initial peak force. Recent study only focused on the performance of fully foam-filled structure compared to the empty column (Hussein, 2017). Scope of work in that research was comparing between 3 different inner materials which is foam, honeycomb and foam+honeycomb. But in this study, partially-filled structures were introduced to reduce the initial peak force of the structure. The foam was prepared in 3 different lengths; 195 mm, 190 mm and 185 mm. These foams were inserted into the square aluminium column to observe the performances of each structure under quasi-static and dynamic condition.

### 1.3 Research Objectives

The principal aim of this research work is to investigate the energy absorption of foam-filled structures. The research focuses on square aluminium (metal) filled with polyurethane (PU) foam to reinforce the structures.

The research objectives are:

- i. To investigate the effect of foam length on energy absorption (EA), specific energy absorption (SEA) and initial peak force (IPF) subjected to quasi-static and impact test
- ii. To optimize the specific energy absorption and reduce the initial peak force of the foam-filled structure by Response surface model (RSM)

### 1.4 Scope

- i. The experimental study is focused on square aluminium alloy type AA6063-T5
- ii. The study was conducted on the thin-walled structure only.
- iii. The study focused on the effect of foam's length reduction
- iv. Optimization was conducted to find the best configuration of foam's length and column's thickness.

## 1.5 Thesis Outline

This thesis consists of a further five chapters as follows:

**Chapter II: Literature Review;** this chapter gives an overview of the design and manufacture of empty and foam-filled structures and the mechanical behaviour of foam-filled structure under quasi-static and dynamic loading.

**Chapter III: Methodology;** this chapter describes the design and experimental procedure in this study, consists of specimen preparation and experimental testing (tensile test, compression test, low velocity impact test).

**Chapter IV: Results and discussion;** this chapter presents and discusses the experimental results of the structures.

**Chapter V: Conclusions;** this chapter summarises the overall findings and discussions alongside recommendations for future work.



UMP

اونيورسيتي مليسيا قهغ

UNIVERSITI MALAYSIA PAHANG

## CHAPTER 2

### LITERATURE REVIEW

#### 2.1 Introduction

This chapter discussed the background of the crash and impact analysis and the previous researches that have conducted to enhance the crash performance of energy absorber. The first part of this chapter describes the vehicle impact regulation and condition. The second part discusses various geometry of energy absorbers and types of foam previously used as filler in energy absorber while the third part explains the optimization method. Previous researches in foam-filled thin-walled tubes as a material for a crash box have been reviewed as references in this chapter. Different materials and shapes of thin-walled tubes discussed. Besides that, types of foam that can increase the performance of the energy absorption device reviewed.

#### 2.2 Vehicle impact

Evolution of new car design had to deal with interminable emerging demands, enforced by new legislation and customer test such as the European New Car Assessment Programme (EuroNCAP) to ensure passenger/pedestrian safety and insurance categorization to enhance vehicle damageability and reparability. The passive safety load cases can be divided into two categories which were high speed and low speed crashes. High speed collision focused more on the effect of front, side and rear impact to the passenger in the car and pedestrian. While low speed crashes commonly implemented as prerequisites test in several standards as well as for insurance classification requirements used by Research Council for Automobile Repairs (RCAR) (Enderich, 2007). More attention was given to the high-speed impact of a vehicle because the effect of impact is worst compared to low speed impact but low speed impact is relatively important to be considered because it usually occurs in the crowded city (Gkritza et al., 2015). Moreover, several national and international standards have enforced the requirement of low speed impacts as a prerequisite to homologate a new car for example Canadian Motor Vehicle Safety Standards (CMVSS) 215 in US (*Safety Bumper Test and Rating Protocol (Version*

VIII ), 2010) or Economic Commission for Europe (ECE-R42) in Europe. The robustness of vehicle under low speed impact crashes has to continuously improved to ensure that the damage of the vehicle to be consistently at minimum level. This may cause the damage cost to be low and leads to lower insurance classification. Allianz Zentrum fur Technik (AZT) or also known as Danner test is one of the crash reparability tests which has been implemented in Europe for insurance rating. The low speed impact test is conducted at 15 km/h velocity, a 40 % overlapped and 0° rigid barrier for front and rear impact.

In developed countries, frontal crashes have contributed 50–70% of the fatalities during accidents (Costas et al., 2013). Therefore, it is important to study on improvement of the frontal part of the vehicle to increase the passenger's safety during crashes. For that instance, the crash box was attached between the bumper and side rails in front of the vehicle. Crash box is a part that expected to be collapsed by absorbing crash energy prior to the other body part (Kim et al., 2014). Thus, damages of the main passenger's compartment can be minimized to ensure the passengers' safety and protecting the expensive parts like fender, hood, intercooler, and radiator (N. N. Hussain, 2015). During a crash event, it is important to understand the energy of the impact and how the loads are transmitted through the system. Higher energy absorption coupled with lower initial peak force should be achieved to prevent the catastrophic collapse and increased passenger survival chances due to crash or impact (Gameiro & Cirne, 2007).

Despite to meet the requirements of emissions legislation, higher aluminum alloys usage in vehicle design was significant for the beneficial performance for example the lightweight characteristic. Application of aluminium in the frontal structure contributes to achieve optimum vehicle weight distribution. In frontal collision, modern automotive design suggested the use of frontal longitudinal structure to act as the primary load path for the impact energy. The structure functioned as energy absorbers to ensure that the inertial forces perceived by the occupant are within an allowable limit. Most vehicles equipped with square and rectangular cross-sections configurations of the frontal longitudinal structures. In designing an energy absorption device for a vehicle, energy-efficient and crash safety requirement are the most important criteria should be considered (Lu & Yu, 2003). An effective design of bumper system plays important role in the event of a frontal collision of the vehicle. The modern bumper systems are consists

of a bumper beam with two crash box (Peraza-hernandez, 2016). Crash box is one of the energy absorbing structures that attached between the vehicle bumper and the front rail. Design of the crash box should be suitable to maximize the energy absorption and minimize the initial peak force during the collision.

The conventional crash box has crash beads to initiate buckling deformation and make the crash box easily collapse. Apart of that, design of crash box should not be massive in terms of weight. Hence, aluminium tubes have been introduced to replaced steel as the reduction of structural component been one of the important issues (Uma Devi et al., 2014). The modern bumper system has the function of absorbing the energy of the low speed impact, thus avoiding damages to expensive parts such as radiator, engine bay component and condenser. The energy absorption capacity of the bumper system during a crash is evaluated by the load-displacement response. The area under the load-displacement curve is a measure of the energy absorbed. The performance of a crash box can be assessed on the basis of the RCAR regulations (Enderich, 2007).

An efficient energy absorber is capable in producing a stable, smooth, repeatable, predictable and controllable crush response with a low initial peak force and have high energy absorption capacity (Duarte et al, 2019). Low initial peak force is important to ensure the deceleration during the crash is lower than the critical values to minimize the injuries to human and reduce damages to the vehicle. Instead of having high energy absorption capability, crash box should not be massive because it will increase the total weight of the vehicle (Rameshchandra, 2018).

### 2.3 Application of Foam-filled Structures

The following sections outline some of the potential applications for foam-filled structures.

#### 2.3.1 Lightweight construction

A few studies have investigated the suitability of foams instead of fiber reinforced composite materials to fulfil both energy absorption capability and lightweight challenge. Cardillac STS has been using energy absorption system made of PU foam as bumper. This kind of bumper is light in weight and has good energy absorption. Other than that,



aluminium foam-filled structure has been used as bottom beam, longitudinal beam, rear beam, roof rack and other parts of Audi A8 (Nianfei Gan et al., 2016).

### 2.3.2 Thermal insulation

Rigid PU (PUR) foams are extensively used as thermal insulation in construction industry, in refrigerated vehicle, pipelines and transportation of liquefied natural gas (LNG) and liquefied petroleum gas (LPG). It performs well in most areas of insulations due to its low thermal conductivity ( $\lambda$ ) that is superior compared to other material, which at 18–28 mW/(m•K) (Kirpluks et al., 2014). In construction, it is more economic to choose a material with a lower thermal conductivity rather than increase the thickness of the insulation in the hold walls. The combination of rigid polyurethane foam with different facing materials produces construction composites materials with important application (Zhi, 2018). Rigid PUR foam has been widely used in the refrigerated vehicle for insulation. The good insulation properties of rigid PUR foam makes the inside space in refrigerated vehicles can be gained. Other than that, PUR is used as the insulation material in pipelines to transport hot or cold medium to prevent loss of heat (Demharter, 1998)

### 2.3.3 Acoustic management

A sound wave incident on a material can be absorbed, reflected and/or transmitted by the material. These three phenomena are all possible depending upon the types of material. The noise reduction coefficient (NRC) of the composite material increased twice compared to rigid polyurethane material only (Tiuc et al., 2016). Acoustic performance or sound absorption efficiency of the material is valued by the sound absorption coefficient. Sound absorption coefficient of sound absorbing materials was determined using an impedance tube (Wei et al., 2020).

### 2.3.4 Energy absorbers

Instead of in automotive industry, thin-walled structures are applied as energy absorbers in modern civil and military industries. Due to the increasing extreme events and threats related to blast attack on buildings, many blast resistant facades/panels were developed to reduce the blast-induced damage on the buildings (Wang et al., 2017).



Besides this, the 'soft' connection (like energy absorption connector) was usually employed to attach the blast resistant façades to buildings, which could further reduce the damage on buildings by means of dissipating part of blast energy and reducing peak blast load transferred to buildings

## **2.4 Energy absorber design**

### **2.4.1 Hollow Thin-walled Structure**

The automotive design should satisfy both safety and weight reduction criteria (Prasad et al., 2016). Therefore, applications of lightweight materials are beneficial in terms of weight reduction and crashworthiness (Zhaokai et al., 2017). Lightweight metals such as aluminium have been studied with different geometries and design to satisfy the requirement of the crash energy absorbers. These metal structures are cost effective, malleable and can be integrated easily in the vehicle body structure (Nianfei Gan et al., 2016). Moreover, thin-walled structures are advantageous in automobile industry because they are great at dissipating impact energy by a stable progressive deformation when subjected to axial compressive load (Baroutaji et al. 2017)

These structure can be design in various such as circular (Goel, 2015), square (Hussein et al., 2017), rectangular (Estrada et al., 2017) and other polygonal shapes. Abramowicz and Jones (Abramowicz & Jones, 1986) have analysed the theory on crushing behaviour of thin-walled square tubes. For similar predicted buckling load, the onset of buckling is strongly affected by the initial imperfection. For static axial crushing, the square tube has generated three types of progressive buckling mode which are extensional, asymmetric B and symmetric. For that reasons, the crushing behavior of hollow columns were discussed with respect to the initial peak force (IPF), energy absorption (EA) and specific energy absorption (SEA).

Four types of shapes which is hexagon, octagon, 12-sided star and 16-sided star has been studied by Fan et al. Conclusion made that increasing the number of corners can improve the energy absorption of the column but it is limited to a certain extent (Fan et al., 2013) Square, hexagonal and circular tapered tubes have been studied by Gan (Nianfei Gan et al., 2016). Circular tapered hollow absorbed the maximum energy compared to the other shapes for hollow part.

Instead of shapes, thickness of thin-walled structures affects the energy absorption ability. Subramaniyam et al (Subramaniyan et al., 2013) performed an experimental study on circular tubes with different thickness. The research concluded that the thicker column has better energy absorption capability than that of the former. In other hand, Niknejad (Niknejad et al., 2017) has introduced new method to increase the energy absorption of a thin-walled column. The energy absorption capacity of the quadrangular column is higher of the corresponding simple column. Tabacu (Tabacu, 2015) conducted experimental study on the circular structure with rectangular insert subjected to axial loading condition. The simulation data showed that when the cross section area of the insert becomes higher, the crushing behavior of the structure was comparable to a foam-filled structure (Yin et al., 2014). Moreover, increase in cross section area simultaneously increases the peak force and mean crushing force. Ly and Phom has investigated the behaviour of single and double hat section and concluded that crushing force of double hat tube is higher than top hat section (Ly & Pham, 2016).

However, application of metal column has some limitations such as a high initial peak force, a large fluctuation in the mechanical response during the crushing process and a moderate energy absorption performance under dynamic loading (Baroutaji et al., 2017). Furthermore, the thin-walled column is weak when subjected to non-axial load and may cause Euler buckling (Nianfei Gan et al., 2016). The most common way to increase the mean crushing force is by increasing the wall column thickness. However, increasing the wall thickness might as well increase the column mass. One of alternatives recommended to solve this issue is by inserting a low-density cellular material in a thin-walled structure. It was proven to increase the energy absorption capability while sustaining the SEA (Dirgantara et al., 2018).

#### **2.4.2 Foam-filled Thin-walled Structure**

Cellular materials such as foams and honeycombs are commonly utilized in many engineering applications as modern structural components due to their excellent physical, chemistry and mechanical properties (Liu et al., 2009). A cellular solid is developed by a formation of interconnected network of solid struts that form edges and faces of cell. There are three typical structures which are two-dimensional cellular which is commonly called honeycombs, three-dimensional cellular with solid edges only is called foam with open cells and three-dimensional cellular with solid edges and faces is called foam with

closed cells. Cellular foam can be manufactured in many different techniques. As for polymeric foams, the gas was inserted into a liquid monomer or a hot polymer at high pressure and expanded into bubbles, then the bubbles were allowed to grow and stabilise, and finally solidified by cross-linking or cooling. While for metallic foams, mixture of powdered metal and powdered titanium/zirconium hydride were compacted and heated to form those type of foam (Gibson & Ashby, 1999). Cellular materials can be classified by the cells' size, variability in cell size (stochastic or periodic), type of pore (open or closed) and the relative density of the structure (Wadley, 2002). Foam, with either open or closed-cells, have a random microstructure, falling in stochastic category (Gibson & Ashby, 1999).

Hanssen (Hanssen et al., 2000) made strong evidence that insertion of foam-filler material significantly increases the energy absorption capability of the thin-walled column but concurrently increases the initial peak force. Song (Song et al., 2005) quantified that there is a significant interactive effect between foam-filler and thin-walled tube, making the total energy absorption of filled tube substantially higher than the summation of their individual contributions. During axial crushing the foam functioned as an elastic foundation to the tube walls, minimize the local buckling distance and allow extra progressive folds to be generated (Costas et al., 2017).

### 2.4.3 Polymeric foam

The characteristics of polymeric foams are recognised in industry and researches as it can be found in many research papers (Duarte et al., 2018, Duarte et al., 2019, Gan et al., 2018, Sun et al., 2017) and book (Wadley, 2002). Generally, density of polymeric foams is lower compared to metal foams. However, both types of foam can sustain large compressive strains that makes them enthralling as energy-absorption devices. One of the ways to achieve these properties in energy absorber is by filling the hollow metal or composite structure with cellular materials such as polymer foam, metal foam and honeycomb.

Polymeric foam has been used in wide range of applications such as weight-reduction purposes, insulation, buoyancy, energy absorption devices, convenience and comfort. It can be divided into two categories which are closed or open cells. Closed cell foams consist of a cellular formation with entrapped air bubbles within a continuous

macromolecular phase such as the polystyrene cup. While open cell foams have a cellular network where continuous channels are available throughout the solid macromolecular phase such as the polyurethane seat cushion. Commonly closed cell foams are rigid and open cell foams are flexible (Khemani, 1997).

Polyurethane (PU) are unique polymer material with wide range of physical and chemical properties (Subramaniyan et al., 2013) that is widely used in energy absorption's application such as in passive safety mechanism in automotive industries. It has the ability to absorb energy while deforming due to the mechanics of cell crushing (Zhang et al., 2019). Figure 2.1 shows the PU foam prepared for material properties test. Polyurethane foam-filled structure may compensate irregular overall buckling and the unstable effect during crushing process (Hangai et al., 2018) Besides, foam-filled thin-walled tubes were introduced to enhanced the energy absorption while maintaining the mass of the vehicle.



Figure 2.1 PU foam prepared for testing

Source : Hussein et al. (2017)

PU is a polymer produced from the exothermic addition reaction of polyisocyanates with polyols, containing hydroxyl groups. It can be found as solid products in flexible, semi-rigid and rigid form depends on the ratio of mixture and the manufacturing process (MRM Rejab, 2004). Each form of PU was applicable for different application depends on the density. The flexible PU usually used for seating cushion and insulation while the rigid PU is applied as a core material in sandwich structures or as filler in energy absorbers.

PU material have great properties in versatility in finished product and ease of production. Besides, PU performed a good behaviour in energy absorption capability compared with that of the solid as shown in Figure 2.2. The figure shown that the PU foam has a plateau phase which cause the foam to increase the energy absorption capacity compared to solid.

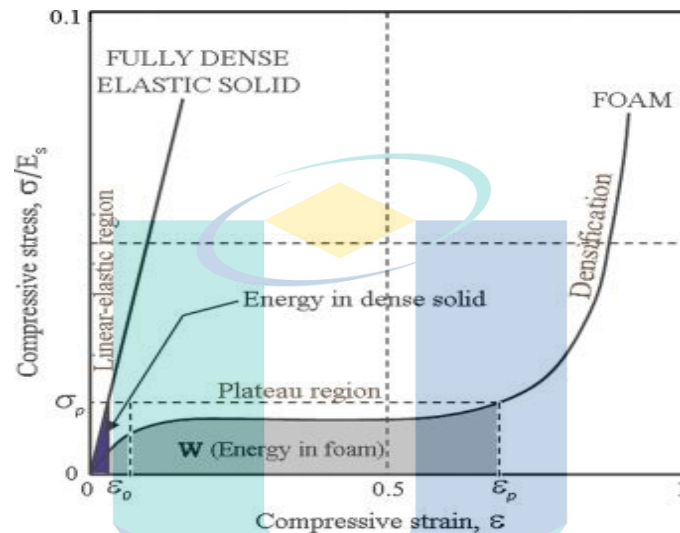


Figure 2.2 Comparison of solid and polymeric foam by energy absorption under the graph at constant load.

Source : Linul et al. (2017)

A few researchers have proven that filling column with PU can increase the energy absorption of the column. Subramaniyam (Subramaniyan et al., 2013) revealed that energy absorption capacity of PU foam-filled tubes was higher than the empty one. An experimental investigation conducted by Hussien (Hussein et al., 2017) has shown an agreement with Subramaniyam study. The results showed that energy absorption (EA) and specific energy absorption (SEA) increased by 104 % and 40 % compared to the hollow tube. Thinwongpituk and Onsalong (Onsalung et al., 2014) has shown that although the energy absorption of the foam-filled column increases, the SEA of the column given contra results. Instead of that, aluminium covblumn can be filled with polyurethane foam to compensate irregular overall buckling and the unstable effect during crushing process (Reddy & Wall, 1988). This effect commonly happens in a very thin tubes (diameter/ height > 500).

Besides, Zhou (Zhou et al., 2016) has reported that SEA of the foam-filled steel beam and magnesium extrusion was 6 times and 1.9 times higher compared to the simple



beam respectively. SEA of magnesium sheet was 2 times higher compared to steel sheet for the same density of the foam. In other research, the energy absorption was proven to be increased by using the higher density of PU by Thinwongpituk (Thinwongpituk et al., 2016). The same conclusion was reported by Yu (Yu et al., 2018) which concludes that SEA and mean crushing force (CFE) of the column increased with the increases of foam average density. The similar investigation was conducted by Azarakhsh (Azarakhsh et al., 2015) that investigated on foam-filled bitubular brass cylinder. Results demonstrated that by filling the bitubular brass with PU, value of EA is increased but SEA value almost constant. In this study, dynamic amplification factor (DAF) was applied to predict the dynamic effect from static analysis. The DAF of the empty bitubular is higher than that of the foam-filled structures.

To support the energy absorption capability of PU, Niknejad (Niknejad et al., 2015) presented a theoretical formula to predict crushing force and absorbed the energy of PU foam-filled quadrangle tubes by considering the interaction effects between the tube wall and the foam and then conducted an experiment to verify the theoretical analysis. From the experimental measurement, the formulas have been proven to be used for different materials and size of tubes. To expand the authors' theory, they then performed a quasi-static test on PU foam-filled circular aluminium tubes (Niknejad et al., 2012).

Moreover, Abedi (Abedi et al., 2012) studied PU foam-filled square and rectangle column subjected to axial loading. The formula to predict the instantaneous folding force, maximum folding force and absorbed energy of the metal column was derived and verified with experimental study. For the empty tubes, the energy absorption of the larger diameter is less compared to the smaller diameter. While for the foam-filled tubes, the larger diameter tubes gained more energy absorption compared to the smaller one.

For a similar reason, Mirfendereski and Salimi (Mirfendereski & Salimi, 2008) conducted a parametric study on foam-filled tapered rectangular tubes subjected to quasi-static and dynamic loading. The authors reported that frusta tubes gained lowest initial peak force under static and dynamic loading. Darvizeh (Darvizeh et al., 2017) investigated energy absorption characteristic of circumferentially grooved thick-walled tubes. The circular PU foam-filled tubes increased energy absorption capability by 89 % when subjected to quasi-static loading and 26% when subjected to dynamic loading.

Results from this study aligned with other studies which showed that SEA of PU foam-filled grooved sample was up to 49 % higher compared to the empty sample (Montazeri et al., 2018). Besides that, Niknejad and Orojloo (Niknejad & Orojloo, 2016) have introduced a nested longitudinal grooved section as energy absorbers subjected to lateral compression. For a nested system of the same grooved sample, SEA of the foam-filled specimen was 1.74 times of the empty specimen.

Other type of polymeric foam that has been investigated as energy absorbers is polystyrene. It is widely used resin in foamed products manufacturing. Polystyrene foams have relatively lightweight combined, good thermal insulation and high resistance to water, mould, fungi, and bacteria. Production process of polystyrene foams are safe which do not involve dusting and allergies which can contribute to health issues. The conventional production method for foamed polystyrene is a bead foaming. Polystyrene foam is a widely used industrial material in road construction, automobile, architecture and so on (Cui et al., 2016). Polystyrene foam has low density, low thermal conductivity and a high loading bearing strength per weight compared with non-foamed polystyrene plastics.

Toksoy and Guden (Toksoy & Guden, 2005) revealed that deformation mode of the polystyrene foam-filled tubes had changed from diamond to concertina which leads to higher energy absorption capacity. Application of polystyrene as filler material has been prolonged by Aktay (Aktay et al., 2006) who has investigated on crushing response of polystyrene foam-filled aluminium tubes. The foam-filler has reduced the folds' length and increased the number of folds during compression with the increasing of the polystyrene density. This results supported the conclusion made by Toksoy and Guden in their research before (Toksoy & Guden, 2005).

Hybrid foams were produced from two different interpenetrating or particulate-embedded foam-material classes. This combination will enhance the multi functionality of the material (Reinfried et al., 2011). Duarte (Duarte et al., 2019) has developed polymer-aluminium hybrid foam as a filler in aluminium alloy square column to investigate the performance under quasi-static and dynamic response. The results showed that the epoxy-aluminium alloy hybrid foam filled structures exhibits the best performance in terms of crashworthiness.



#### 2.4.4 Aluminium foam-filled column

In late 1990s aluminium foam which has high absorption of impact energy was developed. Metal foam is effective for absorbing energy because it has extended stress plateau in stress-strain traces. The advantages in terms of high stiffness with low density, high corrosion resistance and easy to recycle have increase the demands to aluminium foam. Aluminium foam can be fabricated using powder metallurgy method as it was the most cost effective and flexible method (Hussain & Suffin, 2011). Normally, the aluminium foam is filled in the thin-walled structure to enhance the crashworthiness as in Figure 2.3

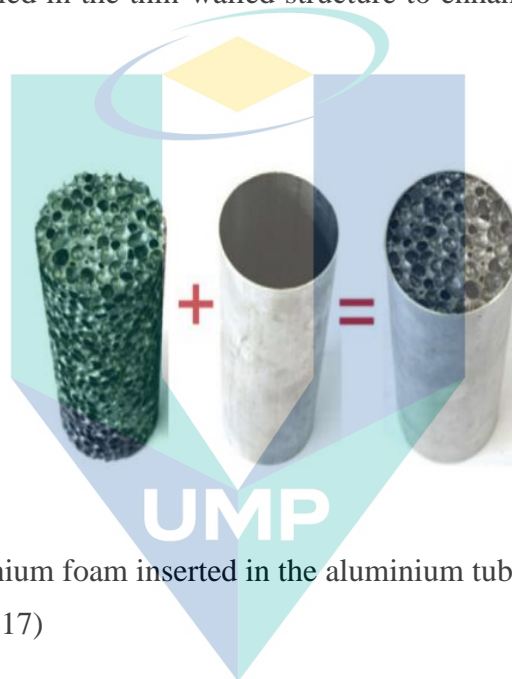


Figure 2.3 Aluminium foam inserted in the aluminium tube

Source : Zhu et al. (2017)

Sun et al investigated the effect of foam-filled in aluminium, steel and carbon fiber reinforced polymer (CFRP) tube. (Sun et al., 2016). Foam-filled aluminium and steel exhibited a stable progressive collapse mode and demonstrated higher value of EA and SEA compared to the empty tube and these values increased with the foam density. But for CFRP, value of EA and SEA decreased for the high-density foam. Shahbeyk et al (Shahbeyk et al., 2005) concluded that random distribution of foam density and impactor inclination did not affect the crushing behaviour of the columns filled with low-density but changed the medium-density foam. Application of aluminium foam between corrugated outer and inner tubes was simulated by Kiliçaslan (Kiliçaslan, 2015). Double corrugated tube filled with aluminium foam with the highest corrugation length,  $\lambda$  achieved the highest SEA which is 19.3 kJ/kg. Goel (Goel, 2015) has modeled aluminium foam core in his simulation and found that the energy absorption increased by 150 %. Aluminium foam used in Gan (Nianfei Gan et al., 2016) study was prepared by patented

process and machined into the tapered shape using computer numerical control (CNC) milling. Test performed on the aluminium foam showed that the foam with highest density absorbed the most energy. To study the effect of foam density with the impactor inclination to the crushing behaviour, three different density for aluminium foam were produced by Hydro Aluminium (Shahbeyk et al., 2005). Result showed that, for  $340 \text{ kg/m}^3$ , small inclination of impactor can cause an unstable global buckling.

Zhu (Zhu et al., 2017) conducted an experimental study on aluminium foam-filled tubes with composite reinforcement. The investigated design succeeded in increasing the SEA by 32 % compared to empty aluminium tubes. Unfortunately, the peak crushing force was also increased by 148 %. This study supported Subramaniyam (Subramaniyan et al., 2013) investigation that concluded the existence of composite in the filler material has increased the energy absorption and the peak force of the tubes.

Multi-tubes configurations have been used to enhance the crashworthiness of a structure. However, these types of design usually lost their weight efficiency. Due to that, foam filler was introduced to increase the absorption energy of the design. Zhang (Zhang et al, 2012) have reported on the performance of single and double circular foam-filled tubes subjected to bending load. Aluminium foam-filled has increased the SEA of the double and single tubes by up to 300 %. Research on double square column was continued by Dirgantara (Dirgantara et al., 2018) that considering the strain rate effect of the foam in the numerical analysis. It was found the consideration of strain rate may lead to the higher crushing performance of the structure. Results on specific energy absorption of the foam-filled structure were in good agreement with other abovementioned studies. Other than that, Li (Li et al., 2018) conducted experimental study to determine effect of shape and geometrical design on the energy absorption characteristic of foam-filled structures. The corner part of the foam-filled single and double square tends to tear under axial compression but the structures with foam-filled corners demonstrated progressive folding collapse mode. This stabilize collapse manner has led to the higher energy absorption gained by this foam-filled design.

This result was supported by Alavi Nia and Parsapour (Alavi Nia & Parsapour, 2013) that investigated on crushing behaviour of square multi-cell. According to the experimental results, SEA and peak load of the square multi-cell tubes were increased by 92 % and 79 % compared to the simple tubes. The research also showed by simulation

that the newly proposed multi-cell can increase the SEA and peak load by up to 227 % and 298 % accordingly. Wangyu investigated the performance of aluminium foam with positive and negative poisson's ratio. They proposed a new mixed foam model (MPR) and analysed capability of the foam-filled structure under axial dynamic impact. It was found that foam-filled double tubes showed the highest SEA and eliminated diamond mode of the inner tube (Wangyu et al., 2018). Altin conducted a study to investigate the effect of different percent of foam inserted into a circle and square tubes (Altin et al., 2017). Experimental results showed that the energy absorbed was increased by the increasing in percent of foam that filled in the aluminium structure. Furthermore, performance of square foam-filled structures was better than the circle one in this study.

Later, Kumar (Kumar et al., 2019) performed an experimental study on aluminium foam-filled in circular, square and rectangle tube under different strain rates. It was observed that highest strength and energy absorption capacity are acquired at a strain rate of 10 mm/s and lowest are at 1 mm/s. The foam-filled structure showed the higher EA and SEA compared to the empty one mostly for the circular structure. Yang (Yang et al., 2019) established the analysis of foam-filled and geometry of structure effect on the transition of the crushing mode. The mean crushing forces corresponding to the concertina and the diamond modes are measured and the transition zones identified for different lobes in the analysis. Mode classification chart indicated that the diamond mode occurred when  $R / t > 25$  and  $\sigma_{\text{foam}} / \sigma_{\text{yt}} < 0.015$ , and in concertina mode vice versa.

#### 2.4.5 Honeycomb filler

Honeycomb is one of the filler materials that has been used widely to increase the energy absorption capability of the structure instead of foam. Design of bee's honeycomb has inspired the researchers to developed the hexagonal structure that performed excellent behaviour in various application which is called honeycomb structure. Honeycomb structures as shown in Figure 2.4 is other type of cellular materials that have been employed in many engineering applications. Some of the application are in safety equipment, automotive sector and engineering sector due to their advantageous mechanical properties including lightweight, high strength, heat insulation and high energy absorption capability (Q. Zhang et al., 2015). Research on honeycomb for a better crashworthiness structures have become more demanding. Similar to foam, the stress-strain curve of a honeycomb is divided into three phases which is linear elastic, plateau

and a densification phase. Energy absorption capability of the structure which controlled by elastic/plastic buckling and plastic collapse of the cells depends on the plateau phase (Qiao & Chen, 2016). Mechanical properties of a honeycomb structure are determined by the matrix material as well as the cell topology properties (Galehdari & Kadkhodayan, 2015). Therefore, any changes in the geometrical parameters including cell type, cell size and ratio of wall thickness-to-length, mechanical property and energy absorption capability of honeycombs will be differs (Liu & Zhang, 2009).

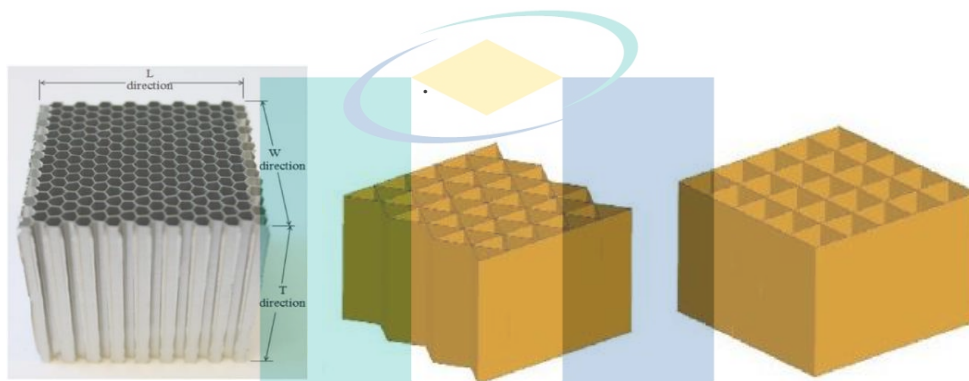


Figure 2.4 Aluminium honeycomb in (a) hexagonal cells can enhance the energy absorption of a structures (b) triangular and (c) square honeycomb

Source : (a) Zuhri et al. (2014) (b) Hussein et al. (2017)

Despite of increasing the energy absorption and the load-carrying capacity, application of honeycomb-filled structures may lead to the higher initial peak force compared to the hollow one. Moreover, stability of honeycomb-filled structures under axial loading are better than that of the conventional structures (Z. Wang, 2019). However mechanical responses of honeycomb-filled structure were highly dependent on the role of dominant part.

Wang (Wang et al., 2016) studied on honeycomb-filled square tube (HFST) verified that employment of honeycomb filler reduced the instability problems occurred in long honeycomb structure. Furthermore, reasonable matching parameter is remarkable to achieve the most favorable effect in term of energy absorption capacity and SEA. The study on matching effect prolong by Wang and Liu (Wang & Liu, 2019) by investigating on honeycomb cells filled with circular aluminum tubes (HFCT). Finite element analysis showed that HFCT structures outperform than the conventional honeycomb and multi-

tubes in terms of plateau stress and EA but the SEA value is mostly similar to multi-tubes.

Balaji and Annamalai (Balaji & Annamalai, 2018) evaluated the performance of honeycomb filled structures. Results shown that compared to hollow column, honeycomb filled structure showed better EA and SEA. They also discovered that combination of honeycomb with carbon fiber as filler showed better performance.

Hussein (Hussein et al., 2017) has investigated the effect of filling aluminium honeycomb-filled tubes, polyurethane foam-filled tubes and aluminium tubes filled with both polyurethane foam and aluminium honeycomb to the crushing behaviour of square hollow aluminium tubes. Combination of polyurethane foam and aluminium honeycomb as filler has shown the highest increment in energy absorption capability. Similar results gained by Zarei and Sadighi (Zarei & Sadighi, 2011) in their study. They concluded that by filling the hexagonal honeycomb with PU foam, the ratio of peak load and mean crushing force were decreases and this value decreasing more by using higher density of PU foam. Similar study conducted by Zhang (Zhang et al., 2019) introduced dynamic impact analysis on honeycomb-filled with expanded polypropylene (EPP). SEA values of the foam-filled honeycomb were decreased compared to the bare honeycomb due to the increases of mass. They suggested that the foam-filled single-cell with least foam was effective in improving the load resistance.

A quasi-static crushing and 3-point bending was performed on a square carbon fiber reinforced polymer (CFRP) filled with metallic honeycomb to study the response of this design (Liu et al., 2017). Result presented that 2 modes of failure which is progressively symmetrical crushing in two vertical sides and unstable crushing in one side occurs. Sun (Sun et al., 2016) investigated the effect of honeycomb-filled in aluminium, steel and CFRP. For steel tube, honeycomb-filled has increase the EA and SEA value compared to the empty one but for CFRP, the SEA values were decreased. While for honeycomb-filled aluminium, values of SEA almost constant.

Xiao (Xiao et al., 2018) studied on factors that influenced the bending resistance of honeycomb-filled composite thin-walled square tubes. It was found that energy absorption capacity of filled CFRP increases by the increment in tube wall thickness but restricted to certain limit. Besides, in terms of fiber direction, better crashworthiness



performance possesses by the tubes with wide angle fiber direction for outer layer, and a small angle for inner layer. As for the impact velocity, higher velocity not suitable to improve the energy absorption characteristics of a honeycomb-filled CFRP.

Although many researches have been conducted on honeycomb structure with hexagonal cells, but it is not acceptable in all approaches. Therefore, in few decade back, researchers have investigated on other types of honeycomb structures such as triangular (Zuhri et al., 2014), square cells (Souza et al., 2018), kagome (Zhang & Zhang, 2013) and auxetic (D. Xiao, Dong, Li, Wu, & Fang, 2019). Square and triangular honeycomb made of natural fiber based material were investigated by Zuhri et al (Zuhri et al., 2014). Energy absorbing characteristic for both structures were modelled using numerical analysis. It was found that energy absorption characteristics of the square honeycomb were better than the triangular honeycomb. Next, crush resistance of rhombic and kagome honeycombs were analysed theoretically and numerically by Zhang and Zhang (Zhang & Zhang, 2013). A theoretical model to predict the mean crushing force of angle elements were proposed and then validated with finite element analysis.

Auxetic materials is a unique material with negative poisson's ratio that expanding laterally when stretched longitudinally. To investigate the effect of honeycomb cell-wall thickness, Dong (Dong et al., 2019) has performed experimental study on thick-walled and thin-walled auxetic honeycomb. The study indicated that the critical cell-wall thickness of re-entrant honeycomb is 0.4 mm. In term of energy absorption characteristic, effect of the elastic strain energy to the total energy absorption should not be ignored for the thin-walled honeycomb, while the thick-walled honeycomb vice versa. Research on auxetic honeycomb were continued with the study on unidirectional-graded auxetic honeycomb (UGAH) and bidirectional-graded auxetic honeycomb (BGAH) by Xiao (Xiao et al., 2019). They concluded that energy absorption of the BGAH was higher compared to UGAH before the graded layer with the maximum cell-wall thickness was densified. Hu (Hu et al., 2019) introduced the application of bionic honeycomb tubular nested structure (BHTNS) as filler in energy absorbers. The theoretical model to predict the mean crushing force was formulated and verified with the numerical analysis.

In spite of improving the energy absorption capability of a structure, application of honeycombs structure may lead to higher initial peak force. For that instance, Yang introduced that hybrid corrugated honeycomb structure by integrating the triangular tubes

with sine-wave plates honeycomb. This new design structure has improved the energy absorption as well as lowering the initial peak force of structure (Yang et al., 2018). Ajdari (Ajdari et al., 2011) has simulated in-plane dynamic crushing of two dimensional honeycombs with both regular hexagonal and irregular arrangements and found that irregular cellular structures have energy absorption similar to their counterpart regular honeycombs. In the same study, it was concluded that the functionally graded cellular with decreasing relative density in the direction of crushing was succeeded in enhancing the energy absorption of honeycombs at early stages of crushing.

#### **2.4.5.1 Functionally Graded and hybrid foam**

Application of functionally graded foam (FGF) material has been proposed to increase the crashworthiness of foam-filled thin-walled structures. Functionally lateral graded aluminium foam used by Yin (Yin et al., 2013) has proven that the crashworthiness were better than the uniform foam. Later, Yin (Yin et al., 2014) has discovered that the crashworthiness of functionally graded foam-filled tapered tubes with ascending grading pattern (FGFTT-AGP) were less than uniform foam tube (UFT). However, the crashworthiness of functionally grade foam-filled tapered tubes with descending grading pattern (FGFTT-DGP) is generally better than UFT. But Mohammadiha and Ghariblu (Mohammadiha & Ghariblu, 2016) found that ascending grading pattern may increase the energy absorption compared to UFT by using the functionally axial graded aluminium foam. However, Attia (Attia et al., 2012) has concluded that both in axial and lateral grading configurations, energy absorption of the column was improved. Optimizations model of a FGT that varies axially conducted by Li showed the same conclusion as the authors above (Li et al., 2014). Design of the density gradient of foam filler depending on the strain distribution. The functionally grade foam-filled tubes acquired up to 24 % higher in SEA compared to UFT with the corresponding same-weight. This is caused by the high deformation in the border part of foam.

Yang (Yang et al., 2019) has developed a chart to classify diamond and concertina mode collapse due to the radius-to-thickness ratio and the foam plateau stress/column yield stress. Yu (Yu et al., 2018) investigated the effects of gradient pattern, average density of foam, and wall thickness on the deformation of foam-filled structure. An equation to predict the stress strain relation of the aluminium foam with functionally



graded-density was constructed and verified with the experimental results. This study also found that the specific energy absorption and crushing force efficiency of the structure increased with the increasing in average density of foam.

Duarte (Duarte et al., 2019) introduced the newly developed polymer-aluminium alloy hybrid foam as fillers in square aluminium tubes. It was found that the polymer-filled lead to development of rupture in the corners of square tubes due to the hydrostatic pressure that builds up within the tube. The study also shown that epoxy-aluminium alloy hybrid foam obtained higher EA and SEA than that of the silicone-aluminium alloy hybrid foam and the empty tube.

#### 2.4.6 Multi-cell column

The application of multi-cell sections was discovered to be an effective design to improve the energy absorption capability of thin-walled structures. These types of design are implemented in the front frame structure that specifically functioned as the energy absorbers (Kenyon et al., 2018). Alavi and Parsapour has been studied on simple and multi-cell for triangular, square, hexagonal and octagonal shapes. Results shown that all the multi-cell had greater specific energy absorption (SEA) in comparison with the simple structure (Alavi Nia & Parsapour, 2014). Scholar found that the cross-sections corners have key significance to the energy absorption performance of the structure (Guillow et al., 2001). Before that, Alavi Nia and Parsapour (Alavi Nia & Parsapour, 2013) has compared 4 designs of multi-cell in square tubes. They found that the new proposed design elements near the corner has increased the SEA by 227 % compared to the simple tubes. Xie and Wang (Xie & Wang, 2017) developed 5 structures with different arrangement of the interior tube walls and connectivity with the exterior tube walls and conclude that the crushing force and energy absorption influenced by the sectional form of the structure.

While Tran (Tran, 2017) revealed that the average crushing force of multi-cell triangular column due to lateral force is effected by the material flow stress, thickness of tube and length of tube. Multi-objectives optimisation design for multi-cell was investigated by Tran and Baroutaji (Tran & Baroutaji, 2018) to find the optimal design which exhibit the best crashworthiness performance under various loading condition. Multi tubular circular with lateral and axial foam-filled design were investigated using

FEA by Altin. They concluded that SEA and CFE of the tri-tubular with lateral foam-filling were found to be better than the axial foam-filled column (Altin et al., 2018). Goel has been studied on crashworthiness of square and circular tubes for single, double and three tubes. The finite element simulation using Altair RADIOSS shown that energy absorption of three tubes is 110% higher than single tube for the square shape (Goel, 2015).

Kenyon (Kenyon et al., 2018) concluded that the nine-cell structure outperformed the five-cell and four-cell cross-section in specific energy absorption (EA) and crushing force efficiency. Zhang (Zhang et al., 2018) proposed a numerical study on bionic multi-tubes with different number of cell. It was found that the best design to achieve maximum SEA and minimum IPF is by filling the middle wall with cylindrical tubes. Qiu (Qiu et al., 2015) investigated the hexagonal column with 6 configurations of multi-cell. Results shown that the number of corners affected the energy absorption capacity for the same cell number structure. The multi objective optimization was performed to maximize the energy absorption and minimize the initial peak force for single load case and multiple load cases.

Wu (Wu et al., 2016) performed numerical analysis on the effect of number of cells and the topological configurations of multi-cell column to the energy absorption characteristic. They found that the MCF and SEA increased proportionally with the number of cells. Zhang and Zhang (Zhang & Zhang, 2014) investigated the circular multi-cell under quasi-static loading as in Figure 2.5. Experimental results showed that energy absorption of specimen with the single, double, triple and quadruple cells were higher than the conventional one. Mean crushing forces of the circular multi-cell structure can be predicted using theoretical method proposed in this study.

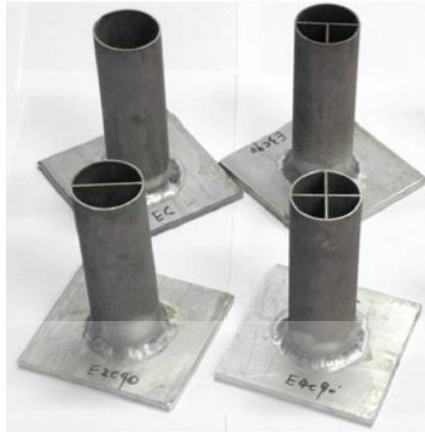


Figure 2.5 Circular multi-cell tubes

Source : Zhang & Zhang (2014)

#### 2.4.7 Corrugated column

Recently, researchers introduced the corrugations tube design to enhance the crashworthiness characteristic of energy absorbers. The corrugation design is suggested to compel the plastic deformation to appear at prearrange intervals on the column. The objectives are to improve the stability of the load-displacement response of axially crushed tubes, forecast and manage the collapse mode so that the energy absorption capacity of the structure can be optimized (Deng & Liu, 2019) . It is interesting to note that corrugation is formed in rows of wavelike folds or basically shaped into a series of regular folds that look like waves (Mahdi et al., 2006). The investigation on corrugated tubes indicated that corrugation could enhance the energy absorption capacity of structures in comparison to traditional straight tubes. Besides that, application of the corrugated tubes has led to the progressive deformation which decreases the initial peak force of the tubes. Alkhatib (Alkhatib et al., 2016) found that the corrugated tapered tubes (CTT) exhibits lower peak force and mean crushing force under different angle of impact. Then, Alkhatib continues their study by investigating crushing behaviour and energy absorption capability of CTT under axial loading (Alkhatib et al., 2017). They concluded that the parameters that influence the crash performance are wall thickness and amplitude of corrugation. Although the EA and SEA of the CTT were lower than the conventional tapered tube, but it succeeded in reducing the initial peak force of the structure.

Experimental study by Eyvazian (Eyvazian et al., 2018) proven that deformation mode of the corrugated metal tubes are more stable and controllable. Besides, the deep corrugation tube has succeeded in reducing the initial peak force compared to the shallow corrugation of the metal tube but the negative effect is the energy absorption were decreased simultaneously. Deng and Liu (Deng & Liu, 2019) carried out the crashworthiness study on sandwich sinusoidal lateral corrugated (SSLC) tubes and optimization showed that the maximum crushing force and SEA can be reduced compared to that of the single tubes. The truncated conical sandwich shell with corrugated (TCSS) was fabricated and optimized by Yang (Yang et al., 2019) has shown great potential to be applied as crashworthiness structure. Deformation mode of the TCSS shown an additional plastic hinges due to strong interaction effect of the face sheet and the core which relates with the excellent energy absorption capacity. Dynamic crushing simulation on single and double corrugated tubes has been simulated by Kiliçaslan (Kiliçaslan, 2015). Aluminium foam-filled double corrugated tubes in Figure 2.6 was proven to have the best energy absorption capability among all. SEA of the foam-filled double corrugated tubes was 31 % better compared to straight tubes.

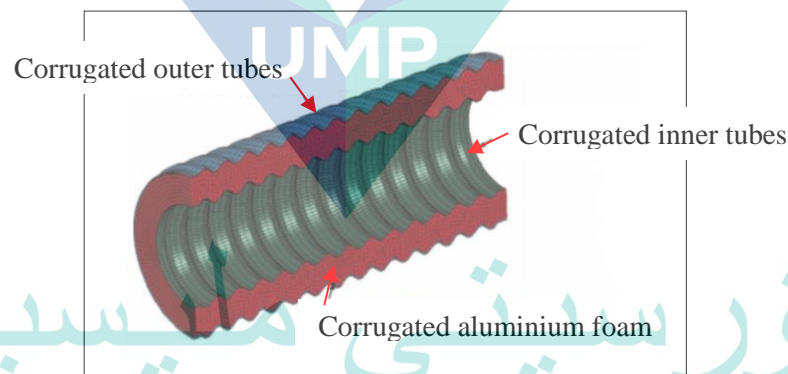


Figure 2.6 A foam-filled double corrugated tubes  
Source : Kiliçaslan (2015)

In other studies, Yan (Yan et al., 2013) have tested the aluminium foam-filled corrugated tubes under axial compression. The foam-filled corrugated sandwich panel showed increments in compressive strength and SEA by 211 % and 157 % respectively. A similar study on PU foam-filled aluminium and composite corrugated core by MR Mat Rejab (MRM Rejab, 2013) proven that energy absorption of aluminium corrugated core was increased by 300 % and 50 % compared to glass fiber and carbon fiber respectively.

Eyvazian (Eyvazian et al., 2016) proven that corrugated column design is effective in decreasing the initial peak force of the simple column but reduce the energy absorption capability. The corrugated composite column was introduced and has increased the SEA of corrugated column by 53 %.

A circular tubes with internal diameter of 22 mm, 27 mm and 32 mm for the corrugation tubes were modeled in LS-Dyna (Kiliçaslan, 2015). Although corrugated design managed to reduce the difference between initial peak force and mean force, but this design increased mass of the structure. This problem can be resolved by using the double-tube corrugated design.

Furthermore, Yan (Yan et al., 2014) has proven that foam-filled corrugated sandwich have increased substantially the mean crushing strength and energy absorption capacity of the beam. Other than that, this design has altered the failure mode and increased the bending resistance of the metallic beams. Similar results obtained by Mahbod and Asgari (Mahbod & Asgari, 2018) shown that foam-filled corrugated tubes has improved the energy absorption capacity in axial and oblique loading condition. The study also proven that by increasing the foam density, the SEA of the tubes has increased simultaneously while crushing force efficiency decreased. Later, Deng and Liu (Deng & Liu, 2019) carried out the crashworthiness study on sandwich sinusoidal lateral corrugated (SSLC) tubes and optimization showed that the maximum crushing force and SEA can be reduced compared to that of the single tubes. Su (Su et al., 2018) studied performance of sandwich cylindrical shells with corrugated cores.

The results showed that the sandwich structure demonstrates superior performance of energy absorption capacity and IPF compared to conventional one. The energy absorption increased due to the coupling effect between face sheet and corrugated cores, which caused the number of lobes developed increase. Other sandwich tube called truncated conical sandwich shell with corrugated cores (TCSS) in Figure 2.7 was fabricated and optimized by Yang (Yang et al., 2019) has shown great potential to be applied as crashworthiness structure. Deformation mode of the TCSS shown an additional plastic hinges due to strong interaction effect of the face sheet and the core which relates with the excellent energy absorption capacity.



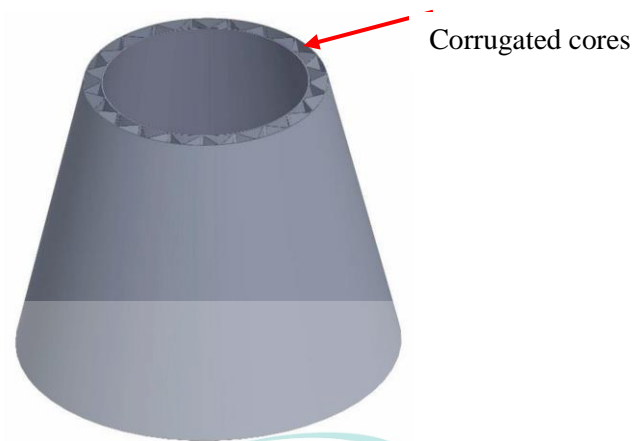


Figure 2.7 Configuration of the TCSS tube  
Source : Yang et al. (2019)

#### 2.4.8 Functionally Graded Thickness Column

The optimization method conducted by Li (Li et al., 2014) proven that the foam-filled functionally graded tubes (FGT) tubular structures was superior to counterparts with uniform thickness under axial loading and multi-objective optimization design shown that graded thickness structure achieve high specific energy absorption (SEA) and low initial peak force. Later, Sun (Sun et al., 2017) has introduced axial and lateral functionally graded thickness thin-walled tubes. The lateral functionally graded tube exhibits better energy absorption compared to uniform tube but axial functionally graded tube is more efficient in decreasing the peak force of the column. Then An (An, Gao, Fang, Sun, & Li, 2015) found that under axial crushing condition showed that specific energy absorption of functionally lateral graded thickness tubes are always greater than those of uniform tubes. Apart from that, a quasi-static axial crushing experiments was performed by Zheng (Zheng, Pang, Sun, Wu, & Li, 2016) and concluded that laterally variable thickness multi-cell tubes are of certain advantages over the uniform tubes.

Besides, Zhang (Zhang et al., 2014) investigated the thickness gradient in cross-section consist of single surface gradient (SSG) and double surface gradient (DSG) tubes as in Figure 2.8. They concluded that this design succeeded to increase up to 30–35 % of specific energy absorption without increasing the initial peak force. The optimization method used has proven that the SEA can be increased by adding the material in the corner part.



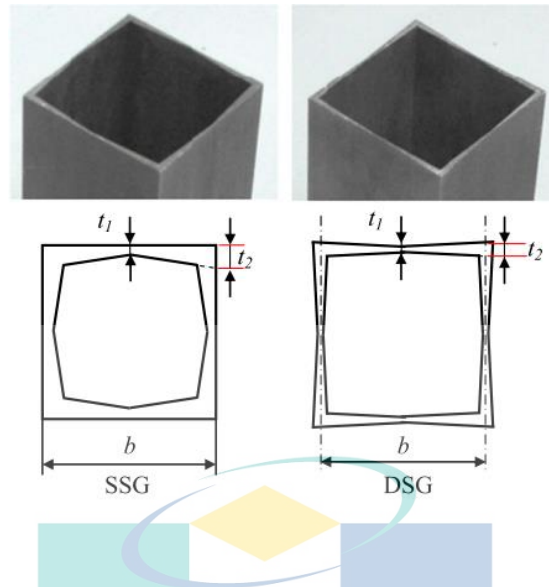


Figure 2.8 Configuration of the SSG and DSG tubes

Source : Zhang et al. (2014)

#### 2.4.9 Composite Thin-Walled Structure

It has been proven that Carbon Fibre Reinforced Plastic (CFRP) is an effective energy-absorbing material. However, the issue as to how to decide the best possible structural configuration still presents a challenge. Composite structures filled with lightweight materials have also attracted considerable interest due to their potential to enhance the energy-absorbing capability of composite structures (Xiao et al., 2018). Carbon fiber reinforced plastic (CFRP) composites, as one class of most promising lightweight materials, have recently been introduced in vehicle engineering; and are expected to play a more important role in contributing on lightweight design in the coming years. Not only is this attributable to their high specific strength and high specific stiffness, but also to their high capacity to dissipate crash energy for protecting passengers and goods (Zhu et al., 2018).

A few years back, natural fiber has been introduced as the alternative to carbon and glass fiber. Interior and exterior vehicle components made of natural fiber are effective in reducing the kerb weight of the vehicle and increasing its fuel efficiency. Daimler Chrysler, Mercedes Benz and Toyota are the companies that employed natural fiber in some of the parts (Holbery & Houston, 2006). Weager has choose natural fiber

due to its' good mechanical properties as well as safe to environment (Weager, 2010). The results found that the newly used material produced door with 60 % lighter than the same steel part with the same stiffness, while for Jaguar's prototype is roughly 35 % lighter than a glass filled polypropylene component with the same thickness. Sun (Sun et al., 2018) studied on the crushing characteristic of CFRP and aluminium tube under oblique loading condition. In this study, crushing mode of aluminum is an axisymmetric concertina mode for low degree of impact angle, and irregular diamond mode for higher degree of impact angle. In average, it can be concluded that energy absorption capacity of both the aluminum and CFRP were higher under low degree of impact angle.

Composite tubes were introduced as a crash box due to strength to weight ratio factor. Empty composite tubes without trigger mechanism generally collapsed in progressive crushing mode. Foam-filled composite tubes stabilized crushing mode but were ineffective in increasing the crushing loads of the composite tubes compared to the sum of the crushing loads of empty composite tube and foam (Sun et al., 2019)

Patel (Patel et al., 2019) investigated homogeneous and heterogeneous ply orientation of composite materials for the best performance for lightweight application in automotive industry. Heterogeneous structure showed superior crashworthiness parameters compared to the homogenous composite. For the heterogeneous structure, initial peak force of the CFRP column is 16.3 % lower compared to the glass fiber reinforced polymer (GFRP) column. Yan (Yan et al., 2014b) study on the application of polyurethane foam filled flax fabric/epoxy tubes under lateral crushing as in Figure 2.9. It was found that the foam filled flax/epoxy tubes were capable of spreading the deformation. The PU-foam suppressed the fibre fracturing and increased the energy absorption during flattening process. Energy absorption and peak load of the higher diameter for the same number of layers. This theory was aligned with Rezaei's (Rezaei et al., 2015) conclusion that stated SEA during splitting of the PU foam-filled circular composite tubes during the axial splitting process showed an increment compared to the empty sample. Sebaey and Mahdi's investigation on the polyurethane-filled CFRP rectangular tubes has mostly the same conclusion (Sebaey & Mahdi, 2017). The CFRP tubes were strengthened with a few inner configurations. The strengthening configuration has increased 25 % of the SEA compared to the foam-filled tube without it. Besides, the strengthening configuration increased the peak load from 13 % to 75 %.



Figure 2.9 (a) Foam-filled flax/epoxy tube (b) empty flax/epoxy tube  
 Source : Yan et al., (2014b)

The results were different in an experimental study on PU foam-filled CFRP tapered tubes. Foam-filled tapered circle and hexagon shape have shown the value of SEA by 4.3% and 3.1% higher respectively compared to the empty tubes. SEA of the hollow hexagon shape was the highest among all but decreased by 25% for the PU foam-filled tubes. SEA of the PU foam-filled tapered tubes increased by 30% compared to the Al foam filled Al alloy tapered tubes (Gan et al., 2016).

Mostly the same results are shown by Sun (Sun et al., 2016) . They investigated the crashworthiness of aluminium foam-filled CFRP tube. As for the empty CFRP tubes, the highest SEA was gained by the highest number of ply tubes with the lowest length-to-diameter ratio. For the aluminium foam-filled CFRP tubes, the SEAs were decreased due to mas of the foam filler. Furthermore, lateral expansion of aluminium foam caused circumferential and axial cracks in the foam-filled CFRP tubes. Guden (Guden et al., 2007) also found that the aluminium foam-filled E-glass woven fabric polyester composite tube and thin-walled Al/polyester composite hybrid tubes were ineffective in increasing the crushing loads and SEA values of the empty tubes. But the foam filler stabilizes the crushing process of the tubes. Similar results found in Sun (Sun et al., 2016) study on aluminium foam-filled CFRP tubes.

The foam-filled composite tubes with a proper design have potential to be lateral energy absorber structure and comparable to aluminium (Elahi et al, 2017). Although the foam-filled composite tubes were found to be ineffective in increasing the crushing loads over the sum of the crushing loads of empty composite and foam in the progressive

crushing region the foam-filled composite tubes induced a more stable tube crushing triggers and progressions.

Liu (Liu et al., 2018) conducted research to study performance of CFRP and aluminium under repetitive impacts. This type of impact usually occurred in vehicles stack up during heavy traffic. Results demonstrated that residual SEAs of the CFRP tubes and aluminium tubes were insignificant of the number of impacts. It also showed that performance of the CFRP tube is superior compared to aluminium under repetitive impact and residual crushing test. Other study on multi-impact was conducted by Amaro (Amaro et al., 2013) on GFRP. It was found that for the same value of energy, the sole impact was more detrimental compared to the cumulative impact or usually called multi-impact.

Sun (Sun et al., 2019) investigated the performance of aluminium/CFRP hybrid tubes subjected to three point bending test. The CF-AL tube (aluminium tube is inserted into the CFRP tube) and AL-CF (CFRP tube is inserted into the aluminium tube) demonstrated higher IPF, SEA and EA compared to the sole aluminium while for CFRP tube, IPF and EA were increased but the SEA value was decreased. Nevertheless, SEA values of the CF-AL tube were higher and the IPF value lower compared to AL-CF tube. The characteristic performed by CF-AL is remarkable for energy absorption structure. A research on metal-foam-composite hybrid tubular sandwich structures introduced by Sun (Sun et al., 2019). To address this issue, numerical and experimental study conducted on 4 configuration of hybrid sandwich structures which were AFA (aluminum outer tube, foam core and aluminum inner tube), AFC (aluminum outer tube, foam core and CFRP inner tube), CFA (CFRP outer tube, foam core and aluminum inner tube) and CFC (CFRP outer tube, foam core and CFRP inner tube). The hybrid structures showed higher IPF, SEA and EA compared to sole aluminium tube while for SEA sole CFRP was higher than that of the hybrid tubes. CFC tube obtained the highest value of SEA but the value of IPF also maximum among all configurations.

#### **2.4.10 Triggering mechanism**

Despite shape configuration, triggering mechanism is perceived as one of the most influential design factors for crashworthy performance. Formation of trigger at appropriate location of the structures caused stress concentration which capable of avoiding the load transfer to the whole structure effectively. It also prevents structures

from collapse catastrophically and induces a progressive failure mode to maximize the energy absorption. Moreover, triggering mechanism is an effective method to reduce the maximum crushing load,  $P_{max}$  during impact. Jiang has proven that a square tube with narrower ditch has succeeded in increasing the SEA by 51.9%. (Jiang et al., 2017). But use of triggering mechanism was found to be effective only if it employs at the appropriate location (Nurul Izzah et al.,2019)

A trigger has been identified as one of the contributing factors in increasing the energy absorption capability of the energy absorber. Triggers are irregularities that are created to reduce force variation in composite tubes by causing a stable crushing on composite tubes. Yan (Yan et al., 2014a) investigated on the PU foam-filler effect on a natural flax/epoxy composite tubes with triggering factor. The foam-filler has decreased the peak force and increased SEA of the tubes. Besides cutting grooves, foam filling is proved to be efficient in increasing the energy absorption and in improving the stability of the tubes and numerous investigations have been made into their effect.



Figure 2.10 Types of trigger mechanism that can be applied

Source : Hussain et al. (2017)

To study the effect of trigger configuration, Hussain (Hussain et al., 2017) chose the GFRP cylinder with three types of triggers shown in Figure 2.10. Results showed that the SEAs value for specimen with trigger were higher compared to the conventional cylinder. Nevertheless, only trigger B and C succeeded in reducing the initial peak force. It was observed that development of different types of trigger can vary the deformation mode of the specimen. As for this study the introduction of fillet on the edge of the crash box given the best performance.

While Estrada (Estrada et al., 2017) evaluated the effect of hole on the tube to crashworthiness characteristic of the structure. Numerical analysis conducted on double



cell tube with hole in different length of the tube. the best performance of crashworthiness was when discontinuities located at the top part of the walls of the rectangular column. study suggests a limit for the discontinuity size. This study concluded that IPF decreased with the increment in hole diameter but subjected to the proposed the limits of the hole perimeter,  $P_h$  with the size of structure,  $W$ , which is restricted by the relation  $0.46W \leq P_h \leq 0.67W$ . Montazeri (Montazeri et al., 2018) compared performance of holed and grooved column. For the mild steel structure, results showed that crushing performance of the holed tube is greater than grooved tube. It also found that the holed steel tube was better compared to the holed aluminium tube because it was relatively higher in term of SEA. Rouzegar et al studied the effect of geometrical discontinuities to energy absorption characteristics of structure. Results shown that energy absorption capacity was affected by numbers and position of notches. Compared to other specimen, composite tubes are more affected by the length of notches (Rouzegar et al., 2015).

## 2.5 Impact parameter

### 2.5.1 Conservation of energy

The conservation of energy principle is expressed in First Law of Thermodynamics which states that energy cannot be created or destroyed. It can change from one form to another. Energy balance can be expressed as

$$\Delta E = E_{in} - E_{out} \quad 2.1$$

Where  $\Delta E$  =change in energy  $E_{in}$  = energy in to the system  $E_{out}$  =energy out of the system

During a vehicle collision, energy is transferred from the vehicle to the object that being collided. The energy from the crash can be either absorb by the object or possibly transfer back to the vehicle. In inelastic collisions, although total energy is conserved but not the kinetic energy. It is converted into another form of energy such as heat and sound during collision. Motion during the collision can be determined by using the equation of momentum considering that momentum is conserved.



Kinetic energy, KE is energy that gained by a system as a result of its motion relative to a reference frame. When a system moves with the same velocity, the KE can be expressed by

$$KE = \frac{1}{2}mv^2 \quad 2.2$$

where m is mass of the impactor and v is the velocity of the impactor before striking the specimen.

Potential energy, PE is energy possesses by a system as a result of its elevation in a gravitational field. PE can be expressed by (Yunus A. Cengel & Boles, n.d.)

$$PE = mgh \quad 2.3$$

where m is mass of the impactor and g is the gravity acceleration and h is the height of the impactor from the specimen

Equating Eqs.4.6 and 4.7, the initial or striking velocity, v is defined as:

$$v = \sqrt{2gh} \quad 2.4$$

### 2.5.2 Crashworthiness parameter

*Initial Peak Force (IPF)*

IPF is defined as the first maximum force obtain by a structure during the crushing process as shown in Figure 2.11

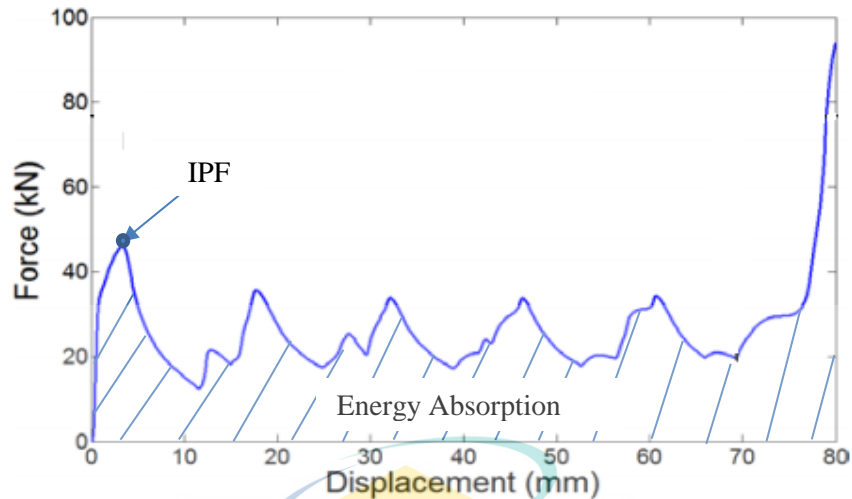


Figure 2.11

IPF in force-displacement curve

### Mean Crushing Force (MCF)

MCF is determine as the mean crushing force over displacement from 0 mm to 60 mm.

MCF is determined by the equation 2.5

$$MCF = \frac{1}{b-a} \int_a^b F d\delta \quad 2.5$$

Where a and b are the 0 mm and 60 mm by referring to Figure 2.11. F is force and  $\delta$  is displacement.

### Crushing Force Efficiency (CFE)

CFE is defined as the ratio of MCF and IPF. For energy absorber design, high value of CFE is desirable. There's no specific range stated but the foam-filled square design has CFE value 3.14 times larger than the empty design (Altin,2017) and foam-filled specimen have 0.64 of CFE compared to 0.32 in one of the configurations in Dirgantara's study (Dirgantara 2018)

$$CFE = \frac{MCF}{IPF} \quad 2.6$$

### *Energy Absorption (EA)*

EA is state as the energy dissipated by the structure during the compression process. It is calculated from the area under the force-displacement curve as in 2.7 by referring to Figure 2.11.

$$EA = \int_a^b F d\delta \quad 2.7$$

Where F is force and  $\delta$  is displacement. Where a and b are the 0 mm and 60 mm respectively

### *Specific Energy Absorption (SEA)*

Considering mass is crucial in energy absorbers design, the specific energy absorption was another important parameter considered in this study. The specific energy absorption, SEA is defined as the dissipated energy divided by the specimen mass, m as in equation 2.8

$$SEA = \frac{EA}{m} \quad 2.8$$

## **2.6 Principle of conservation of momentum**

This principle states that when two or more bodies act on each other, the total momentum remains constant, provided there is no external forces acting towards them. In a collision, the total momentum of the two objects before the collision is equal to the total momentum of the two objects after the collision as stated in equation 2.9

$$m_1 v_1 = m_2 v_2 \quad 2.9$$

## **2.7 Crash Optimization**

### **2.7.1 Optimization method**

Optimization is a potential method to acquire the best possible solution of various engineering planning and design problems. Other than that, it can be refers a method to improve the performance of a system, process, or product to achieve the maximum

performance of it (Bezerra et al., 2008). The methods are widely used in engineering design since years. However, with the development in computing technology, optimization method becomes more advantageous in selecting the best solution of various engineering problems. The current optimization methods and tools are sufficient enough to be applied in industrial applications.

In engineering design, capability or effectiveness of a new innovation is analysed using simulation and verified with experiment. But combination of these two methods involves high cost. To decrease the cost of these method, statistical method combine with the finite element were introduced (Boria, 2017). An optimization technique is commonly stated by determination of objective and constraint functions to find a solution as illustrated in Figure 2.12. With the development in computer technology, optimization have become a part of computer aided design. Metamodels are used in the optimisation design to reduce the computational cost. Some of the commonly used metamodels techniques are response surface methodology (RSM), radial basis function (RBF), Kriging (KRG), support vector regression (SVR) and polynomial response surface (PRS). Every metamodel has its disadvantage and advantage, and different metamodels are suitable for fitting different functions (Djamaluddin, 2019)

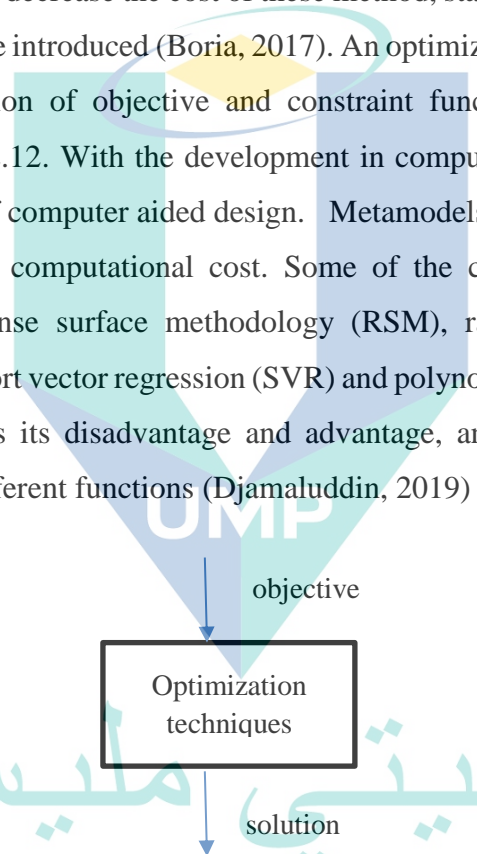


Figure 2.12 The operation of analysis models  
Source : Djamaluddin (2019)

An RBF apply a few basic functions that are symmetric and centered at each sampling point. It was initially created for scattered multivariate data interpolation. RBF usually applied in case of ocean depth measurement, altitude measurement, rainfall interpolation, surveying, mapping, geographic and geology. But one of the disadvantages of RBF is that RBF model fitness can't be examined using ANOVA.(Fang et al., 2005). Mullur and Messac (Mullur & Messac, 2006) proposed a new metamodeling approach

which is the extended radial basis function (E-RBF) method that provide favourable output.

Tran conducted a new type of method named multi objective optimisation for multiple loading cases (MOMLC) to optimise the triangular multi-cell structure. it was showed that mean crushing force is affected by the loading angle and number of cells. This method is suitable to optimize the multi-cells structure subjected to multiple loading as it evaluates all impact loading cases concurrently (Tran & Baroutaji, 2018).

An increase in SEA often leads to an increase in PCF, so that to consider for these two different design criteria, the design problem can be imposed in the multiobjective optimization framework. Wu (Wu et al., 2016) concluded that RBF model is the most promising than that of RSM and KRG models.

### **2.7.2 Optimisation design for crashworthiness**

In automotive industries, the design time is reducing by using Computer-Aided Engineering (CAE) at design stage. Although optimization method may reduce the duration to achieve the best design objectives, but in term of technical view, there are some problems when it comes to crashworthiness. This basically cause by the highly complicated and irregularities of the crush function. Moreover, more complex design needs more comprehensive response which can be obtained from experimental testing or simulation. This type of high-end simulation uses a replacement model (summary of an efficient and detailed model) which called metamodel (Ryberg, 2013)

For crashworthiness optimization, RSM has been the predominant method because it provides efficient and accurate solution. Besides, analysis of variance (ANOVA) can be used to predict model suitability before it can be implemented in design optimization (Fang et al., 2005). In study conducted by Baroutaji (Baroutaji et al., 2015), the optimization of circular structures under lateral loading were investigated employing the RMS method. Energy absorption capacity and peak load were designed as output responses for the input factor of diameter, thickness and width of the tube. In addition, Hou (Hou et al, 2014) studied the new thin-walled cellular configurations to enhance the crashworthiness of the vehicle part. The replacement model method using RSM was adopted in this research. Besides, RSM has been employed by Yin et al to optimised the design parameter of a functionally graded foam-filled structures (Yin et al., 2014). The

multiobjective design optimization (MDO) process, polynomial functional metamodels of SEA and PCF were utilized to decrease the computational cost of crash simulations by finite element method. However, RSM that is using the second order polynomial response surface models is not suitable to construct global models for the complex design with complicated nonlinear problems. Table 2.1 shows a few researches on optimization of the crashworthiness in thin-walled column.

Table 2.1 Optimisation design of crashworthiness for energy absorbers

Authors	Tube design	Loading	Model
Fang et al (2014)	Functionally graded foam-filled	bending	Kringing model
Tran (2015)	Multi-cell square	Axial	Response Surface Method
Altin et al (2018)	Multi-tubular circular	Axial	Response Surface Method
Deng (2019)	Corrugated tubes	Axial	Kringing model
Wang et al (2019)	Multi-cell square	Axial	Response Surface Method

### 2.7.3 Optimisation Algorithm

Optimisation design can be solved by using different types of algorithms. The local optimisation algorithm is a favoured technique because the capability of solving problem with many design variables and the effectiveness of the results achieved. Most local optimisation algorithms are based on gradients to determine optimum solutions (Alan, 1987).

However, global optimisation is need in most cases because it provides a better solution in determination of the most favourable values globally. It solves optimisation cases by generating determinative point that emphasis on the optimum solutions globally. The stochastic algorithm is used to solve non-linear local optimisation by using random point generation for searching techniques. This technique commonly has low limitation in mathematical features, capable for larger design cases and don't need gradient data. Stochastic optimisation algorithm is commonly suitable for multi objectives cases because the metamodel evaluation time is lower. Genetic algorithm and swarm particle optimisation were example of stochastic optimisation algorithms.



#### 2.7.4 Multi objective optimisation for structure

To optimize the best arrangement of foam-filled thin-walled structure that provide enhancement in crashworthiness, many researches has been executed in few years back. The optimisation methods have been implemented in structural design. For example, Xiong (Xiong et al., 2018) investigated and optimized the crashworthiness of novel foam-filled ellipse column. Taguchi-method used to develop design of experiment (DOE) which is applied to study the effect of each parameter. Grey relational analysis (GRA) is implemented to find the optimal design of foam-filled elliptical column for maximum SEA and minimum IPF. Asanjarani (Asanjarani et al., 2017) conducted a multi objective crashworthiness optimisations on square taper tubes with indentation. Response Surface Method were used to formulate the objective functions which are SEA and CFE. Sun (Sun et al., 2010) employed the swarm particle optimisation in crashworthiness designs using two-stage multi-loyalty method for a metamodel. Bigdeli and Nouri (Bigdeli & Nouri, 2019) proposed new geometry to increase the crashworthiness characteristic of the structure. The highest influenced parameter of this design is thickness of the structure and the optimum thickness for both configurations was 1.4mm. Optimization performed using Design-Expert software and the MOPSO method in MATLAB software.

In optimisation techniques, metamodel methods are commonly used to decrease the computing period. RBF as a metamodel method is more accurate for non-linear response estimation.

#### 2.7.5 Response Surface Methodology (RSM)

In the 50s, Box and collaborators instigated response surface methodology (RSM) in optimization RSM was invented from the graphical perspective generated after fitness of the mathematical model, and its use has been chosen in texts on chemo metrics. It comprises of a group of mathematical and statistical techniques that are based on the fit of empirical models to the experimental data obtained in relation to experimental design. The linear or square polynomial functions are applied to describe the system objectives to explore experimental conditions until its optimization (Bezerra et al., 2008). RSM imposes a few stages includes selecting the independent variables of major effects on the system studied, selecting the experimental design and carrying out the experiments

according to the selected experimental matrix, the mathematic–statistical treatment of the experimental data through the fit of a polynomial function, evaluating the model’s fitness, verifying the necessity and possibility of performing a displacement in direction to the optimal region and obtaining the optimum values for each studied variable (Myers et al., 2016).

Chapter 2 presented the literature review on types of energy absorbers that commonly used in the automotive industries. Also discussed on PU foam that has been used as filler for the metal energy absorbers and properties of PU. Besides, this chapter also looked into an overview of energy absorption of hollow structures, foam-filled structures and a few designs of energy absorbers in the industries. The optimization method that was widely used in engineering planning and design is also elaborated in this chapter. Hussien (Hussein et al., 2017) in his study has concluded that the PU foam-filled column has succeeded in increasing the EA. The axial crushing behaviour of square aluminium tubes with different filled material which was PU, aluminium honeycomb and combination of PU and honeycomb. The configuration of PU foam-filled was by filling the whole length of the column with foam. However, there is no study that reported on the effect of reduction of foam length to the IPF and SEA of the column. With knowledge supported from chapter 2, the next few chapters will present the performance and test data of this study

اونيورسيتي ملايسيا قهغ

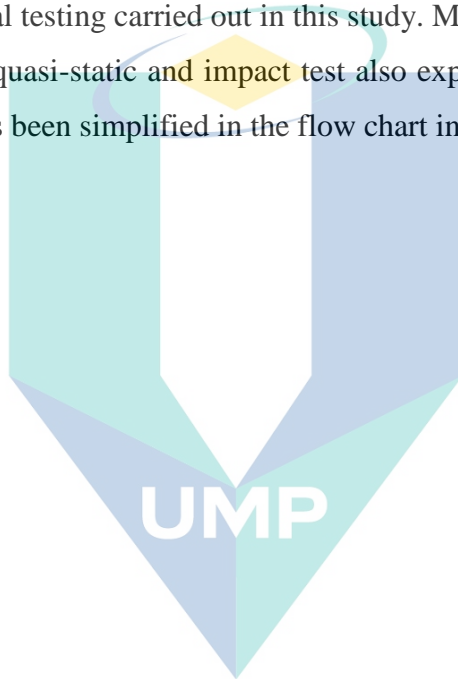
UNIVERSITI MALAYSIA PAHANG

## CHAPTER 3

### METHODOLOGY

#### 3.1 Introduction

This chapter describes on specimen fabrication process, calculation of foam density and mechanical testing carried out in this study. Mechanical testing is conducted on specimen such as quasi-static and impact test also explained in details. The flow of the research works has been simplified in the flow chart in Figure 3.1.



اونيورسيتي مليسيا قهغ

UNIVERSITI MALAYSIA PAHANG

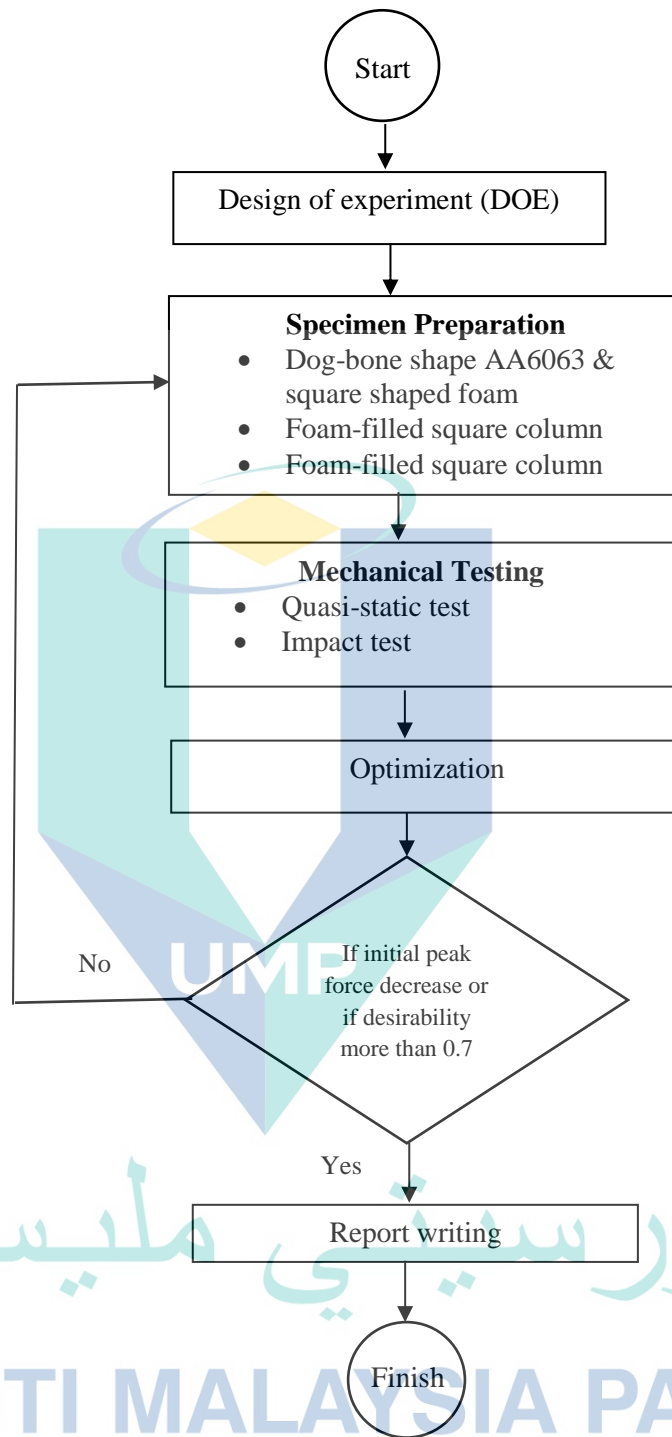


Figure 3.1 Methodology flow chart.

### 3.2 Design of Experiment (DOE)

DOE is prepared to identify number of specimens that was produced in order to achieve the specified objectives. Table 3.1 showed DOE that has been prepared for this study.

Table 3.1 Design of experiment.

	Code	Test	Thickness (mm)	Length of Foam (mm)
1	A1.4P0	Quasi-static	1.4	No foam
2	A1.4P185	Quasi-static	1.4	185
3	A1.4P190	Quasi-static	1.4	190
4	A1.4P195	Quasi-static	1.4	195
5	A1.4P200	Quasi-static	1.4	200
6	A2.0P0	Quasi-static	2.0	No foam
7	A2.0P185	Quasi-static	2.0	185
8	A2.0P190	Quasi-static	2.0	190
9	A2.0P195	Quasi-static	2.0	195
10	A2.0 P200	Quasi-static	2.0	200
11	A1.4P0	Impact	1.4	No foam
12	A1.4P185	Impact	1.4	185
13	A1.4P190	Impact	1.4	190
14	A1.4P195	Impact	1.4	195
15	A1.4P200	Impact	1.4	200
16	A2.0P0	Impact	2.0	No foam
17	A2.0P185	Impact	2.0	185
18	A2.0P190	Impact	2.0	190
19	A2.0P195	Impact	2.0	195
20	A2.0 P200	Impact	2.0	200

Notification of the specimen was indicating by the thickness of the square column and the length of foam. The 1.4 mm thickness square tubes were notified with A1.4 and the 2.0 mm thickness square tubes was notified with A2.0. Then follows by the length of foam. For the empty column, the notification used is P0, for length of foam of 185 mm, the notification used is P185, for length of foam of 190 mm, the notification used is P190, for length of foam of 195 mm, the notification used is P195 and length of foam of 200 mm was notified with P200. For example; aluminium square tubes with thickness of 1.4 mm that filled with 200 mm of foam was notified as A1.4P200 and aluminium square tubes with thickness of 2.0 mm that filled with 195 mm of foam was notified as A2.0P195. Before conducting the experiment, the foam-filled specimen was prepared accordingly. The preparation processes were described in detail in the subsection below.

### 3.3 Specimen preparation

Test specimens in this study were divided into two groups as listed in Table 3.1. All of these test specimens had an initial length of 200 mm. The first group was square aluminium tubes with thickness of 1.4 mm. The second group was square aluminium tubes with thickness of 2.0 mm. Foam with 4 different configuration of length which are 200 mm, 195 mm, 190 mm and 185 mm were inserted into the square aluminium tubes.

#### 3.3.1 Preparation of aluminium alloy square column

The specimens were prepared with square cross-sectional extruded column with dimension of 80 mm x 80 mm. The square dimension has been chosen considering the geometrical restriction in designing a crush box using aluminium tubes. The optimization procedure state that the tube width must be more than 70 mm (Zarei & Kröger, 2008). L/D (where L is height of the column and D is width of the square) ratio is set approximately 2.5 to avoid global buckling upon experimental observation. (Nikkhah et al., 2017). Therefore, the column is cut into 200 mm in length for each specimen with 1.4 mm and 2.0 mm thickness. Aluminium alloy AA6063-T5 used in this study was supplied by FM Global Trading based in Pekan, Pahang. This material has been chosen for all the specimens prepared due to the high strength to weight ratio which is 0.19 compared to steel which is 0.14 (Fentahun & Savas, 2018) . Figure 3.2 shown the aluminium column which has been cut to 200 mm each for both thicknesses.



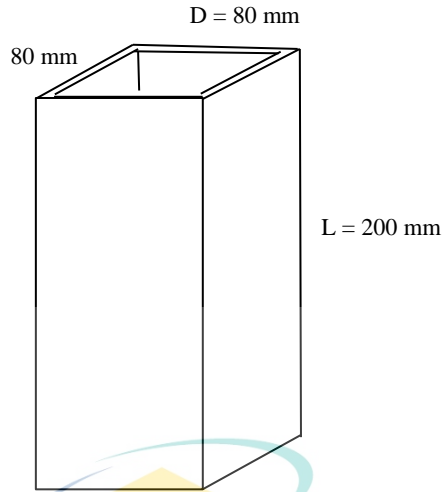


Figure 3.2 Aluminium column.

### 3.3.2 Product acceptance/ material assurance process for aluminium

For the purpose of data comparison with the previous study, the material properties test has been conducted on the aluminium alloy AA6063-T5. The tensile test was conducted according to ASTM E8/E8M standard (ASTM E8/E8M, Standard Test Methods For Tension Testing Of Metallic Materials, 2010). This test was conducted as part of the optimization procedure for the material acceptance/assurance method for AA6063.

Specimen were cut from the side wall of the 1.4 mm thickness tube in longitudinal direction using wire cut machine as in Figure 3.3 for sub size specimen.

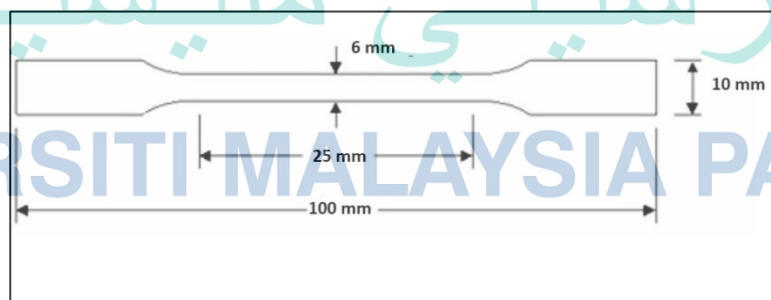


Figure 3.3 Dimension of sub size specimen for tensile test.

Three specimens with gauge length of 25 mm, width of 6 mm, overall length of 100 mm and width of grip section of 10 mm that have been prepared for material properties test for aluminium alloy

Tensile test was conducted using 50 kN Instron Universal Testing Machine (model 3369) in Faculty of Mechanical and Automotive Engineering Technology, Universiti Malaysia Pahang (UMP). During the tensile test, ultimate tensile strength is required to break a material in such a manner. When two ends of the specimen were pulled in opposite direction during the tensile test at constant cross-head velocity of 2 mm/min to maintain the quasi-static condition, it was undergone elastic and plastic deformation phases. Initially, the specimen deformed elastically which is shown by the linear line in the load vs extension graph (graph is shown in Figure 4.1 and 4.2).

### 3.3.3 Preparation of polyurethane foam (PU foam)

PU foam was prepared before inserted into the aluminium column. Mould with the suitable sizes were prepared before the square shape with the required sizes can be fabricated. The mould was produced from mild steel with 12.5 mm thickness. The mould was designed so that it can be open up to remove the foam. Sizes of the square is 77.2 mm x 77.2 mm for the 1.4 mm column and 76 mm x 76 mm for the 2.0 mm column.

Inside part of the mould should be apply with mould release wax so that the foam can be easily removed from the mould. The wax was applied to each and every part of the mould so that the foam produced can be removed perfectly as square column from the mould.

Polyol and isocyanate used in this study was supplied by Growchem Sdn Bhd which based in Semenyih, Selangor. Density of the polyol and isocyanate were 1070 kg/m<sup>3</sup> and 1220 kg/m<sup>3</sup> respectively. First, 100 g of polyol and 100 g of isocyanate was weighted in different beaker using weighting scale. Then the isocyanate was poured into the polyol beaker. After that, they were mix together using hand-mixer with constant speed of 2760 rpm. Tachometer was used to determine the speed of the hand-mixer. It was done by directed the tachometer to the rotating blades and the speed was shown on the tachometer screen. The process was shown in Figure 3.3. After approximately 10 second, the mixture turned into milky colour. Then liquid mixture of PU was poured into the square moulds and leave for foaming process. The foaming time for the foam is approximately 35 second.

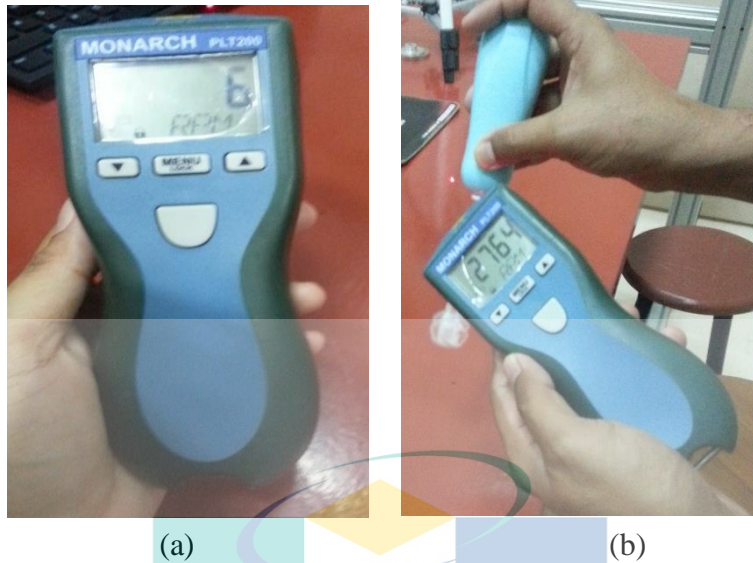


Figure 3.4 (a) Tachometer that has been used to define the speed of the hand mixer (b) the tachometer was directed to the rotating blades.

After 30 minutes, the mould can be opened up to remove the foam. It takes some time to make sure that the foam has been cooling down so that the removing process can be easier. After cutting out the dome part, the foam was measured and cut into the designed length according to the DOE. The skin of the foam was removed before inserted into the aluminium column to make sure that the specimen tested shown the characteristic of PU foam. The process of producing the foam is controlled by using the hand-mixer to make sure that the process is consistent and the time of foaming is the same for all the specimen used.

### 3.3.4 Product acceptance/ material assurance process for PU foam

#### i. Calculation density of foam

Foam density was measured as described by ASTM D1622/D1622M (ASTM D1622/D1622M-10, Standard Test Method for Apparent Density of Rigid Cellular Plastics, 2010). Density was calculated by dividing the weight of each sample by its corresponding volume. Three different cubical samples of 30 mm × 30 mm × 30 mm (length × height × width) for each specimen were measured. The data and average value of density were reported.

Density of the PU for mixture of both components which are growfoam (polyol) and grownate (isocyanate) with ratio 1:1 was calculated using the general equation of density:

$$\rho = m/V \quad 3.1$$

Where  $\rho$  = density (kg/m<sup>3</sup>)  
m = mass (kg)  
V = volume (m<sup>3</sup>)

### 3.3.5 Compression test of polyurethane (PU) foam

Preparation of PU specimen for material properties were conducted according to ASTM 1621/1621M (ASTM D1621-10, Standard Test Method for Compressive Properties of Rigid Cellular Plastics, 2010). The PU used in this study consists of two chemical substances which are Polyol and Isocyanate. Both substances were mixed in a weight ratio of 1:1. Deb (Deb et al., 2015) has concluded that PU foam has the best energy absorption effect with this ratio

The mould was custom made to shape the PU to the size needed. The mould was developed from mild steel that was fix together to form a square 30 mm (width) x 30 mm (length) and 200 mm (height). In order to produce PU specimen, the polyol and isocyanate were weighted to ratio 1:1 in different beaker using weighting scale. Then the isocyanate was poured into the polyol beaker. After that, they were mix together using hand-mixer with constant speed of 2790 rpm. Then liquid mixture of PU was poured into 30mm x 30mm square mould with 200 mm in height. Foaming time for the foam is about 35 second.

After curing, the foam was extracted from the mould was opened and the foam was cut into 30mm in length to form 30 mm x 30 mm x 30 mm cubes. The cutting process were conducted using the sectioning cut off machine in Material Laboratory, Universiti Malaysia Pahang.

After cut into shapes, the specimen's width, length and height were measured and recorded. Volume and mass of each specimen were calculated and recorded. Figure 3.5 shows the samples of specimen after being cut into cube shapes.

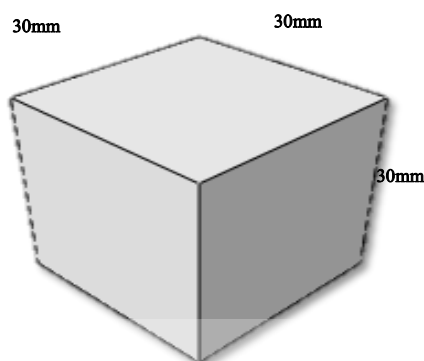


Figure 3.5 Schematic diagram of PU in cubic shapes prepared for testing.

Compressive test was conducted using 50 kN Instron Universal Testing Machine in Faculty of Mechanical and Automotive Engineering Technology, Universiti Malaysia Pahang (UMP). The samples were subjected to a controlled compression at constant cross-head velocity of 2 mm/min. All specimens were crushed up to 70% of their original length. The ultimate tensile strength, breaking strength and maximum elongation can be identified in the graph.

### 3.4 Mechanical Testing

Quasi-static compressive test and impact test were performed on specimens in both groups to study their deformation modes and obtain their load- displacement curves, from which energy absorption could be calculated. The compressive test of each configuration were repeated three times to check consistency of the experimental result.

#### 3.4.1 Quasi-static compressive test

For the quasi-static test, a constant slow speed compression testing has been carried out according to ASTM E9 standard (ASTM E9-89a, Standard Test Methods of Compression Testing of Metallic Materials at Room Temperature, 1989) by using the 1000 kN Instron Universal Testing Machine in Faculty of Civil Engineering Technology, Universiti Malaysia Pahang. The speed for the compression test was set at 6 mm/min. Specimens was axially crushed between two parallel steel flat platens, one static and one moving as in Figure 3.6. The fixed platen was fitted with a load cell from which the load signal was taken directly to the computer. For each test, the crush load was plotted on the Y-axis and the crosshead displacement on the X-axis. From the graph performed in Figure 4.12 and 4.14, there are two important parameters can be identified which is the initial peak load and also the energy absorption capability of each of the specimens tested.



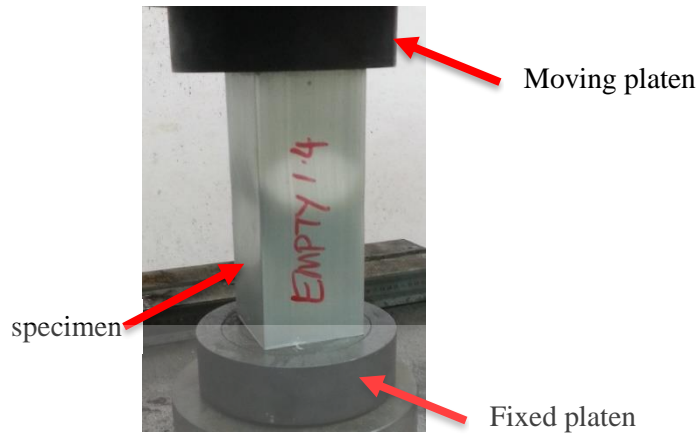


Figure 3.6 Specimen was placed between two platens.

### 3.4.2 Low velocity impact test

A drop weight impact test typically determines a material's resistance to a sudden external force. The low impact test of the foam-filled aluminium column was conducted using Dynatup drop-weight impact tester as shown in Figure 3.8. The impact test relies on the pneumatic assisted drop hammer of a known mass to supply the energy required to crush the specimen. The kinetic energy of the impactor can be adjusted by varying its drop height or its mass. In this study, a 38 kg impactor,  $M$  was used over a range of velocities of 5.18 to 5.40 m/s in order to characterise the dynamic response of the structures. A flat circular impactor, with diameter of 130 mm was used to strike the specimens with the impact energy of 246 J.

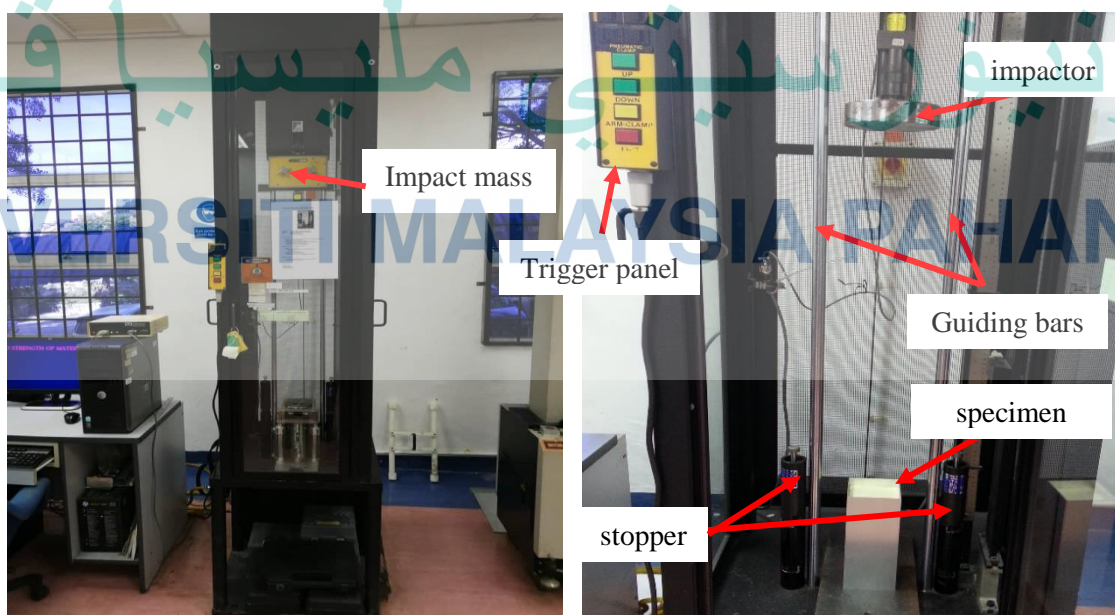


Figure 3.7 Instron Dynatup impact tester



When the impactor in contact with the top surface of the specimen, it progressively crushed. This movement was restricted by two stoppers in both sides of the rail. The kinetic energy is assumed to be completely absorbed by the specimen by neglecting the small rebound energy.

### 3.5 Optimization

Optimization has been conducted using Design Expert software version 7.0. This software is designed to assist in field of design and interpretation of multi-factor experiments. It proposes a broad range of designs such as factorials, fractional factorials and composite designs. In Design Expert software, before add in the input data, the suitable method has to be chosen from factorial, combined, mixture and response surface. For this study, response surface method is chosen. RSM has been dominant technique in crashworthiness optimization mainly because of it provides efficient and accurate solution. Besides, analysis of variance (ANOVA) can be used to predict model suitability before it can be implemented in design optimization (H. Fang et al., 2005).

Generally, formulating the mathematical relationship between SEA and IPCF considering the material properties, geometrical nonlinearities, and contact-impact nonlinearities is a bit challenging (Fang et al., 2014). A few techniques are suggested such as the response surface method to considered those effects of suitable parameters in designing energy absorbers (Mahbod & Asgari, 2018). The design variables are expressed mathematically as follows for the RSM method.

$$y(x) = \sum_{i=1}^p \beta_i \varphi_i(x) \quad 3.2$$

where  $p$  denotes the number of basic functions, and  $\beta_i$  is the unknown coefficient to be determined. By using the least-square method, the coefficients  $b = (\beta_1, \beta_2, \dots, \beta_n)$  of the polynomial terms can be obtained as:

$$b = (\Phi^T \Phi)^{-1}(\Phi^T y) \quad 3.3$$

where  $\Phi$  is a matrix consisting of basic functions  $\varphi_i(x)$  evaluated at these  $M$  design sampling points and can be written as:

$$\Phi = \begin{bmatrix} \varphi_1(x^1) & \cdots & \varphi_n(x^1) \\ \vdots & \ddots & \vdots \\ \varphi_1(x^M) & \cdots & \varphi_n(x^M) \end{bmatrix} \quad 3.4$$

By substituting Eq. 3.3 into Eq. 3.4, the coefficient vector  $b = (\beta_1, \beta_2, \dots, \beta_n)$  can be determined.

Objective function of this optimization algorithm is to minimize the initial peak force and maximize the specific energy absorption. The input functions were thickness of the aluminium column and the length of foam while the output responses were initial peak force and specific energy absorption.

### 3.6 Verification of optimization results

In optimization, the verification of the results should be conducted to close the cycle. As for that the verification has been conducted using simulation in Abaqus software to compared the suggested values in Design Expert Software with simulation results.

### 3.7 Conclusion

Chapter 3 presented details of the fabrication of the foam-filled structures with different length of foam, the experimental set-up as well as the testing procedure for both quasi-static and impact test. In this chapter, the fabrication process and the geometry of each specimen were explained in detail. The basic mechanical properties of the materials were examined through tensile test for Aluminium and compression test for foam. Finally, the foam-filled aluminium column was test to investigate the effect of applying different length of foam on the compression response of these aluminium structures.

## CHAPTER 4

### RESULTS AND DISCUSSION

#### 4.1 Introduction

This chapter discussed the experimental results of the research work. The chapter begins with the material properties test of aluminium alloy AA6063-T5 and polyurethane foam, then subsequently followed by the quasi-static and dynamic compression response of the empty and foam-filled square structure. Quasi-static and dynamic compression tests were conducted to measure the mechanical response of the structures under impact.

#### 4.2 Mechanical Properties of Materials

##### 4.2.1 Stress and strain of the aluminium alloy

For aluminium alloy, tensile test was conducted according to ASTM E8/E8M standard (ASTM E8/E8M, Standard Test Methods For Tension Testing of Metallic Materials, 2010). The engineering stress versus engineering strain curve was plotted as shown in Figure 4.1 and 4.2. The graphs shown the average engineering stress and strain for 3 tested samples for each thickness.

اونيورسيتي ملايسيا قهغ

UNIVERSITI MALAYSIA PAHANG

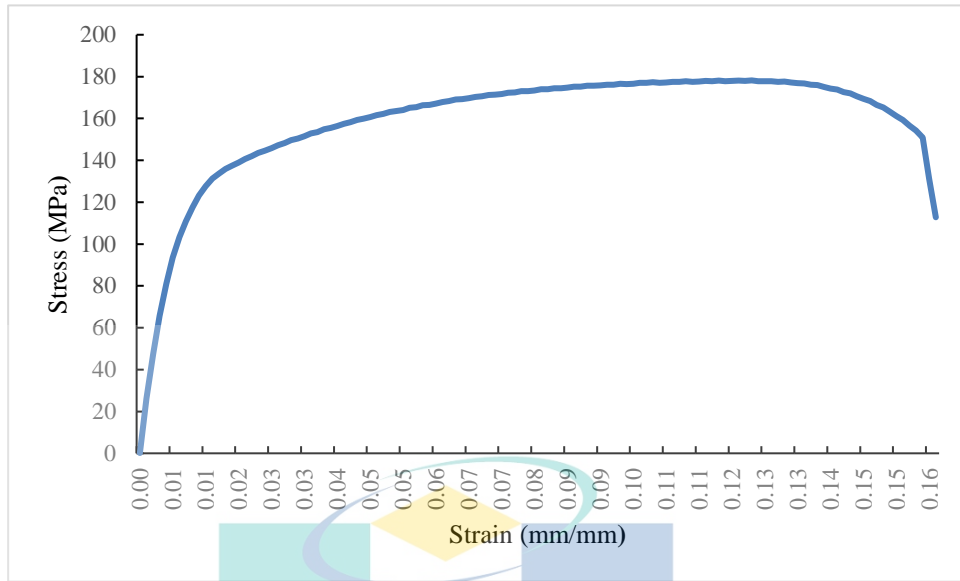


Figure 4.1 Engineering stress vs engineering strain graph for AA6063-T5 for 1.4 mm thickness.

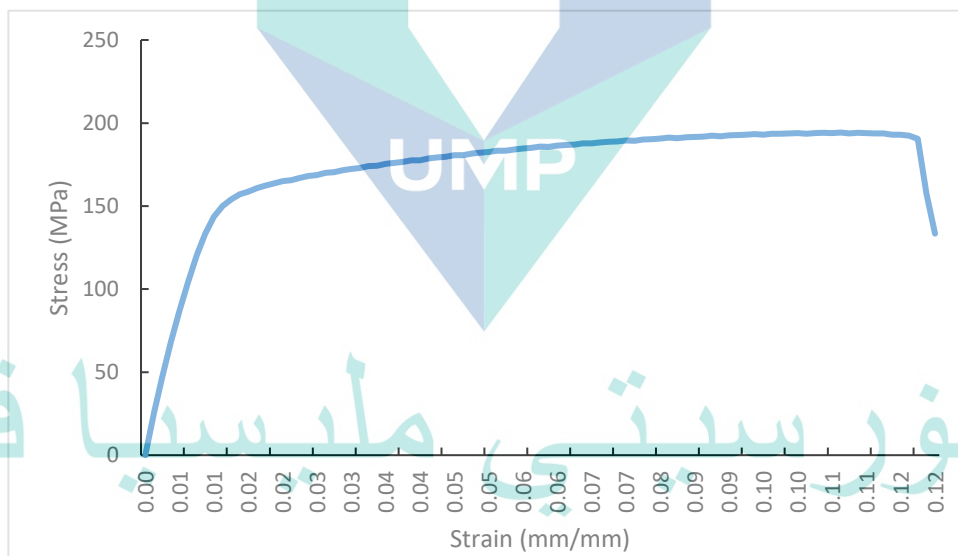


Figure 4.2 Engineering stress vs engineering strain graph for AA6063-T5 for 2.0 mm thickness.

This data is then used to calculate stress and strain for the sample which were then used to find the modulus of elasticity. The theoretical and tested value of material properties for the aluminium AA6063-T5 was recorded in Table 4.1.

Table 4.1 Material Properties of Aluminium 6063-T5

Material Constant	Theory	Experiment
Young Modulus	68 GPa	69 GPa
Yield Stress	150 MPa	158 MPa
Ultimate tensile stress	180 MPa	185 MPa
Elongation at break	11%	12%

#### 4.2.2 Density of the rigid polyurethane (PU) foam

Three specimens were prepared to measure density of the foam. The test was conducted in the standard laboratory atmosphere of  $23^{\circ}\text{C} \pm 2^{\circ}\text{C}$  and  $50 \pm 5\%$  relative humidity. Cross-section of the PU foam is illustrated in Figure 4.3 (a) while sketching of the areas of distributed cells is in Figure 4.3 (b). The outer layer of the foam is called skin. Layer next to skin is the microcells and fine cells are found approximately the centre of the foam. Presence of void can reduce the strength of the foam.

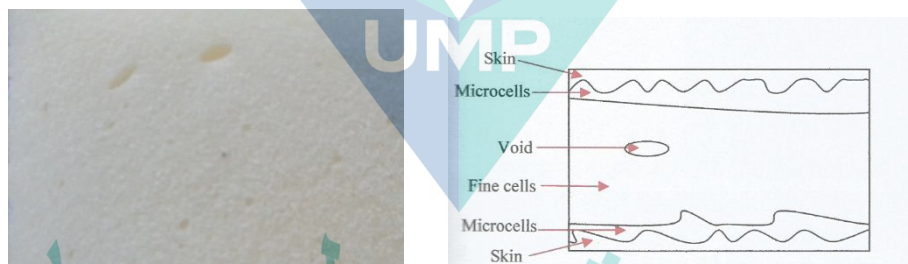


Figure 4.3 (a) Cross-section of PU foam. (b) sketching of the cross-section

Source : Mat Rejab (2004)

The geometrical dimensions of the rigid PU foams for determination of density and material properties test were cut to 30 mm x 30 mm x 30 mm. The skin parts were removed and the part with voids should be avoided to ensure the specimen prepared are acceptable. The weight of specimen was measure by electronic weight scale with precision of four. Then the density of PU foam was calculated. Dimension and mass of each specimen for the foam was measured and recorded in Table 4.2. Density was estimated density of the foam. It was a rough calculation to determine the product density according to standard.

Table 4.2 Calculation for foam density.

No	Mass (kg)	Width (m)	Length (m)	Height (m)	Volume (m <sup>3</sup> )	Density (kg/m <sup>3</sup> )
A	$2.23 \times 10^{-3}$	$2.74 \times 10^{-2}$	$2.74 \times 10^{-2}$	$2.72 \times 10^{-2}$	$2.042 \times 10^{-5}$	109.20
B	$2.32 \times 10^{-3}$	$2.75 \times 10^{-2}$	$2.72 \times 10^{-2}$	$2.77 \times 10^{-2}$	$2.072 \times 10^{-5}$	111.97
C	$2.30 \times 10^{-3}$	$2.76 \times 10^{-2}$	$2.76 \times 10^{-2}$	$2.71 \times 10^{-2}$	$2.064 \times 10^{-5}$	111.41
D	$2.23 \times 10^{-3}$	$2.74 \times 10^{-2}$	$2.72 \times 10^{-2}$	$2.72 \times 10^{-2}$	$2.027 \times 10^{-5}$	110.01
E	$2.33 \times 10^{-3}$	$2.73 \times 10^{-2}$	$2.76 \times 10^{-2}$	$2.73 \times 10^{-2}$	$2.057 \times 10^{-5}$	113.27
Average density						111.17

#### 4.2.3 Stress and strain curve of polyurethane (PU) foam

For the rigid polyurethane (PU) foam, two properties to be determined are the compressive strength and energy absorption characteristics. In this study, the effect on the energy absorption capability of PU foam was investigated. The 30 mm x 30 mm x 30 mm PU foam was compressed using UTM according to standard as in Figure 4.4. The specimen was placed between two platens of the machine and was compressed at 2 mm/min.

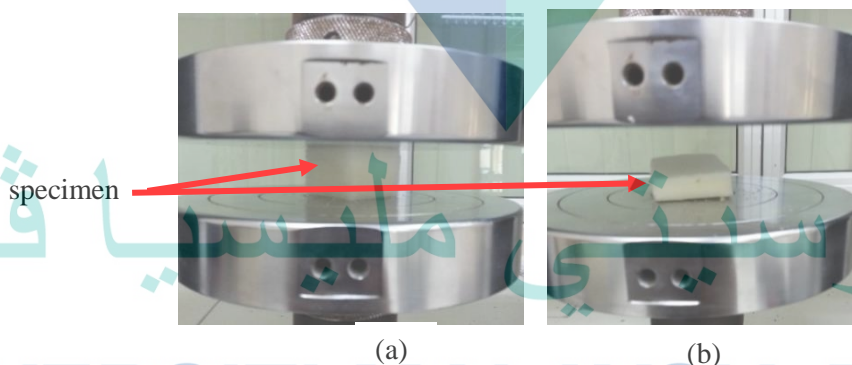


Figure 4.4 Compression of PU foam (a) initial setup (b) after 70% compression.

Based on data from the experiment, the stress and strain data were calculated. The compression process of foam has a general feature of localised progressive collapse (Gibson & Ashby, 1999). The stress-strain curve during the uniaxial compression test for the PU foam is plotted in Figure 4.5.



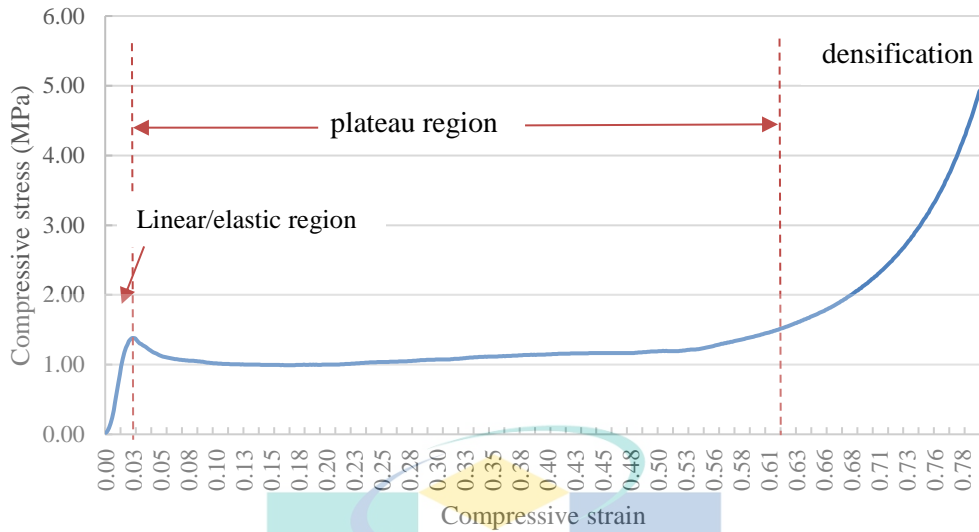


Figure 4.5 Stress-strain curve for the tested PU foam.

Stress-strain curve PU foam in Figure 4.5 can be divided into three phases of response. Initially, the linear phase indicates the elastic part where the stress increases uniformly (Gibson & Ashby, 1999). After the linear phase, the specimen entered the plastic plateau region. During this phase, the foam cells start to collapse by either elastic buckling, plastic yielding or brittle crushing. Deformation continues at constant force and cause the development of plateau stress until it touches the opposite walls in the cells. Final phase is called densification which occurs when the specimen was completely deformed (Avalle et al., 2001). Densification causes the stress to increase usually at 60% strain rate. In this study, the rigid PU foam was assumed to behaves as an isotropic material, so that the compression response is uniform in all principle directions. Increasing the relative density of the foam increases the Young's modulus, raises the plateau stress and reduces the strain at which densification begins (de Vries, 2009) . The theoretical and tested value of material properties for the polyurethane foam was recorded in Table 4.3. The theoretical data from Wang's study has been using PU with density of  $100 \text{ kg/m}^3$  while in this study, the density of PU is  $110 \text{ kg/m}^3$ . The lower value of density has resulted in lower value of densification strain.

Table 4.3 Material properties of polyurethane.

Material Constant	Theory (Wang et al, 2020)	Experiment
Plateau stress	-	1.05 MPa
Densification strain	0.74	0.78
Density	100 kg/m <sup>3</sup>	110 kg/m <sup>3</sup>

### 4.3 Quasi Static Test

The specimens were crushed under quasi static loading condition with speed of 6 mm per minute. To ensure the reliability of the results, three samples have been tested for each configuration. The force-displacement traces for all of the configuration were shown in Figure 4.12 (for thickness 1.4 mm specimen) and 4.14 (for thickness 2.0 mm specimen). Crashworthiness parameters such as initial peak force (IPF), energy absorption (EA) and specific energy absorption (SEA) for all the experiments were also calculated and discussed. Notification of each specimen is stated in Table 4.4

Table 4.4 Specimen notification.

Notification	Column thickness (mm)	Foam length (mm)
A1.4P0	1.4	No foam
A1.4P185	1.4	185
A1.4P190	1.4	190
A1.4P195	1.4	195
A1.4P200	1.4	200
A2.0P0	2.0	No foam
A2.0P185	2.0	185
A2.0P190	2.0	190
A2.0P195	2.0	195
A2.0P200	2.0	200

#### 4.3.1 Crushing behaviour of specimen with 1.4 mm thickness

The specimens were crushed under quasi static loading condition with speed of 6 mm per minute. Crushing progresses at constant load with little fluctuation. After a certain level of compression, the load starts to increase rapidly, possibly indicating the starting of foam densification.

Square structures may be collapsed in inextensional mode, extensional mode or mixed mode (Baroutaji et al., 2017) depends on the width to thickness ratio ( $b/t$  where  $b$  refers to the square dimension and  $t$  refers to the thickness of the specimen) in Figure 4.6. When crushed under quasi-static loading, 1.4 mm thickness specimen began to form the inward and outward lobe at the adjacent surface edge of the square. For the A1.4P0 the fold initiated around the middle part of the specimens with two lobes around the sections as in Figure 4.7. The deformation mode of A1.4P0 which was identified as an inextensional mode. Since  $b/t$  ratio in this study is 57.1, it is aligned with theory which state that the inextensional crushing mode occurred for specimen with  $b/t$  ratio more than 40.8 (Baroutaji et al., 2017).

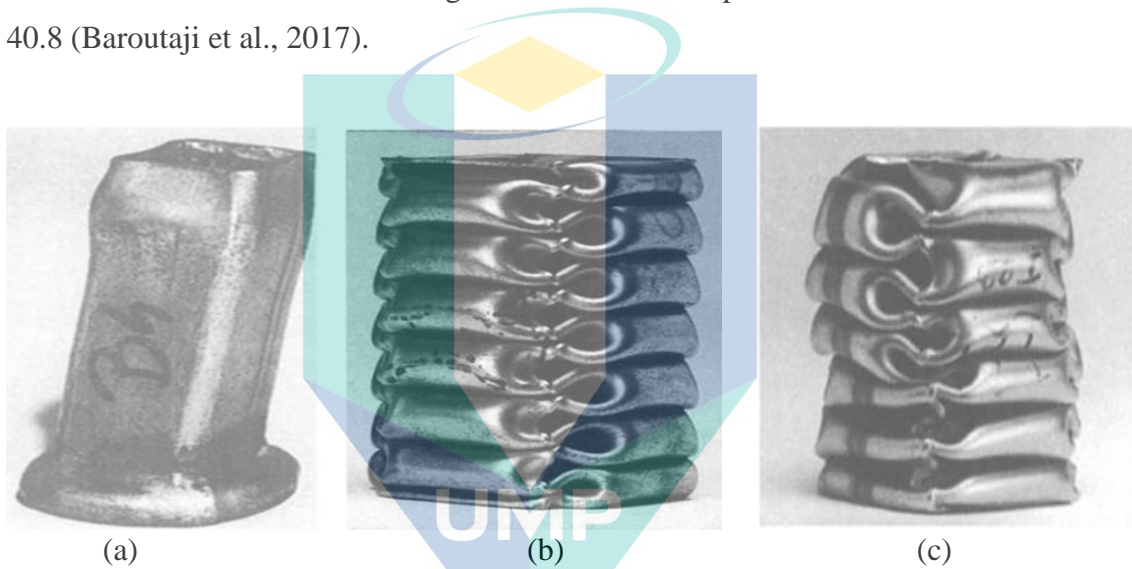


Figure 4.6 Axial progressive deformation mode of square tubes: (a) extensional mode (b) inextensional mode (c) asymmetric mixed mode

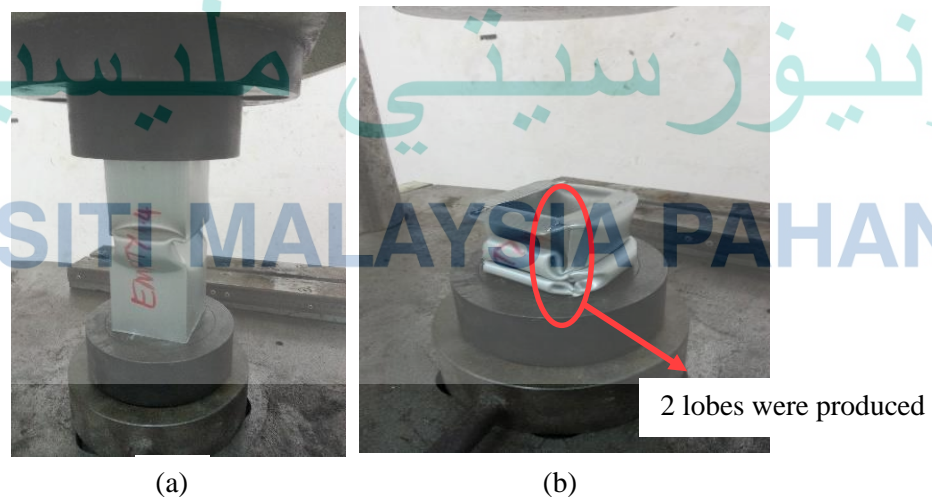


Figure 4.7 Deformation of A1.4P0 (a) initial crush (b) after 70% crush.

When filled with foam, the number of lobes for A1.4P185, A1.4P190 and A1.4P200 was increased in inextensional crushing mode. For a structures without any factitious trigger, the initial lobe is formed in a random distance along the length direction (X. Zhang et al., 2014). For the foam-filled specimens (except A1.4P195), fold was initiated at about 60 mm away from the upper end of the column (Figure 4.8a) continues to the middle region and finally to the lower end. Almost all foam-filled structures (except A1.4P195) crush consistently lobe by lobe in inextensional mode, Specimen P185 produced 3 inextensional folds (Figure 4.8b) which was less than A1.4P190 and A1.4P200 which produced 4 inextensional folds. Moreover, it was observed that after the compressive load is removed, the foam sprang back elastically by a certain distance to form a convex shape at both specimens' ends

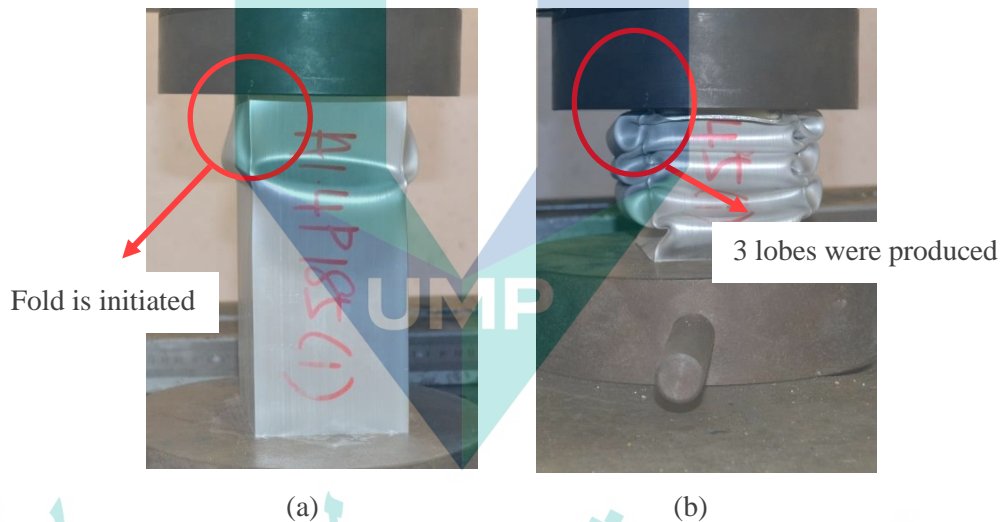


Figure 4.8 Deformation of A1.4P185 (a) initial crush (b) after 70% crush.

For specimen A1.4P195, the fold started about 80 mm below the upper end of the column in Figure 4.9a. The folds continued until the middle region with inextensional mode. As the compression continues, the folds become irregular at the bottom part towards the lower end and the deformation mode turned to diamond. Specimen A1.4P195 formed 3 folds with mixed mode deformation (combination of inextensional and diamond mode) shown in Figure 4.9b.

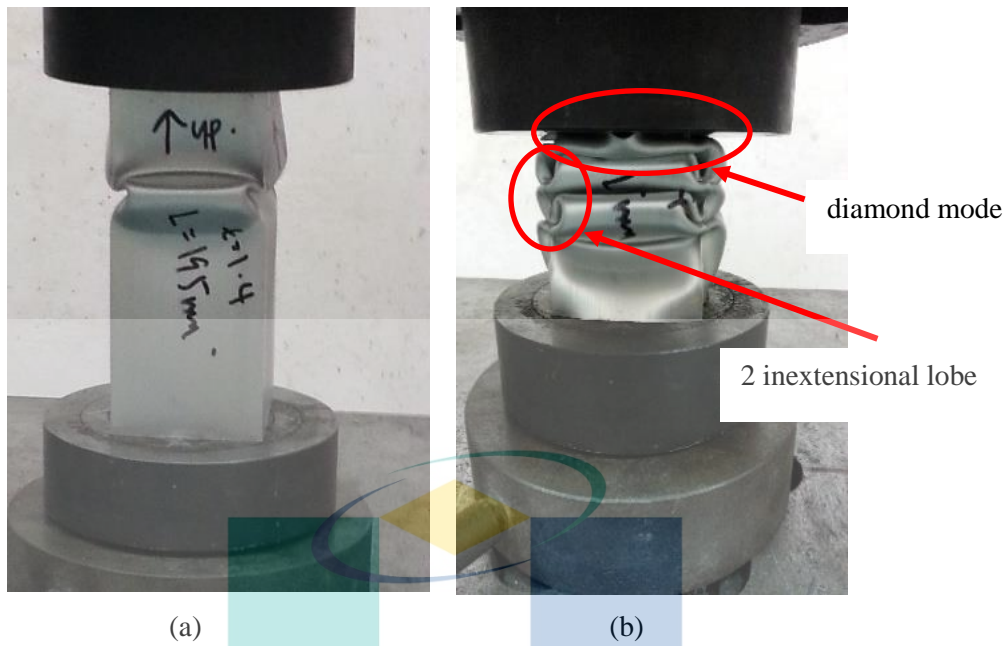


Figure 4.9 Deformation of A1.4P195 (a) initial crush (b) after 70% crush.

#### 4.3.2 Crushing behaviour of specimen with 2.0 mm thickness

It can be observed that crushing behaviour of the A2.0 structures were different from A1.4. For A2.0P0 structure, the first lobe is formed around the middle part of the specimens at initial stage of the compression process (refers figure 4.10a). But as the compression continues, at displacement of 15mm, tearing deformation occurred at two edges of the structures. Moreover, the development of a lobe with a big folding wavelength also influences the formation of tear (X. Zhang et al., 2014). Folding wavelength relates to the sizes of lobe produced during the compression process. The tears become more severe until the final stage as shown in Figure 4.10.



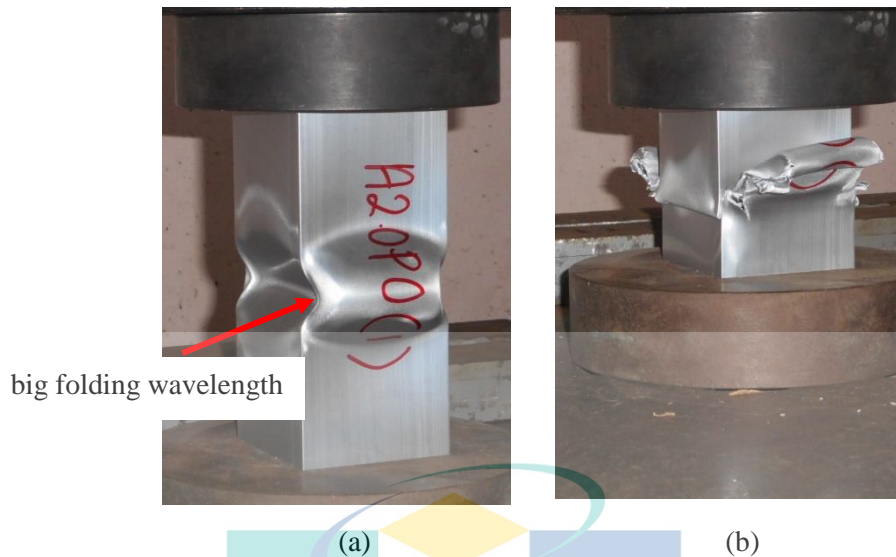


Figure 4.10 Deformation of A2.0P0 (a) initial crush (b) after 70% crush.

While for the foam-filled structures (A2.0P185, A2.0P190, A2.0P195 and A2.0P200), although the buckle also initiated around the middle part of the specimens but tear development started a bit late which is at displacement of 20 mm. The tear propagation started at the corners at both sides as shown in Figure 4.11a. The tear should be initially formed due to the stress concentration that weakens the corner region. The tear of the foam-filled structures is worse compared to A2.0P0 as in Figure 4.11b.

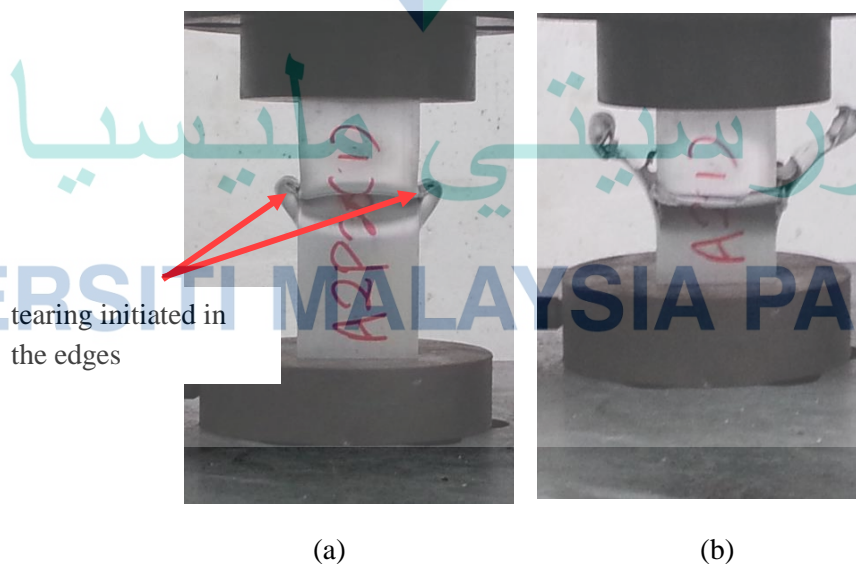


Figure 4.11 Deformation of A2.0P200 (a) initial crush (b) after 70% crush.



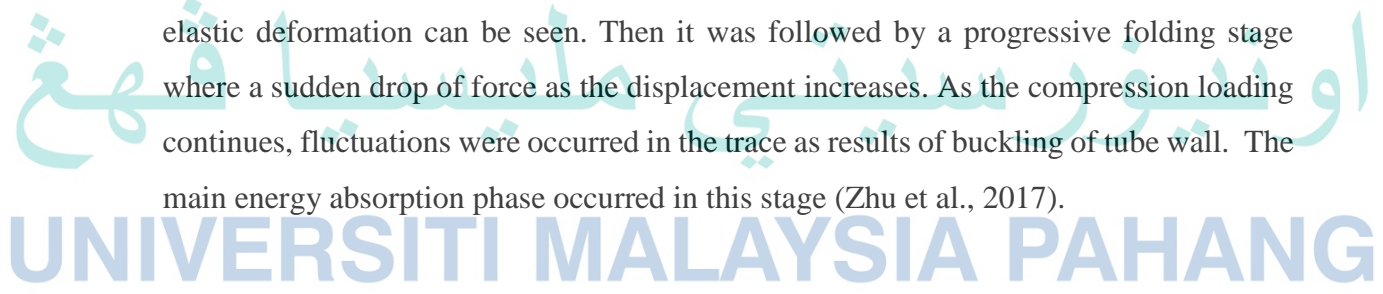
The crushing mode of all specimen used in this study under quasi-static test were summarize in Table 4.5 below.

Table 4.5 Summary of collapse mode for the specimen all specimen

Length of foam	T1.4	T2.0
0	Inextensional mode	Tearing
185	Inextensional mode	Tearing
190	Inextensional mode	Tearing
195	Asymmetric mixed mode	Tearing
200	Inextensional mode	Tearing

#### 4.3.3 Effect of length of foam to crushing response of specimen with 1.4 mm thickness

From the experiments, the force-displacement traces for all of the configuration were produced as in Figure 4.12. The results shown that the foam-filled column traces were higher compared to the empty column traces. At the initial stage, the crushing force increased rapidly until it reaches the initial peak force (IPF) in the elastic stage where the elastic deformation can be seen. Then it was followed by a progressive folding stage where a sudden drop of force as the displacement increases. As the compression loading continues, fluctuations were occurred in the trace as results of buckling of tube wall. The main energy absorption phase occurred in this stage (Zhu et al., 2017).



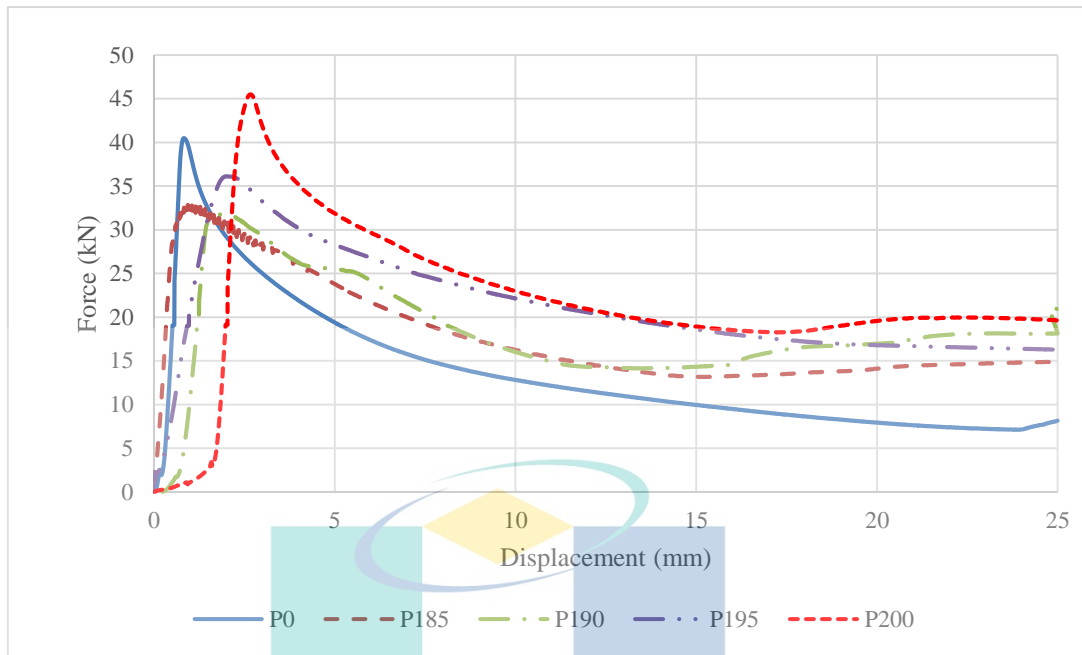


Figure 4.12 Force-displacement traces for P0 (empty column), P185, P190, P195 and P200 (full column) for specimen thickness 1.4 mm.

i. Energy absorption (EA)

Figure 4.12 represents the compression force-displacement traces comparison of empty column and foam-filled column for 1.4 mm thickness specimen. A remarkable increase in the area under the force-displacement traces for the foam-filled column compared to empty column was observed. Since area under the curve represents the energy absorption of the structure, it reflects that the filling of PU foam has increases the energy absorption capacity of the thin-walled structures. Figure 4.12 and Table 4.6 shown the energy absorption (EA) calculated over a displacement from 0 mm to 25 mm. It shown that EA value for specimen A1.4P0 (empty column) is 345 J. By filling the column with foam for the entire length has increased the EA to 547 J. It was aligned with research conducted by Yang (Yang et al., 2019) which concluded that the application foam-filled column is effective in increasing the energy absorption of a structure. In this study, length of foam is reduced to investigate the effect to the initial peak force values. Data in Table 4.6 shown that by reducing the length of foam, the EA of specimen A1.4P195 is decreased to 542 J. While for specimen A1.4P190, the EA also decreased to 503 J and keep reducing to 465 J for specimen A1.4P185. The results of EA exhibit a reduction with the reduced length of foam. Since the cellular material is introduced to increase EA, the energy

absorption capability of the specimen decreased simultaneously with the reduction of foam length.

Table 4.6 Energy absorption indices derived from the force-displacement traces for 1.4mm thickness specimen.

Specimen	Mass (g)	IPF (kN)	EA (J)	SEA (kJ/kg)
A1.4P0	240.2	40.8	345.1	1.4
A1.4P185	350.5	32.9	464.5	1.3
A1.4P190	353.6	32.1	502.7	1.4
A1.4P195	356.5	35.2	541.5	1.5
A1.4P200	358.9	45.5	547.1	1.5

ii. Initial Peak Force (IPF)

Although foam-filled structure has succeeded in increasing the energy absorption, but it also increases the absolute force level which increases the IPF of the structure (Hussein et al., 2017). The reduction of foam is purposely done to reduce the initial peak force. Table 4.6 shows that the values of IPF for all the foam-filled structures are not much different. The IPF of A2.0P200 (full-filled column) is 45.5 kN which is higher than A1.4P0 (empty column). This results aligned with previous research done by Hanssen (Hanssen et al., 2000) which also found that the IPF of the foam-filled column is higher compared to the empty column. This findings also supported the study conducted by G. Balaji (Balaji & Annamalai, 2018). According to Figure 4.13, it can be seen that compared to specimen A1.4P200, reduction in length of foam has reduced the IPF by 23% for the specimen A1.4P195. Next for specimen A1.4P190, the IPF was reduced by 29%. But as the length of foam was reduced in A1.4P185, the IPF reduced by 28%. But since the difference between specimen A1.4P190 and A1.4P185 was relatively small and can be neglected. The conclusion that can be made is that the decrease in foam length demonstrates a promising improvement in initial peak force, but to a certain extent.

iii. Specific Energy Absorption (SEA)

Specific energy absorption (SEA) is one of the important crashworthiness parameters in the determination of the ability of the structure for impact loading conditions. This factor is derived as the ratio of EA to the physical mass of structure (refer

to Equation 2.7). According to Table 4.6, the specific energy absorption (SEA) of specimen A1.4P0 is 1.4 kJ/kg. and for specimen P200 the SEA is 1.5 kJ/kg. For the reduced length of foam, the SEA of A1.4P195 is 1.5 kJ/kg. Next for specimen A1.4P190, the SEA calculated as 1.4 J/kg. Then for specimen A1.4P185, the SEA is 1.3 kJ/kg. It can be observed that the SEA values of A1.4P195 and A1.4P200 tubes are more remarkable than that of A1.4P0 tubes. Hence, for this study, specimen A1.4P195 deserves recommendation due to its higher SEA values compared to another specimen.

iv. Performance of energy absorbers

As the objective of this study is to reduce the initial peak force and at the same time maintaining the specific energy absorption capacity of the structure, the value of SEA and initial peak force for all configuration compared to A1.4P200 specimen were presented in Figure 4.13.

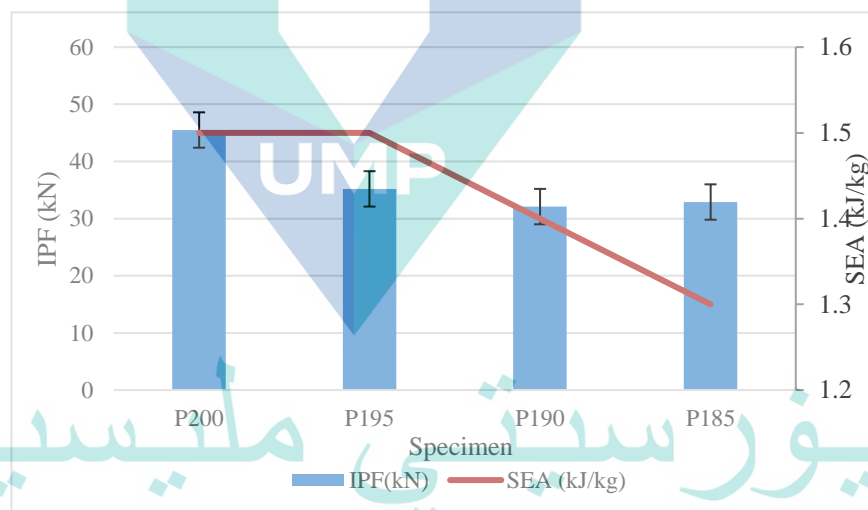


Figure 4.13 Value of SEA and IPF compared to A1.4P200 for 1.4 mm thickness specimen.

In this study, the reduction in SEA have to be minimum and the reduction in initial peak force have to be maximum for the best performance. For specimen A1.4P195, the IPF was reduced by 23% and the SEA just decrease about 1%. Next, A1.4P190 configuration has decrease the IPF by 29% and reducing 8% of the SEA. These two-configuration shown quite good performance in achieving the objective of this research. Then for A1.4P185, the SEA was reducing by 28% and IPF was reduced by 15%. The

conclusion was, at the axial crushing feed rate of 6 mm/min, the A1.4P195 is more desirable due to its low reduction in SEA as well as higher reduction of the IPF.

#### 4.3.4 Effect of length of foam to crushing response of specimen with 2.0 mm thickness

Instead of 1.4 mm thickness specimen, one more specimen thickness was tested to study the effect of foam length to the 2.0 mm thickness specimen to the absorption capacity. Figure 4.14 shows the force-displacement curve for 2.0 mm thickness column. The formation of initial lobe at random distance, to some extent may, increases the irregularity of the force-displacement curves. Moreover, the irregularities were also contributed by the existence of tearing on the corner part of the structure. It can be seen that the second peak force is almost demolished due to the tearing.

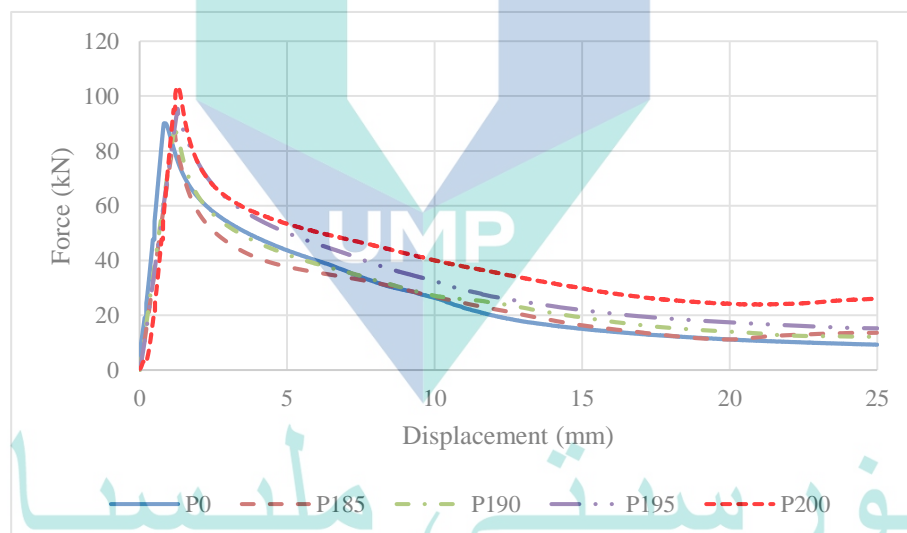


Figure 4.14 Force-displacement traces for P0 (empty column), P185, P190, P195 and P200 (full column) for specimen thickness 2.0 mm.

#### ii. Energy absorption (EA)

Figure 4.14 represents the force-displacement curve for specimen with 2mm thickness. In terms of energy absorption capacity, A2.0P200 curve is highest while the A2.0P0 curve is the lowest. Table 4.7 shows the relevant energy absorption indices such as energy absorption (EA), specific energy absorption (SEA) and initial peak force (IPF) calculated over a displacement from 0 mm to 25 mm. By filling the column with foam for the entire length, A2.0P200 the EA gained is 945 J. As the foam's length is reduced,

the EA is decreasing to 841 J for specimen A2.0P195. While for specimen A2.0P190, the EA decreased to 703 and keep decreasing to 607 J for specimen A2.0P185. This results was aligned with Hussien study (Hussein et al., 2017) on foam-filled column. By reducing the length of foam, the energy absorption was reduced proportionally.

Table 4.7 Energy absorption indices derived from the force-displacement traces for 2.0 mm thickness specimen.

Specimen	Mass (g)	IPF (kN)	EA (J)	SEA (kJ/kg)
A2.0P0	324.8	90.6	594.5	1.8
A2.0P185	433.1	85.9	606.5	1.4
A2.0P190	435.9	91.6	702.5	1.6
A2.0P195	437.7	97.3	840.8	1.9
A2.0P200	440.9	100.1	944.8	2.1

iii. Initial Peak Force (IPF)

Compared to the 1.4mm thickness, the initial peak force for specimen with thickness 2.0 mm was quite higher. This was expected because for the thicker materials, more force is required to initiate the deformation to the column (Subramaniyan et al., 2013). Figure 4.14 and Table 4.7 shows that the highest initial peak force was gained by A2.0P200 which is 100.1 kN as the force is required to deform column filled with full length of foam. This results is supported by Hussien (Hussein et al., 2017) that stated the IPF of foam-filled tubes were higher than the empty tubes. But as the length of foam is reduced, the IPF was reduced to 97.3 kN for the specimen A2.0P195. Then for specimen A2.0P190, the IPF was decrease to 91.6 kN and keep decreasing to 85.9 kN for specimen A2.0P185. It shown that decreasing the length of foam in the aluminium column is effective in reducing the initial peak force compared to fully foam-filled column (A2.0P200)



iv. Specific Energy Absorption (SEA)

According to Table 4.7, the specific energy absorption (SEA) of the specimen A2.0P200 is 2.1 kJ/kg. For the reduced length of foam, the SEA of A2.0P195 is 1.9 kJ/kg. Next for specimen A2.0P190, the SEA calculated as 1.6 kJ/kg. Then for specimen A2.0P185, the SEA is 1.4 kJ/kg. However, for this study, specimen A2.0P195 deserves recommendation due to its higher SEA values compared to another specimen.

v. Performance of energy absorbers

To observe the objective of this study, the percentage reduction in energy absorption and initial peak force for all configuration compared to A2.0P200 specimen were presented in Figure 4.15

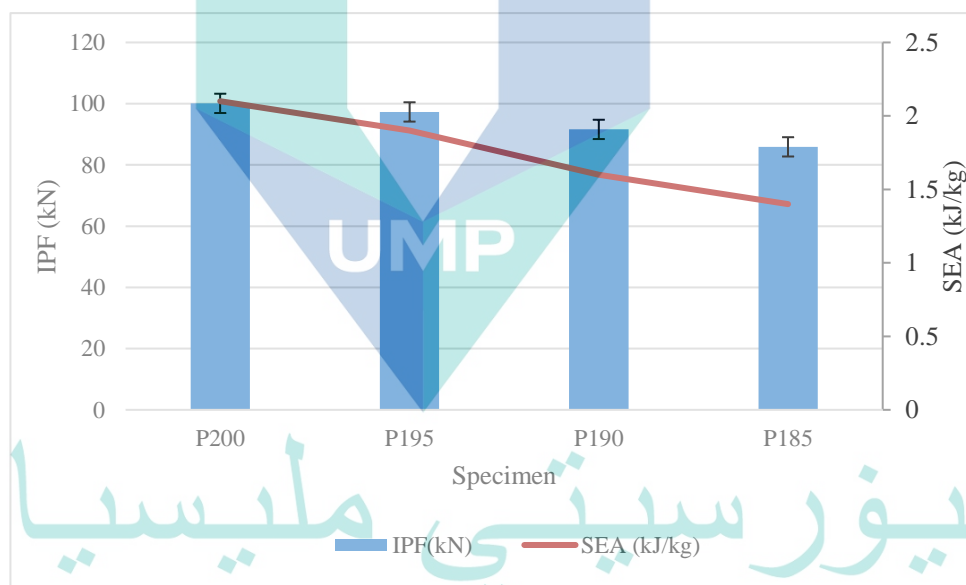


Figure 4.15 Value of SEA and IPF compared to P200 for 2.0mm thickness specimen.

But for the same thickness material, the initial peak force of the column varies with the length of foam. For specimen A2.0P195, the SEA and IPF was decreased by 10% and 3% respectively compared to A2.0P200. Next for specimen A2.0P190, the SEA was reduced 24% by and IPF was reduced by 8%. The maximum reduction was shown by specimen A2.0P185 with 33% in EA and 14% in IPF. It can be concluded that for 2.0 mm thickness specimen, the IPF is decreased proportionally with the EA due reduction of foam length.

#### 4.3.5 Effect of wall thickness to crushing response of specimen

Two thickness of for each structure which is 1.4 mm and 2.0 mm was tested to study the effect of specimen thickness to the energy absorption indices.

##### i. Energy Absorption (EA)

To observe the EA capacity of specimen A2.0 compared to A1.4, bar chart that contains the EA data of each specimen were constructed. Figure 4.16 shows EA obtain by each specimen for both thicknesses.

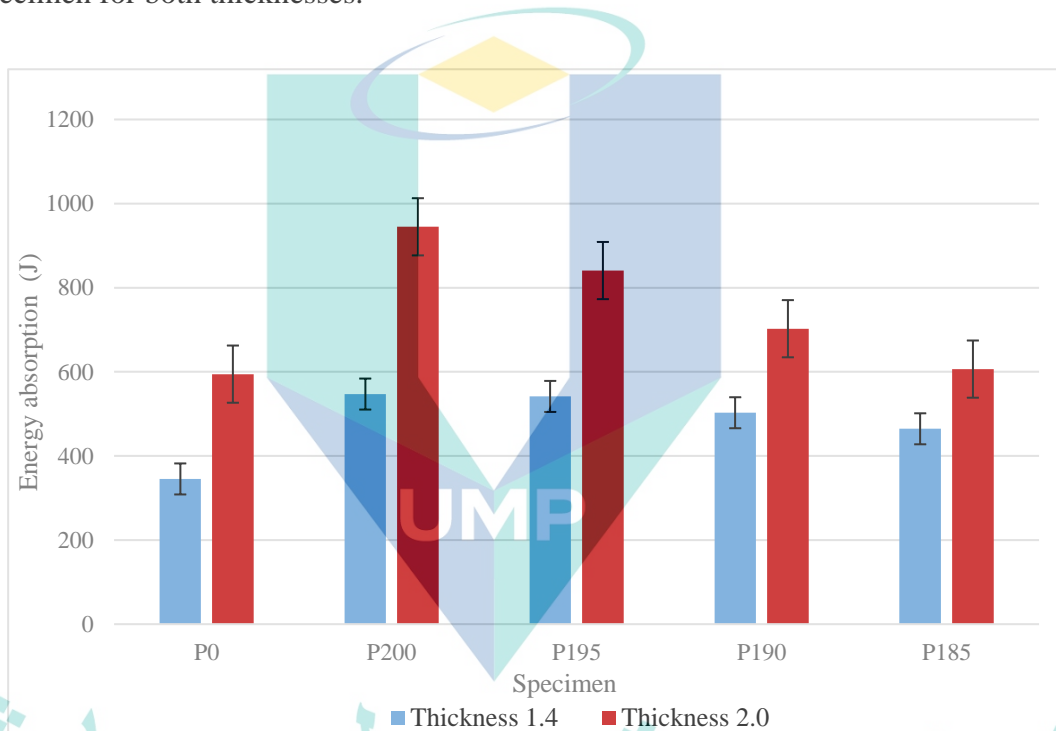


Figure 4.16 Energy absorption gained by 1.4 mm and 2.0 mm thickness specimen.

From chart in Figure 4.16, it can be observed that the EA of A2.0 specimen is higher than that of the A1.4. For specimen P0(empty) and P200, the EA value of A2.0 is increased by 42% compared to A1.4. Next for specimen P195, the EA is increased by 36%. While for specimen P190 the EA value is also increased by 28% and finally for specimen P185 the EA value increased by 23%. It can be concluded that all the thicker specimen gained higher EA compared to the thinner one. This is because, the force needed to deform the thicker structure is higher than the thinner. Higher peak force may cause the area under the force-displacement curve to be higher. These results were supported by Subramaniyam (Subramaniyan et al., 2013) in his study.

ii. Initial peak force (IPF)

To compare the initial peak force of A2.0 with A1.4, bar chart in Figure 4.17 was developed.

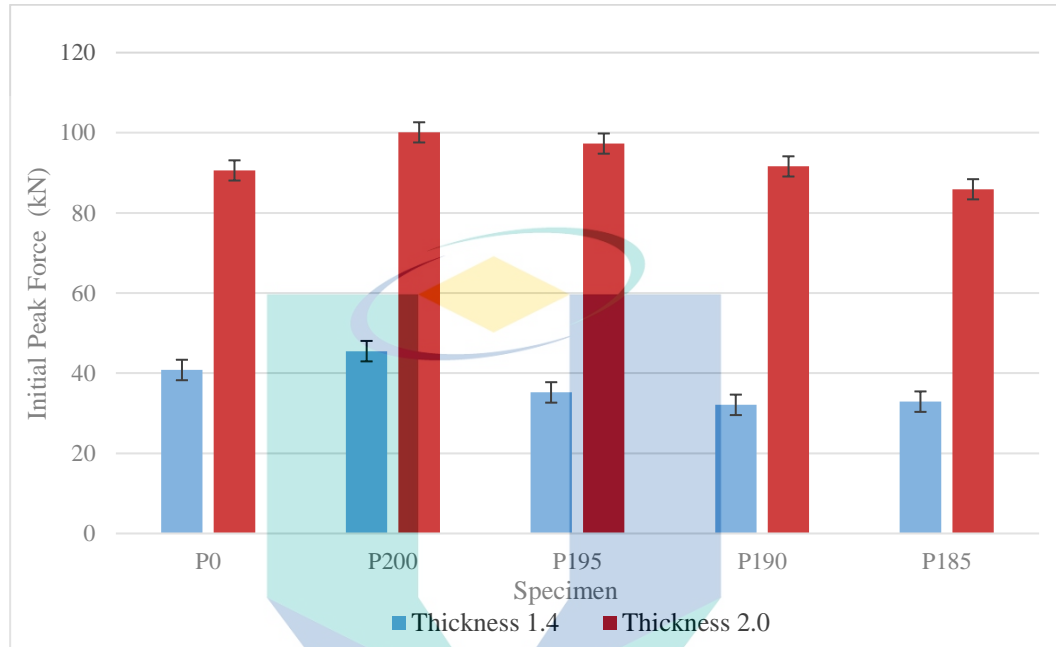


Figure 4.17 Initial peak force achieved by 1.4 mm and 2.0 mm thickness specimen.

According to Figure 4.17, it can be seen that the IPF of A2.0 specimen is higher than that of the A1.4. For specimen P0 (empty) and P200, the EA value of A2.0 is increased by 55% compared to A1.4. Then the IPF is increased by 63% for specimen P195. While for specimen P190 the IPF value is increased by 65% and for specimen P185 the IPF value increased by 62%. The observation showed that the A2.0 specimen obtained higher IPF compared to A1.4. Higher IPF value is undesirable and should be avoid in energy absorbers design. These results were supported by Subramaniyam et al (Subramaniyan et al., 2013) in his study.

iii. Specific energy absorption (SEA)

Specific energy absorption obtained by 1.4 mm and 2.0 mm thickness specimen Figure 4.18 shows that the SEA of A2.0 specimen is better than that of the A1.4. SEA of specimen A2.0P0(empty) is increased by 21% compared to specimen A1.4P0. Next for specimen A2.0P200, the SEA value is 28% higher compared to A1.4P200. This follows

with the SEA value of A2.0P195 which is increased only by 20% compared to specimen A1.4P195. While for specimen P190 the SEA value is increased by 12% and for specimen P185 the SEA value increased by only 6%. The observation showed that the A2.0 specimen obtained higher IPF compared to A1.4. Energy absorbers design requires high value of SEA. These results were aligned with Niknejad (Niknejad et al, 2013) who concluded that the SEA is increased with the increases in structure wall thickness.

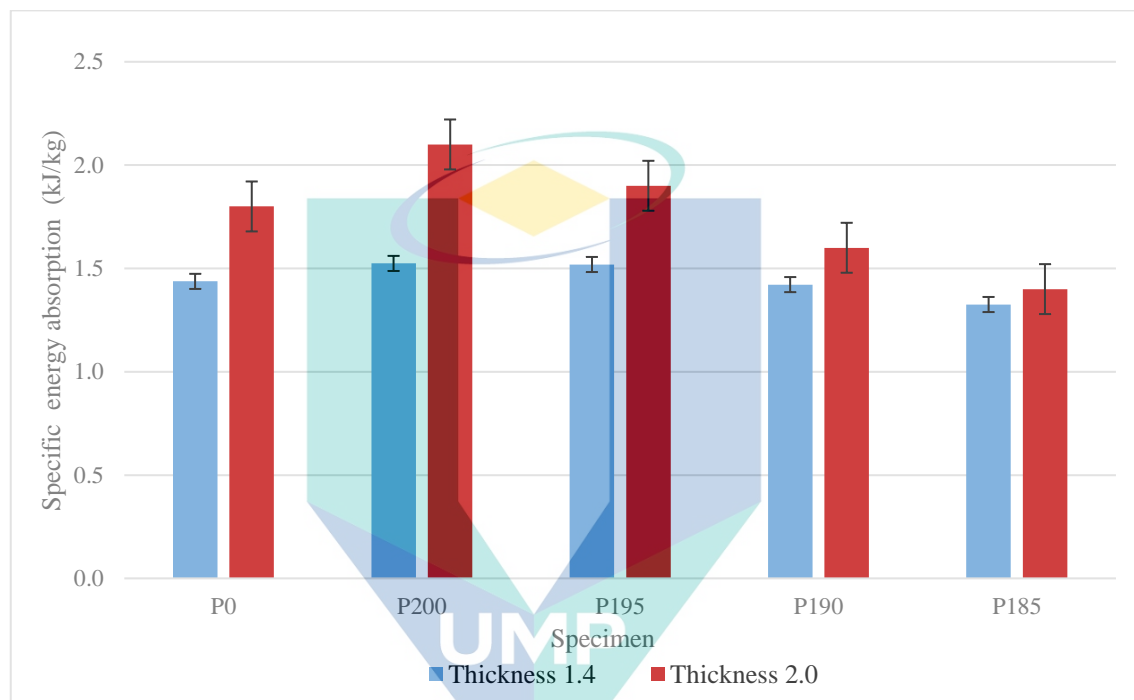


Figure 4.18 Specific energy absorption gained by 1.4 mm and 2.0 mm thickness specimen.

#### 4.4 Low velocity impact test

The impact tests were carried out using Instron Dynatup drop-weight test machine with a mass of 38 kg impacting on the specimen from the same nominal height of 0.66 m. Impact tests were carried out to determine the dynamic compression responses of the specimens. A model for a low velocity impact test was used to determine maximum impact test at certain height. The impactor mass,  $m$  was released from a height,  $h$  to strike the specimen.

#### 4.4.1 Effect of length of foam to crushing response of specimen with 1.4 mm thickness under impact test

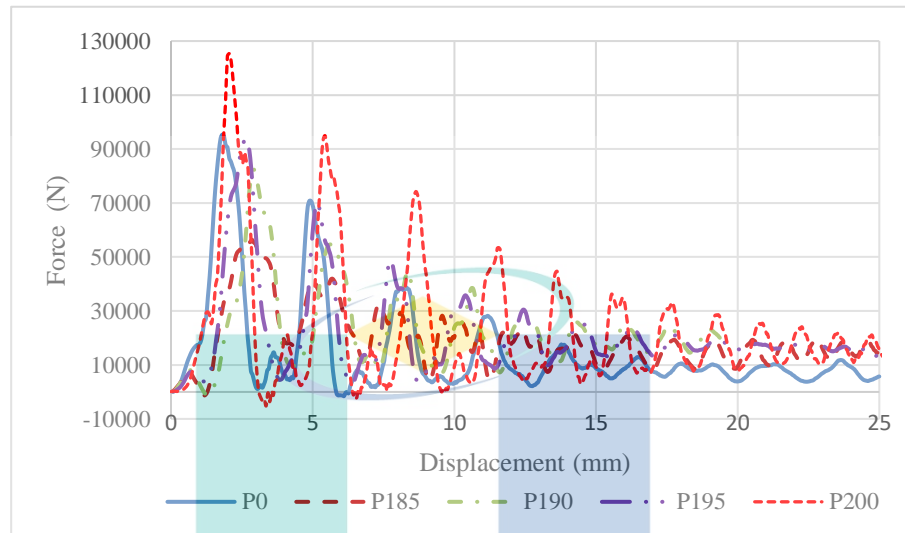


Figure 4.19 Force-displacement traces for A1.4P0, A1.4P185, A1.4P190, A1.4P195 and A1.4P200 under dynamic loading condition.

##### i. Energy Absorption

From the impact test conducted on specimen A1.4P0, A1.4P185, A1.4P190, A1.4P195 and A1.4P200, the force-displacement curves have been produced for a displacement from 0 mm to 25 mm as in Figure 4.19. The graph, shown that A1.4P200 gained the highest curve with the highest energy absorption capacity. The energy absorption for the column which was filled by foam for the entire length (A1.4P200) is 582 J. Then the foam's length is reduced, so that EA for specimen A1.4P195 is decreasing to 529 J. For specimen A1.4P190, the EA decreased to 528 J and decreased to 477 J for specimen A1.4P185. The EA for A1.4P190 did not decrease much than A1.4P195 because the tearing deformation in the latter is severe compared to the A1.4P190. It can be concluded that by reducing the length of foam, the energy absorption was reduced proportionally. This is due to the characteristic of foam that increasing the energy absorption capacity. But the tearing deformation has affected the value of EA in the higher length of foam (for the reduced length only).

Table 4.8 Crashworthiness parameter derived for impact test results for 1.4 mm thickness specimen.

Specimen	Mass (g)	IPF (kN)	EA (J)	SEA (kJ/kg)
A1.4P0	240.2	98.3	386.0	1.6
A1.4P185	350.5	89.3	476.9	1.4
A1.4P190	353.6	93.2	528.4	1.5
A1.4P195	356.5	96.9	529.1	1.5
A1.4P200	358.9	125.4	582.2	1.6

ii. Initial Peak Force (IPF)

Table 4.8 showed that the initial peak of thickness 1.4 mm specimen subjected to impact test. The IPF A1.4P200 was the highest IPF which is 125.4 kN. But when the length of foam was reduced, the IPF was reduced. For specimen A1.4P195, the IPF reduced to 96.9 kN and keep reducing to 93.2 kN for A1.4P190 specimen. When the length of foam is reduced to A1.4P185, the IPF keep reducing to 89.3 kN. It shown that the initial peak force of a foam-filled column is decreasing by reducing the length of foam in the aluminium column but the energy absorption and SEA decreases simultaneously.

Performance of the specimen in term of SEA and IPF of 1.4 mm thickness specimen under impact test were presented in bar chart in Figure 4.20. This chart was developed to observe the achievement of this research objectives.

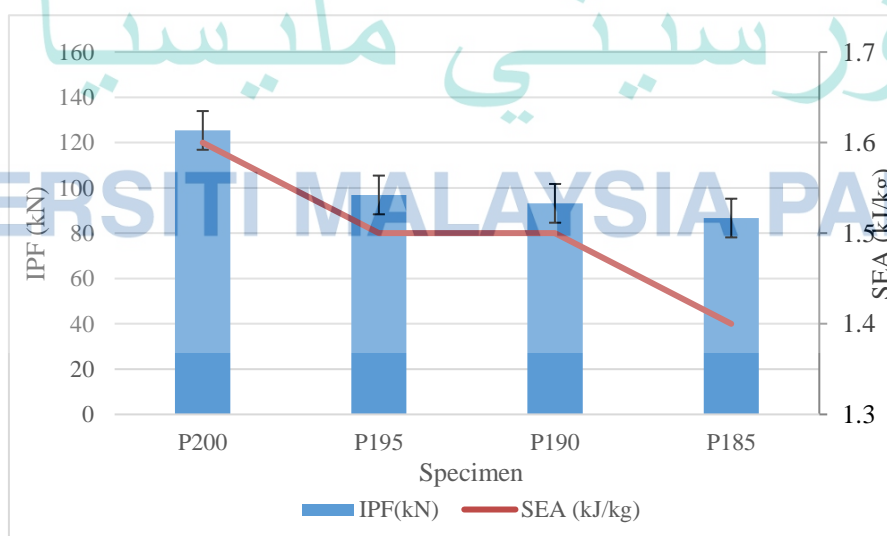


Figure 4.20 Value of SEA and IPF compared to A1.4P200 for 1.4 mm thickness specimen under impact test.



Figure 4.20 shows that specimen A1.4P195 gained reduction of 23% in IPF and SEA was decreased by 6% compared to A1.4P200. Then A1.4P190 configuration has reduced the IPF by 31% while reducing only 6% of the SEA. Finally, specimen A1.4P185 succeeded in reducing 26% of IPF by decreasing 13% of SEA compared to A1.4P200. It can be concluded that under impact test, for 1.4 mm thickness specimen, the A1.4P190 configuration shown the best performance by reducing highest IPF and reducing smallest SEA simultaneously.

### iii. Specific Energy Absorption (SEA)

According to Table 4.8, the specific energy absorption (SEA) of specimen A1.4P200 the SEA is 1.6 kJ/kg. Next, the SEA of A1.4P195 and A1.4P190 is 1.5 kJ/kg. Then the SEA of A1.4P185 is 1.4 J/kg. Hence, for 1.4 mm thickness under impact test, the higher length of foam specimen gained higher SEA and the partially foam-filled specimen A1.4P195 and A1.4P190 deserves recommendation as the SEA reduction is only 6% compared to A1.4P200.

#### 4.4.2 Effect of length of foam to crushing response of specimen with 2.0 mm thickness

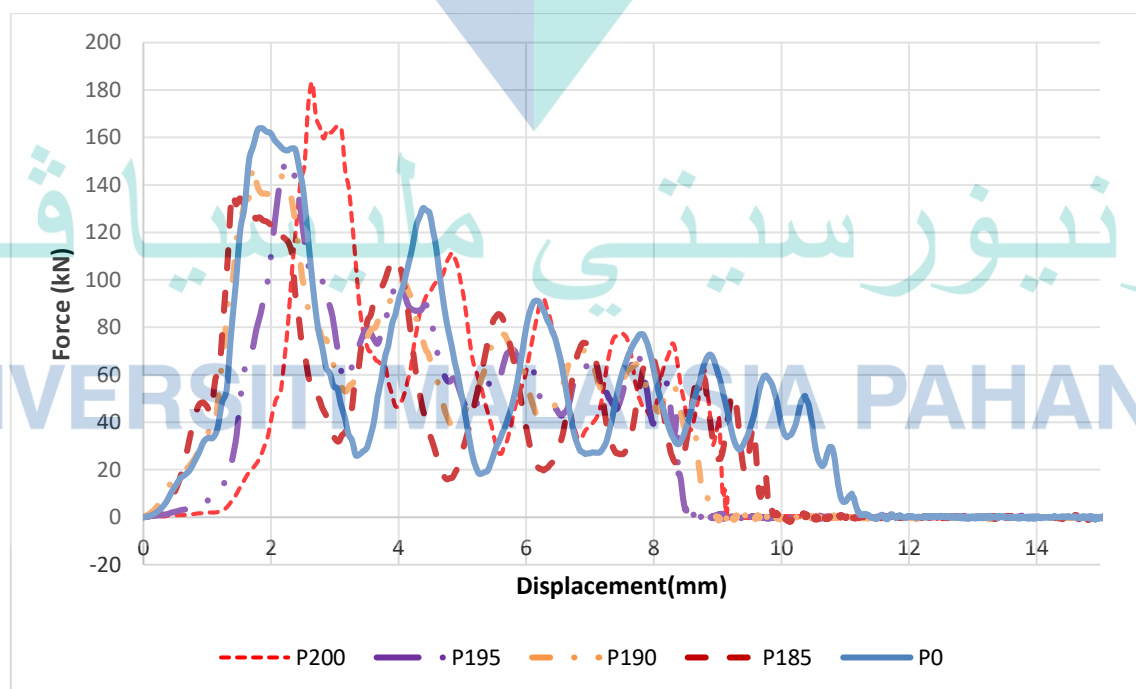


Figure 4.21 Force-displacement traces for A2.0P185, A2.0P190, A2.0P195 and A2.0P200 under impact test for thickness 2.0 mm specimen.

i. Energy Absorption

For 2.0 mm thickness, the force-displacement curves have been produced for impact test as in Figure 4.21. It was shown in Figure 4.23 and Table 4.9 that when the column was filled by foam for the entire length, A2.0P200 the value of EA is 594 J. Then the foam's length is reduced, so that EA for specimen A2.0P195 is decreasing to 575 J. Finally, specimen A2.0P190 and A2.0P185 gained the same value of EA which is 564 J. This shows that the energy absorption is reducing with the reduction of foam's length. This results were aligned with the research conducted by Hussien (Hussein et al., 2017)

Table 4.9 Crashworthiness parameter derived for impact test results for 2.0 mm thickness specimen under impact test.

Specimen	Mass (g)	IPF (kN)	EA (J)	SEA (kJ/kg)
A2.0P0	324.8	167.2	517.1	1.6
A2.0P185	433.1	137.0	564.1	1.3
A2.0P190	435.9	148.0	564.4	1.3
A2.0P195	437.7	154.0	575.2	1.3
A2.0P200	440.9	183.0	594.2	1.3

ii. Initial Peak Force (IPF)

Table 4.9 showed that the initial peak force for thickness 2.0 mm specimen subjected to impact test is higher compared to quasi static condition. The IPF for specimen reference which was A2.0P200 is 183 kN. When the length of foam was reduced, the IPF was also reduced. For specimen A2.0P195, the IPF reduced to 154 kN and keep reducing to 148 kN for A2.0P190 specimen. Then the value of IPF reduced to 137 kN for A2.0P185 specimen.

Performance of the specimen in term of IPF and SEA were presented in bar chart in Figure 4.22. The bar chart was developed to observe the achievement of this research objectives.

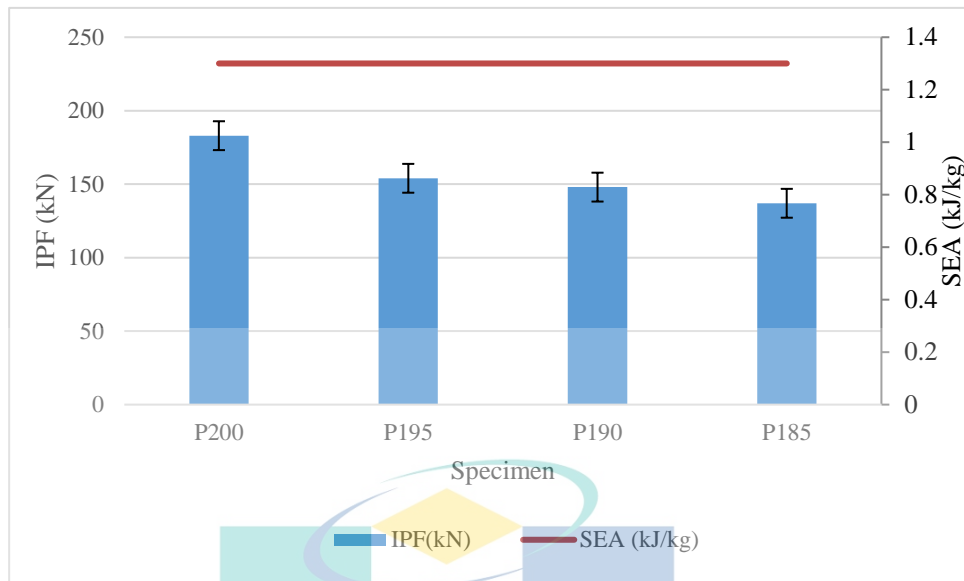


Figure 4.22 Reduction of SEA and IPF compared to P200 for 2mm thickness specimen under impact test.

Figure 4.22 shows the comparison values of SEA and IPF for each specimen with A2.0P200. SEA was decrease by 3% and IPF was decrease by 16% respectively for specimen A2.0P195. Next for specimen A2.0P190, the SEA was decreased by 5% by and IPF was decreased by 19%. The minimum reduction was shown by specimen A2.0P185 with 5% in SEA and 25% in IPF. It can be concluded that under dynamic loading condition, for 2 mm thickness specimen, the IPF was reducing with the reduction in length of foam but the SEA was constant. This shown that application of partially filled structure is efficient as energy absorber for 2 mm thickness specimen under impact test.

iii. Specific Energy Absorption (SEA)

According to Table 4.9, it can be observed that the specific energy absorption (SEA) of specimen A2.0P200, A2.0P195, A2.0P190 and A2.0P185 is 1.3 kJ/kg. Hence, specimen A2.0P0 deserves recommendation due to its higher SEA values which is 1.6 kJ/kg. This shown that for thickness 2.0 mm the partially foam-filled specimen were succeeded in reducing the IPF without reducing the SEA values.

**4.4.3 Effect of wall thickness to crushing response of specimen**

Other than quasi-static, effect of thickness also studied under impact test. Both thicknesses of for each structure which is 1.4 mm and 2.0 mm was tested to study the effect of specimen thickness to the energy absorption indices.

i. Energy Absorption (EA)

Bar chart that contains the EA data of each specimen were constructed to study effect of thickness to EA capacity of specimen A2.0 compared to A1.4. Figure 4.23 shows EA obtain by each specimen for both thicknesses.

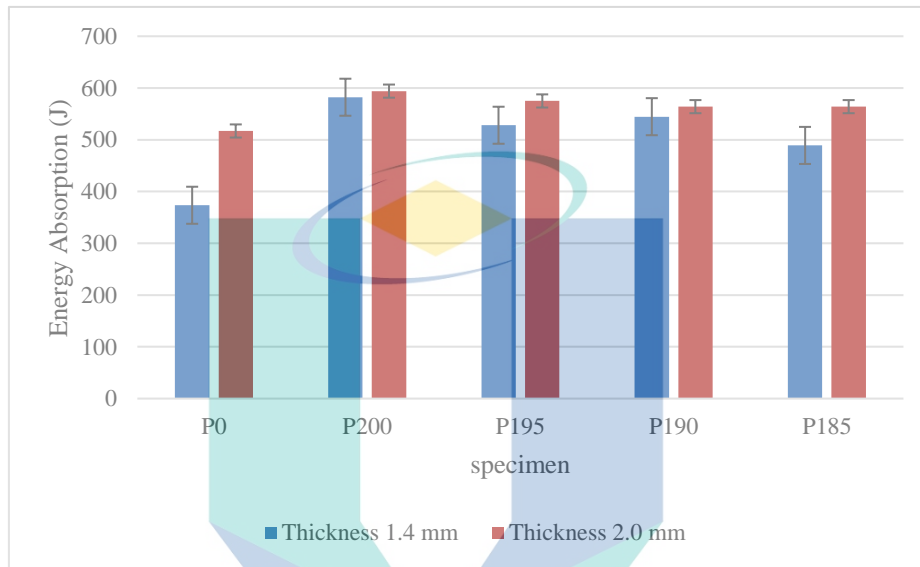


Figure 4.23 Energy absorption gained by 1.4 mm and 2.0 mm thickness specimen.

From chart in Figure 4.23 above, it can be observed that the EA of A2.0 specimen is higher compared to A1.4 but the different is quite small compared to quasi-static data. For specimen P0, the EA value of A2.0 is increased by 28% compared to A1.4. Then for specimen P200, the value of EA increased by just 2%. Next for specimen P195, the EA is increased by 8%. While for specimen P190 the EA value is also increased by 3% and finally for specimen P185 the EA value increased by 13%. It can be concluded that although 2.0 mm have higher EA compared to 1.4 mm specimen, but the different is quite small. This is because, the force needed to deform the thicker structure is higher than the thinner. Higher peak force will cause the area under the force-displacement curve to be higher. These results were supported by Subramaniyam (Subramaniyan et al., 2013) in his study.

ii. Initial peak force (IPF)

To compare the initial peak force of A2.0 with A1.4, bar chart in Figure 4.24 was developed.

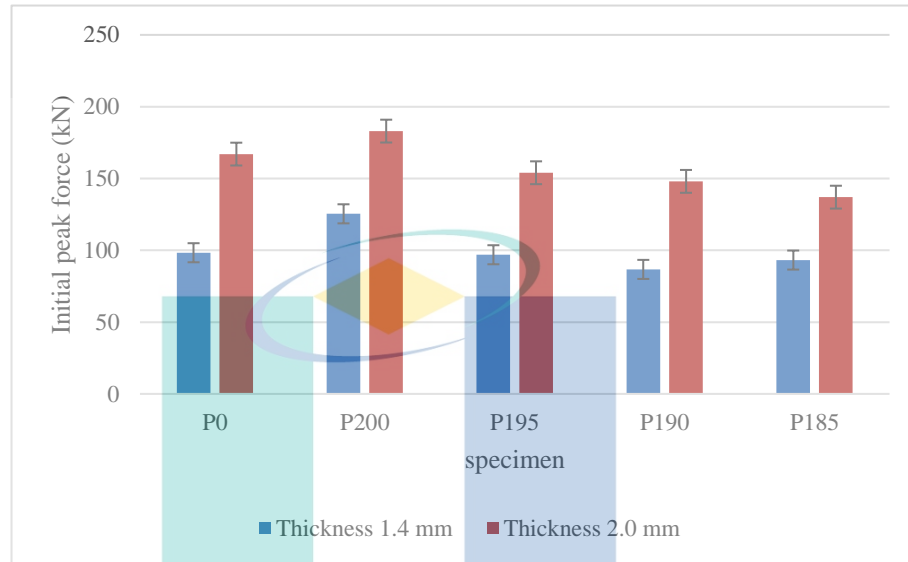


Figure 4.24 Initial peak force achieved by 1.4 mm and 2.0 mm thickness specimen.

By referring to Figure 4.24, it can be seen that the IPF of A2.0 specimen is higher than that of the A1.4. For specimen P0, the EA value of A2.0 is increased by 41% compared to A1.4. Then for specimen P200, the value of EA increased by 31%. Then the IPF is increased by 37% for specimen P195. While for specimen P190 the IPF value is increased by 41% and for specimen P185 the IPF value increased by 32%. The observation showed that the A2.0 specimen obtained higher IPF compared to A1.4. Higher IPF value is undesirable and should be avoided in energy absorbers design. These results were supported by Subramaniam (Subramaniam et al., 2013) in his study.

iii. Specific energy absorption (SEA)

To compare the SEA of A2.0 with A1.4, bar chart in Figure 4.25 was developed.

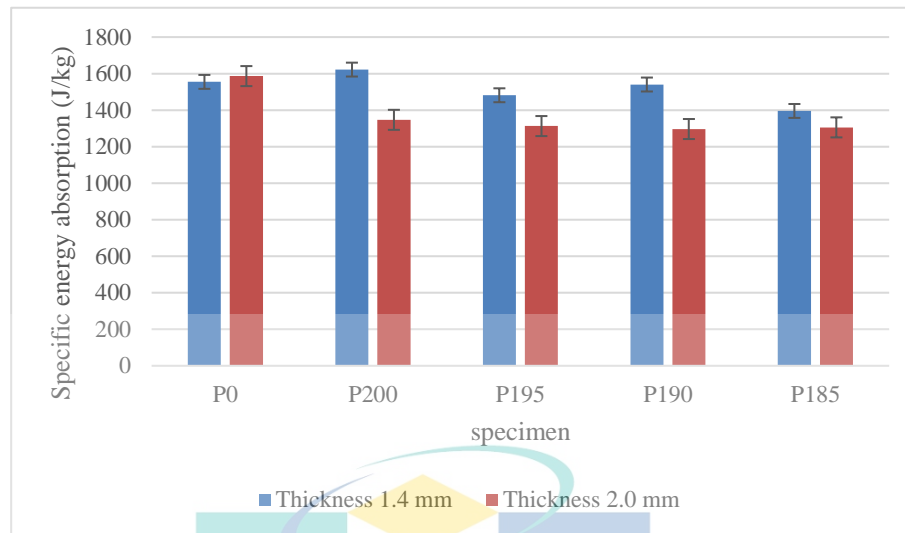


Figure 4.25 Specific energy absorption obtained by 1.4 mm and 2.0 mm thickness specimen.

Figure 4.25 shows that the SEA of almost all A2.0 specimen is lower than that of the A1.4 except for P0. SEA value of specimen A2.0P0(empty) is increased by only 2% compared to specimen A1.4P0. Next for specimen A2.0P200, the SEA value is 20% lower compared to A1.4P200. This follows with the SEA value of A2.0P195 which is decreased by 12% compared to specimen A1.4P195. While for specimen P190 the SEA value is decreased by 18% and for specimen P185 the SEA value decreased by only 7%. The observation showed that the A2.0 specimen obtained lower SEA compared to A1.4. This is because the increment in EA is small compared to mass of the 2.0 column. This suggest that the 1.4mm specimen is more effective in term of SEA compared to 2.0 mm specimen subjected to impact load in energy absorbers application (Bigdeli & Nouri, 2019).

## 4.5 Optimization

### 4.5.1 Optimization methodology

As an energy absorber, the foam-filled structure is required to absorb maximum impact energy. Thus, the energy absorption should be an objective function and be maximized from the optimization perspective. While, the initial peak force of the structure is another significant parameter that relates to the safety of the passenger, which should be minimized.



#### 4.5.2 Historical data Design

The RS model was designed based on historical data method on two levels for two central points in Design Expert software. This research was focused on two parameters which is thickness of the thin-walled tube that were 1.4mm and 2.0 mm and length of foam that ranged from 185mm to 200mm. The data inserted for this study is presented in Table 4.10 for thickness 1.4mm and Table 4.11 for 2.0 mm.

Table 4.10 Experimental data inserted in design expert software for 1.4 mm specimen.

EA indices	Quasi-static			Impact		
	P195	P190	P185	P195	P190	P185
EA (J)	541.5	502.7	464.5	529.1	528.4	476.9
IPF (kN)	35.2	32.1	32.9	96.9	93.2	89.3
SEA (kJ/kg)	1.5	1.4	1.3	1.5	1.5	1.4

Table 4.11 Experimental data inserted in design expert software for 2.0 mm specimen.

EA indices	Quasi-static			Impact		
	P195	P190	P185	P195	P190	P185
EA (J)	840.8	702.5	606.5	575.2	564.4	564.1
IPF (kN)	97.3	91.6	85.9	154.0	148.0	137.0
SEA (kJ/kg)	1.9	1.6	1.4	1.3	1.3	1.3

#### 4.5.3 Response surface model

Response surface model (RSM) was conducted to the experimental data using statistical software named Design-Expert. Response surface model (RSM) was conducted to the experimental data using statistical software named Design-Expert. The RSM prepared an effective method of formulating estimated functions for unknown responses using linear, quadratic, or higher-order polynomials. The commonly used response surface models are those using linear or quadratic polynomials.

#### 4.5.4 Analysis of variance (ANOVA)

In this study, ANOVA was conducted to identify the effect of length of foam and thickness of the thin-walled structure in numerical intensity to energy absorption capability and initial peak force. Each output response was analysed individually for the for both input factors. Table for ANOVA obtained with the aid of Design-Expert consists of value of sum of square which is a quantity that appears as part of a standard way of presenting results of such analysis, mean square which is a measure of the quality of an estimation, F-value which is calculated by dividing two mean squares and determines the ratio of explained variance to unexplained variance, P-value which is the level of marginal significance within a statistical hypothesis test representing the probability of the occurrence of a given event (Mahbod & Asgari, 2018). For the model to be significant, the corresponding P-value shall not exceed 0.05. The estimation of value EA and IPF acquired from the response functions and experimental results. The values of sum of square, mean square,  $R^2$ ,  $R^2$ -adj, p-value and F-value can be observed in Table 4.12 for quasi-static test and Table 4.13 for impact test. Suitability of the RS model can be measure by the larger values of  $R^2$  and  $R^2$ -adj (almost 1).

UMP

اونيورسيتي ملايسيا قهغ

UNIVERSITI MALAYSIA PAHANG

Table 4.12 Analysis of variance (ANOVA) table for quasi static test.

Output response	Source	Sum of squares	Mean square	F-value	P-value	R <sup>2</sup>	adj-R <sup>2</sup>	pred-R <sup>2</sup>	
QS-EA	Model	98822.67	32940.89	223.96	0.0044	0.9970	0.9926	0.9599	significant
	Length	24180.25	24180.25	164.4	0.006				
	Thickness	4430.39	4430.39	30.12	0.0316				
	Residual	294.17	147.08						
	Std. Dev	12.13	C.V. %		1.99				
	Mean	610.17	PRESS		3971.25				
QS-IPF	Model	5127.78	2563.89	331	0.0003	0.9955	0.9925	0.9752	significant
	Length	46.92	46.92	6.06	0.0908				
	Thickness	5080.86	5080.86	655.95	0.0001				
	Residual	5151.02	7.75						
	Std. Dev	2.78	C.V. %		4.45				
	Mean	62.5	PRESS		127.92				
QS-SEA	Model	0.23	0.076	90.67	0.0109	0.9927	0.9818	0.9015	significant
	Length	0.12	0.12	147	0.0067				
	Thickness	0.019	0.019	22.49	0.0417				
	Residual	1.67E-03	8.33E-04						
	Std. Dev	0.029	C.V. %		1.9				
	Mean	1.52	PRESS		0.023				

Table 4.13 Analysis of variance (ANOVA) table for impact test.

Output response	Source	Sum of squares	Mean square	F-value	P-value	R <sup>2</sup>	adj-R <sup>2</sup>	pred-R <sup>2</sup>	
IMP-EA	Model	5778.80	2889.40	9.95	0.0474	0.9995	0.9992	0.9985	significant
	Length	1001.72	1001.72	3.45	0.1602				
	Thickness	4777.08	4777.08	16.46	0.0270				
	Residual	870.78	290.26						
	Std. Dev	17.04	C.V. %		3.16				
	Mean	539.68	PRESS		3966.27				
	Model	4396.65	2198.32	251.11	0.0005	0.9941	0.9901	0.9680	significant
IMP-IPF	Length	151.29	151.29	17.28	0.0253				
	Thickness	4245.36	4245.36	484.94	0.0002				
	Residual	26.26	8.75						
	Std. Dev	2.96	C.V. %		2.47				
	Mean	119.73	PRESS		141.51				
	Model	0.044	0.022	15.9	0.0253	0.9138	0.8563	0.5869	significant
	Length	2.50E-03	2.50E-03	1.8	0.2722				
IMP-SEA	Thickness	0.042	0.042	30	0.012				
	Residual	4.17E-03	1.39E-03						
	Std. Dev	0.037	C.V. %		2.69				
	Mean	1.38	PRESS		0.02				

i. ANOVA of Energy Absorption responses for quasi-static and impact test.

For quasi-static test, energy absorption obtained a two-factor interaction (2FI) model solution. The p-value is smaller than 0.05 indicates that the model term is significant. Value of  $R^2$  indicates the effect of any input factor observed in the model, that influence the changes in the output responses. While value of  $R^2$ -adj specify the real effect of the model input factor on the output responses. The high value of  $R^2$ -adj and its closeness to that of  $R^2$  suggest the desirability of the output model projection. Value of  $R^2$  is 0.9970 is in reasonable agreement with the  $R^2$ -adj which is 0.9926. The higher value of  $R^2$  relates to the higher accuracy of the RS model. Therefore, for EA, the best approximation is found to be 2FI. The equation in terms of actual factor obtained for the energy absorption response in quasi-static test is stated in Eq. 4.1

$$EA^{qs} = 5502.11 - 28.93L - 4615.56t + 26.17Lt \quad 4.1$$

While in impact test, value of  $R^2$  is 0.9995 is in reasonable agreement with the  $R^2$ -adj which is 0.9992. Similar to Tran (Tran & Baroutaji, 2018) study, linear function is found to be the best approximation for EA. The equation in terms of actual factor obtained for the energy absorption response in quasi-static test is stated in Eq. 4.2

$$EA^{imp} = -221.56 + 3.17L + 94.06t \quad 4.2$$

ii. ANOVA of Initial Peak Force responses for quasi-static and impact test.

The results for the IPF response of both quasi-static and impact test led to a linear model with an interaction between the two parameters L and t. Value of  $R^2$  for quasi-static test is 0.994 is in reasonable agreement with the  $R^2$ -adj which is 0.9925. It indicates the output model capability for predicting the response behavior. Model is defined as significance condition when value of  $p < 0.05$ . While for IPF in quasi-static test, the linear function should be used for the optimum design. The equation in terms of actual factor was obtained as Eq. 4.3

$$IPF^{qs} = -232.55 + 0.69L + 97.00t \quad 4.3$$

While in impact test, value of  $R^2$  is 0.9941 is in reasonable agreement with the  $R^2$ -adj which is 0.9901. Linear function is found to be the best approximation compared to other response functions. The equation in terms of actual factor obtained for the energy absorption response in quasi-static test is stated in Eq. 4.4

$$IPF^{imp} = -264.70 + 1.23L + 88.67t \quad 4.4$$

- iii. ANOVA of specific energy absorption responses for quasi-static and impact test.

Hence for the SEA response of both quasi-static and impact test achieved a two-factor interaction (2FI) model solution. Value of  $R^2$  for quasi-static test is 0.9927 is in reasonable agreement with the  $R^2$ -adj which is 0.9818. It indicates the output model capability for predicting the response behavior. Model is defined as significance condition when value of  $p < 0.05$ . For SEA in quasi-static test, 2FI model is used for the optimum design. The equation in terms of actual factor was obtained as Eq. 4.5

$$SEA^{qs} = 10.36 - 0.05L - 9.11t + 0.05Lt \quad 4.5$$

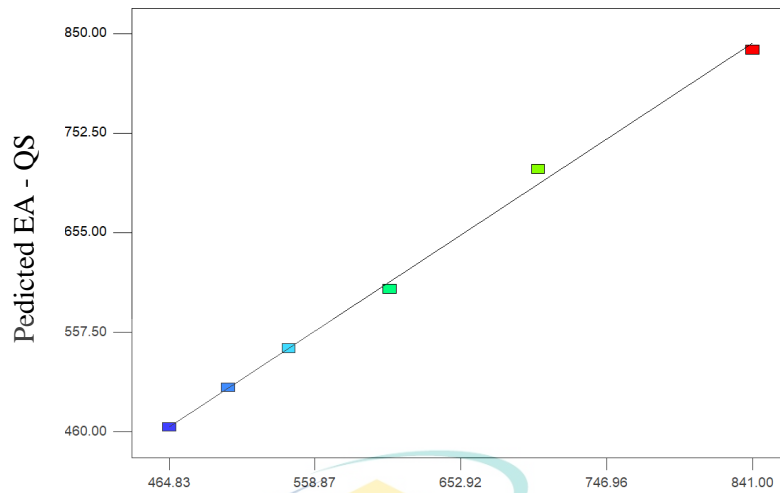
While in impact test, value of  $R^2$  is 0.9138 is in reasonable agreement with the  $R^2$ -adj which is 0.8563. Linear function is found to be the best approximation compared to other response functions. The equation in terms of actual factor obtained for the specific energy absorption response in quasi-static test is stated in Eq. 4.6

$$SEA^{imp} = 0.91 + 5.00L - 0.28t \quad 4.6$$

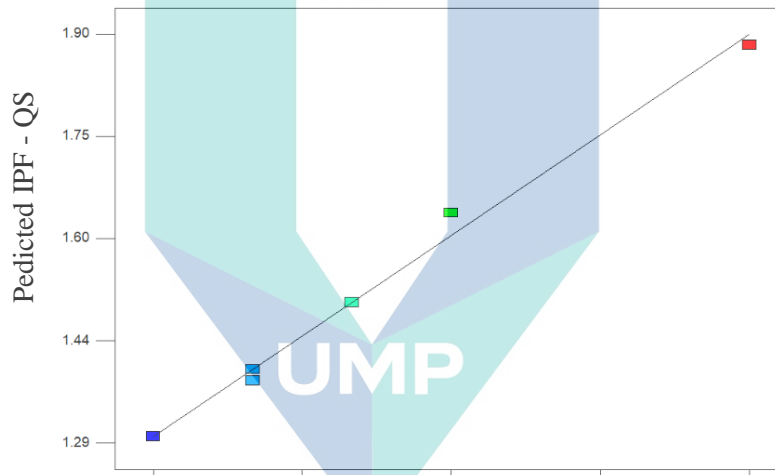
#### 4.5.5 Validation of the Response Surface models

Figure 4.26 and 4.27 shown a scatter diagrams for the distribution of the actual values obtained from the experiment versus the predicted values from output model for each output response. From the diagram, the distribution of the values in the vicinity of the diagonal line mirrors the model capability for predicting the response trends. The graph represents approximation value of the data. QS shown the data gained in the quasi-static test and IMP is for the data gained in impact test.

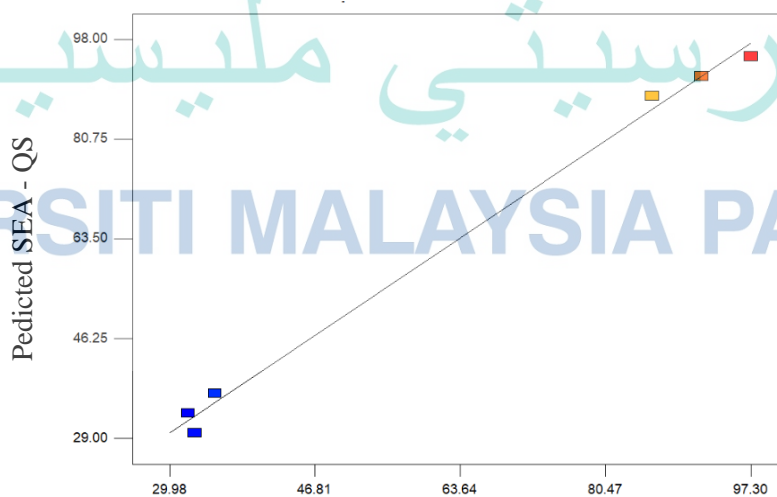




(a) Experimental EA – QS.

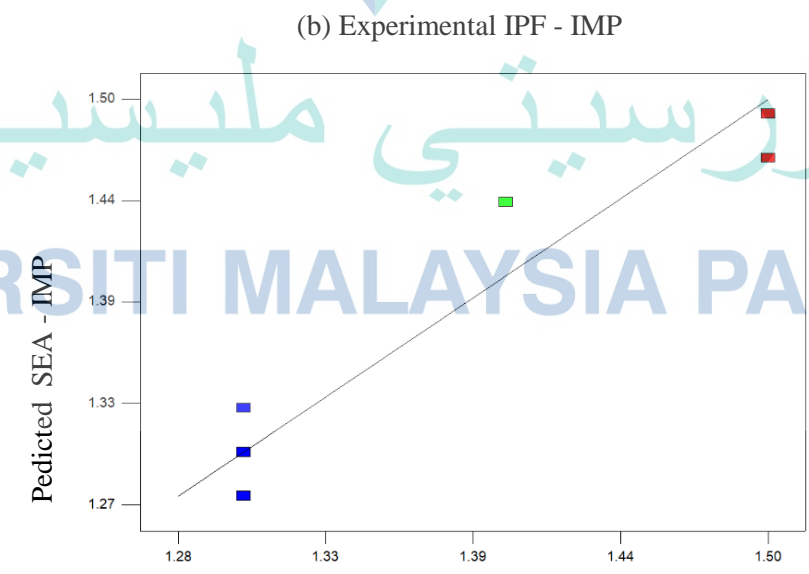
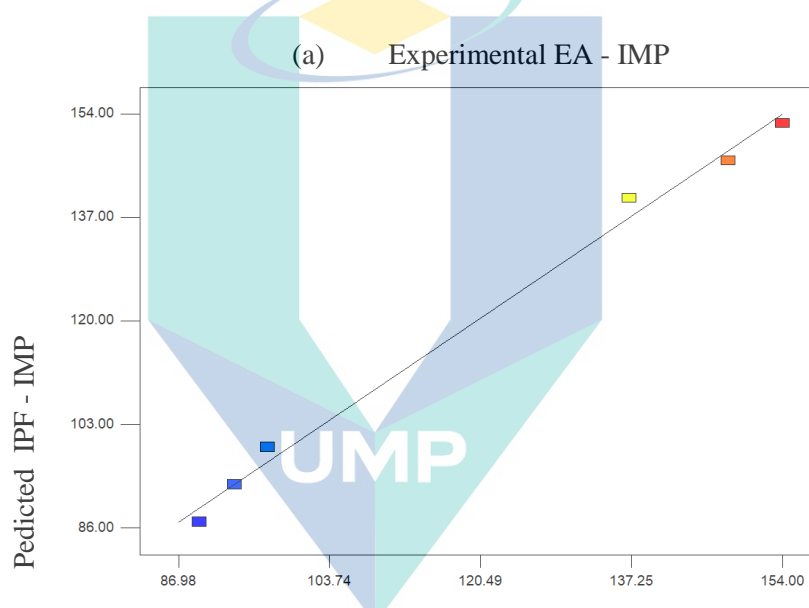
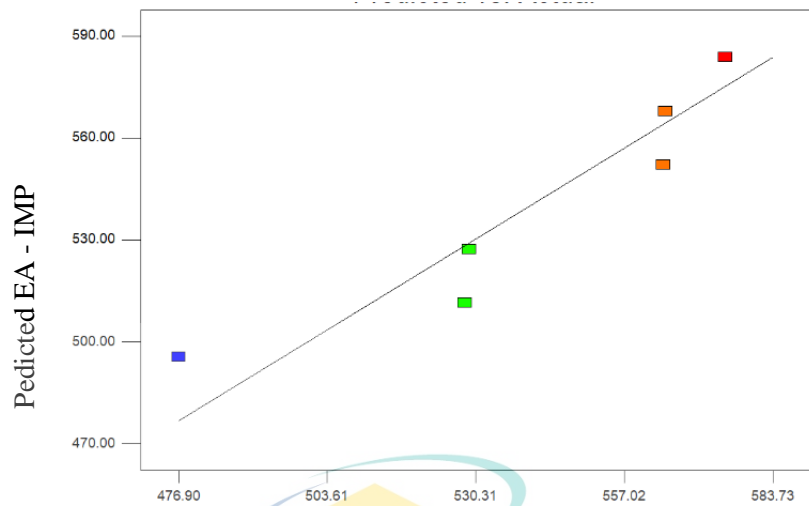


(b) Experimental IPF – QS.



(c) Experimental SEA – QS.

Figure 4.26 Predicted versus experimental graph (a) Energy Absorption response (quasi-static), (b) Initial Peak Force response (quasi-static), (c) Specific Energy Absorption response (quasi-static)



(c) Experimental SEA - IMP

Figure 4.27 Predicted versus experimental graph (a) Energy Absorption response (impact), (b) Initial Peak Force response (impact) (c) Specific Energy Absorption response (impact).

#### 4.5.6 Optimization results

- i. Crashworthiness optimization for quasi-static test.

The experimental data can be observed clearer in Figure 4.28 that shows the variation in EA, IPF and SEA respectively with thickness and length. It shows that both EA and IPF increase with the increment in thickness. Moreover, the EA and IPF displays the decrease trends with decreasing of foam length. In this case, the tube is optimized with the length and thickness as the input factor and EA and IPF as the output response. EA and IPF are modeled by the linear polynomials. Response surface approximation approach has been adopt to obtain the better responses (Hou, Li, Long, Yang, & Li, 2007). The optimum solutions for quasi-static test are shown in Table 4.14, there were 2 design solutions were suggested.

Table 4.14 Design solution given by Design Expert software for quasi-static test.

Solutions	Length, L	Thickness, t	Initial Peak Force	Specific Energy Absorption	Desirability
1	195.00	1.74	69.87	1.72	0.74
2	195.00	1.73	69.12	1.71	0.74

Both configurations shown a desirability value more than 0.7. The desirability function approach has outlined that each response will be transformed into a desirability and the total desirability function, this shown how the geometric mean of each desirability values individually be computed then optimised. The desirability can be stated as if a response is completely undesirable, then the corresponding desirability value will be 0. If the response is totally desirable, then the desirability value will be equal to 1. If the response falls between undesirable and totally desirable, the the desirability value will be between 0 and 1. When the response approaching the target, the desirability value becomes closer and closer to 1(John, 2013). The response for all the combination can be predicted as the sum of overall mean and the factors that leds to the significant factors and interactions. The expected values of the response variables were calculated for all the combination of configurations after the significant factor and interaction was determine. Then, the values were then converted into desirability values. For the final stage, the total desirability for the combinations was calculated.

For length of foam 195 mm and thickness of 1.74 mm, the specific energy absorption is 1.7 kJ/kg and IPF is 70 kN. While the SEA and IPF are 1.7 kJ/kg and 69 kN respectively when the combination foam length of 195 mm and thickness of 1.73 mm is applied. Therefore, the optimum results for EA, IPF and SEA for quasi-static test can be observed in in Figure 4.28

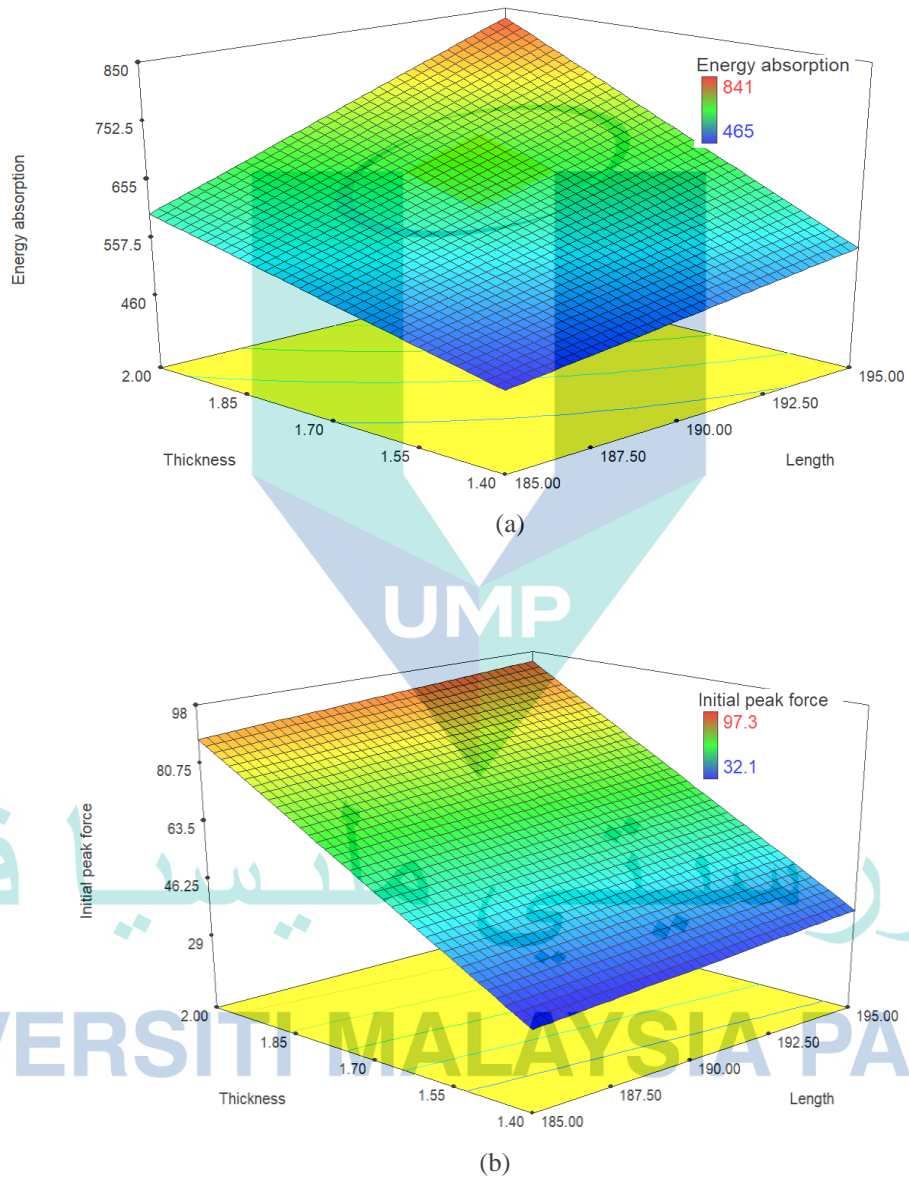


Figure 4.28 Effect of L and t to (a) EA (b) IPF (c) SEA for quasi-static test.

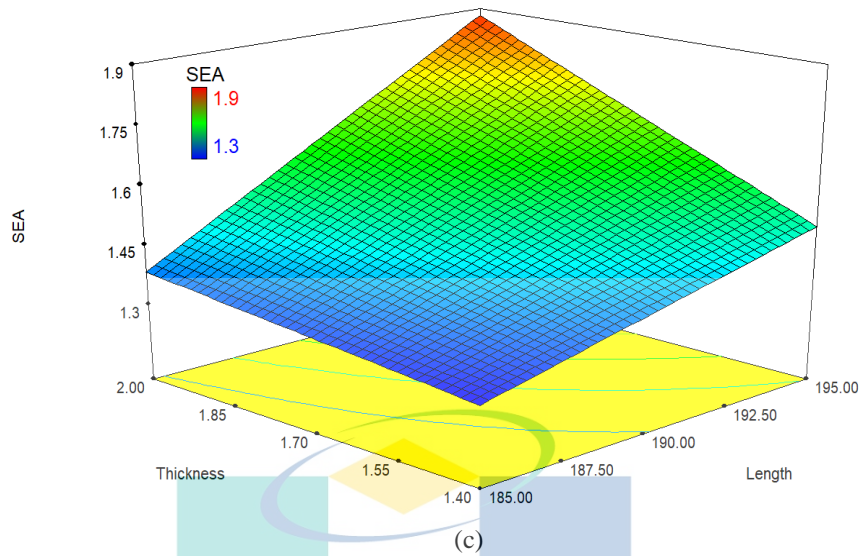


Figure 4.28 Continued

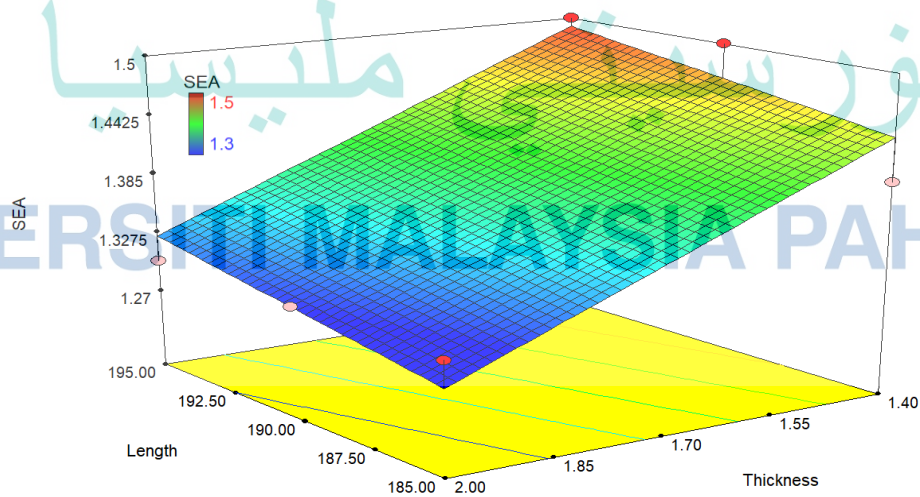
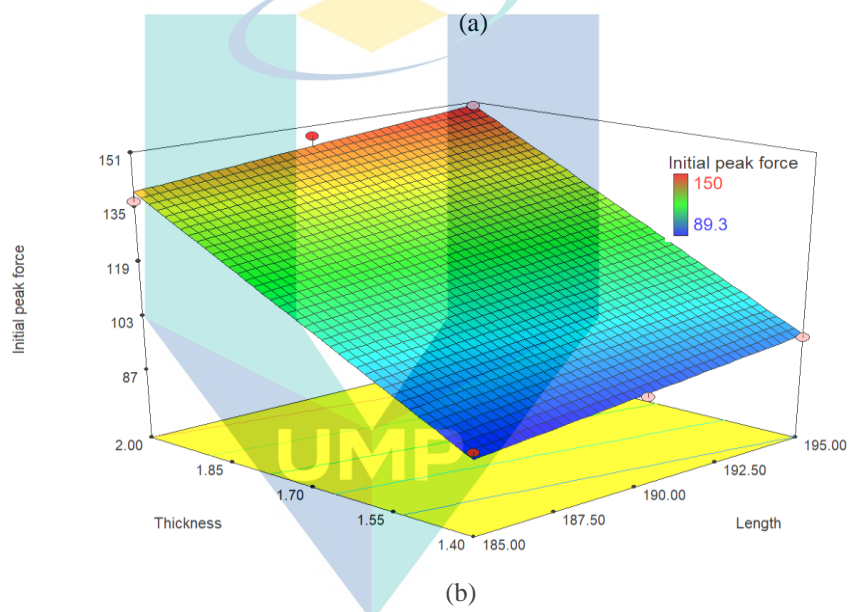
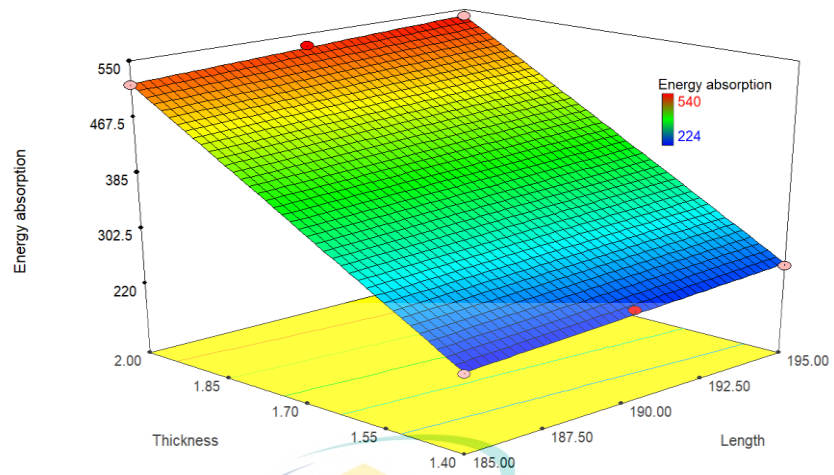
ii. Crashworthiness optimization for impact test

By using the same optimization process, the optimum design variables for impact test are summarized in Table 4.15. Two configurations of length and thickness are suggested for impact test for the optimum value of EA and IPF. The length suggested is 195 mm of foam length with 1.46 mm thickness of the column to achieve the optimal value of SEA and IPF which is 1.5 kJ/kg and 103 kN respectively. Other suggestion is to use length of foam of 195 mm with thickness of 1.47 mm to gained the SEA of 1.5 kJ/kg with IPF of 104 kN.

Table 4.15 Design solution given by Design Expert software for impact test

Solutions	Length, L	Thickness, t	Initial Peak Force	Specific Energy Absorption	Desirability
1	195.00	1.46	103.05	1.47	0.71
2	195.00	1.47	103.56	1.47	0.70

Variation of thickness and length of foam with EA and IPF were shown in Figure 4.29.



(c)

Figure 4.29 Effect of L and t to (a) EA (b) IPF (c) SEA for impact test



#### 4.5.7 Verification of optimization results

The results given by the optimization software was verified using simulation. Abaqus software version 6.14 has been used in the verification process to determine the IPF and SEA value for the thickness and length of foam suggested by Design Expert. Figure 4.30 shows the Finite Element Analysis of specimen A1.4P0 using Abaqus software.

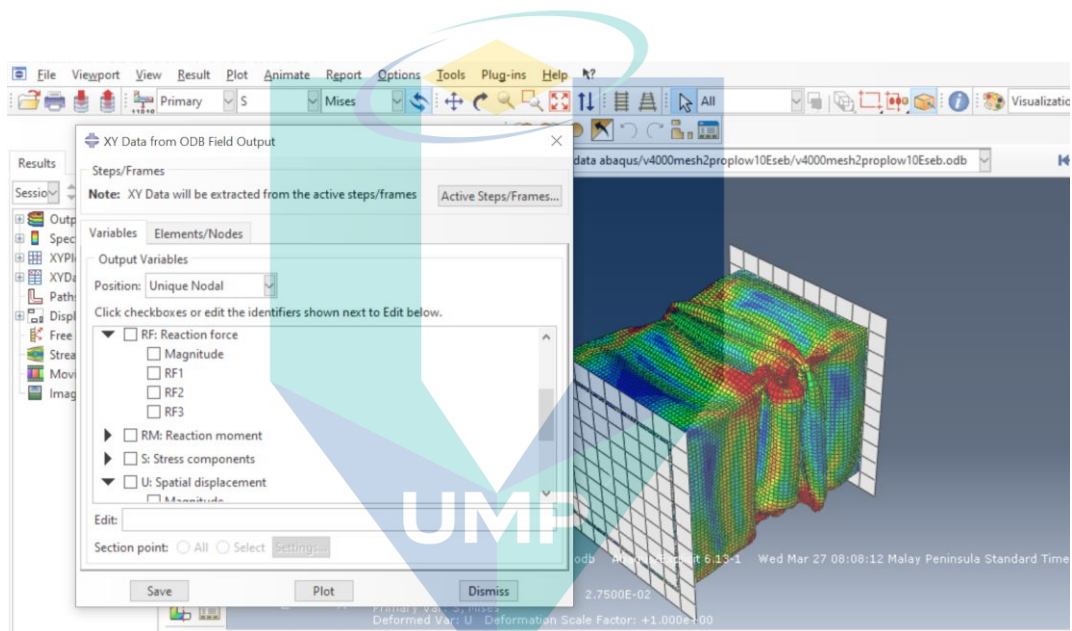


Figure 4.30 Simulation process of specimen A1.4P0

From the simulation, data of force and displacement of each specimen can be extracted to determine the value of IPF and SEA for each specimen. IPF is the first peak point in the force versus displacement graph. While the SEA values were calculated by dividing the EA values with mass of the specimen. Before that, the EA values were calculated from area under the curve for the same graph. Table 4.15 shows the data that determined from the simulation for quasi-static test.

Table 4.16 Simulated value of IPF and SEA for quasi-static test

Length (mm)	Thickness (mm)	IPF (kN)	SEA(kJ/kg)
195.00	1.40	36.89	1.53
195.00	1.74	70.22	1.71
195.00	1.73	69.52	1.71
195.00	2.00	100.25	1.92

The simulation data was determined for the length of foam of 195 mm with different thickness of aluminium column which were 1.4 mm, 1.74 mm, 1.73 mm and 2.0 mm. For the 1.4 mm thickness, the IPF value is 36.89 kN with SEA of 1.53 kJ/kg. Then for the 1.74 mm thickness column, the IPF is 70.22 kN with SEA of 1.71 kJ/kg. While for 1.73mm thickness column, the IPF is 69.52 kN with SEA of 1.71 kJ/kg. Finally for 2.0 mm thickness, the IPF is 100.25 kN with SEA of 1.92 kJ/kg. Results from the optimization was compared with the simulation results. The data is shown in Table 4.17

Table 4.17 Comparison of data in simulation and optimization for the value of IPF and SEA under quasi-static test

Length (mm)	Thickness (mm)	Optimization result		Simulation result	
		IPF (kN)	SEA (kJ/kg)	IPF (kN)	SEA (kJ/kg)
195.00	1.4	-	-	36.89	1.53
195.00	1.74	69.87	1.72	70.22	1.71
195.00	1.73	69.12	1.71	69.52	1.71
195.00	2.0	-	-	100.25	1.92

Value of IPF gained from the optimization for 1.74 mm thickness column, the value of IPF and SEA are 69.87 kN and 1.72 kJ/kg compared to 70.22 kN and 1.71 kJ/kg. As for 1.73 mm, the IPF is 69.12 kN compared to 70.22 kN in simulation. The value of SEA in optimization and simulation is 1.71 kJ/kg.

While the similar simulation was conducted for impact test. The value of IPF and SEA for each specimen were extracted from the simulation data. Table 4.18 shows the data that gained from the simulation for impact test.

Table 4.18 Simulation data for IPF and SEA value under impact test

Length (mm)	Thickness (mm)	IPF (kN)	SEA(kJ/kg)
195.00	1.40	97.19	1.50
195.00	1.46	103.05	1.47
195.00	1.47	103.56	1.47
195.00	2.00	160.33	1.33

The simulation data shows that for 1.4 mm thickness, the IPF is 97.19 kN with SEA of 1.5 kJ/kg. Next, for 1.46 mm thickness, the IPF value is 103.05 kN with SEA of 1.47 kJ/kg. Then for 1.47 mm thickness, the IPF is 103.56 kN with SEA of 1.47 kJ/kg. Finally, for 2.0 mm thickness column, the IPF is 160.33 kN with SEA of 1.33 kJ/kg. The optimization results were compared with the simulation results. The data were shown in Table 4.19

Table 4.19 Comparison of data in simulation and optimization for the value of IPF and SEA under impact test

Length (mm)	Thickness (mm)	Optimization result		Simulation result	
		IPF (kN)	SEA (kJ/kg)	IPF (kN)	SEA (kJ/kg)
195.00	1.4	-	-	97.19	1.50
195.00	1.47	104.52	1.51	103.05	1.47
195.00	1.46	104.44	1.51	103.56	1.47
195.00	2.0	-	-	160.33	1.33

From the optimization, for 1.47 mm thickness column, the value of IPF is 104.52 kN and SEA is 1.51 kJ/kg compared to 103.05 kN and 1.47 kJ/kg in simulation. As for 1.46 mm, the IPF and SEA are 104.44 kN and 1.51 kJ/kg respectively compared to 103.56 kN and 1.47 kJ/kg in simulation.

## CHAPTER 5

### CONCLUSION

#### 5.1 Introduction

This chapter is to conclude the study on polyurethane foam as a filler in the energy absorber application. Some future works and recommendation are also included in this chapter.

#### 5.2 Conclusion

Polyurethane foam-filled structure with different length of foam has been produced using free-rise condition of PU. The foam was tested to determine the mechanical properties under uniaxial compression. The PU foam is extensively studied to analyse the energy absorption characteristic under compression load.

The experiment is designed to decrease the initial peak force of the column and increase the energy absorption accordingly. Specimen A1.4P195, A1.4P190 and A1.4P185 for 1.4mm thickness and A2.0P195, A2.0P190 and A2.0P185 for 2.0 mm thickness filled with foam to increase the energy absorption of the structure. Certain length on the upper region was left empty to reduce the initial peak force compared to the hollow column. From the results obtained, it can be concluded that:

1. The reduction of foam length has effected the energy absorption capacity and initial peak force of the structure. Under quasi-static test, reduction in foam length to 195 mm has decrease the IPF of structure by 23% but it decreases only 1% in reduction of SEA for 1.4 mm specimen and for 2mm thickness specimen, the IPF is decreased by 3% for the reduction of the SEA by 24% for specimen with length of foam of 195 mm. While under impact test, the IPF is reduced by 31% and contributes to the reduction of SEA by only 6% for the length of foam of 190 mm and 1.4 mm thickness structure. The similar results obtained by the 2 mm thickness with maximum reduction of 5% in IPF but the SEA remains constant.

2. Optimization conducted using Design expert software shows that for quasi-static test, the best solution gained by length of foam of 195 mm with thickness of 1.74 mm that produce the initial peak force of 70 kN and SEA of 1.7 kJ/kg while for impact test the best solution gained by length of foam of 195 mm with thickness of 1.46 mm that produce the initial peak force of 103 kN and SEA of 1.5 kJ/kg.

### 5.3 Suggestion for future work

It has been shown that the performance of foam-filled structure with reduction of foam length are better than the full foam-filled structure. Here, some recommendations for future work are given:

- a. The finite element analysis (FEA) can be performed to predict the behaviour of the specimen.
- b. Optimization can be conducted before the experiment work to have clearer value of range for the length of foam by using FEA result
- c. The multi-cell or corrugated foam-filled structure with different length of foam can be studied.
- d. Suitable types of trigger mechanism can be introduced as it may contribute to the reduction in IPF value.

اونيورسيتي مليسيا قهغ

UNIVERSITI MALAYSIA PAHANG

## REFERENCES

- Abedi, M. M., Abbas, N., Liaghat, G. H., & Nejad, M. Z. (2012). Theoretical and experimental study on empty and foam-filled columns with square and rectangular cross section under axial compression. *International Journal of Mechanical Sciences*, 65, 134–146.
- Abramowicz, W., & Jones, N. (1986). Dynamic progressive buckling of circular and square tubes. *International Journal of Impact Engineering*, 4(4), 243–270.
- Ajdari, A., Nayeb-hashemi, H., & Vaziri, A. (2011). Dynamic crushing and energy absorption of regular, irregular and functionally graded cellular structures. *International Journal of Solids and Structures*, 48(3–4), 506–516. <https://doi.org/10.1016/j.ijsolstr.2010.10.018>
- Aktay, L., Toksoy, A. K., & Güden, M. (2006). Quasi-static axial crushing of extruded polystyrene foam-filled thin-walled aluminum tubes: Experimental and numerical analysis. *Materials and Design*, 27(7), 556–565. <https://doi.org/10.1016/j.matdes.2004.12.019>
- Alan R, P., Richard J, B., & Hedengren, J. (1987). *Optimization Methods in Engineering Design*. 330–336.
- Alavi Nia, A., & Parsapour, M. (2013). An investigation on the energy absorption characteristics of multi-cell square tubes. *Thin-Walled Structures*, 68, 26–34. <https://doi.org/10.1016/j.tws.2013.01.010>
- Alavi Nia, A., & Parsapour, M. (2014). Comparative analysis of energy absorption capacity of simple and multi-cell thin-walled tubes with triangular, square, hexagonal and octagonal sections. *Thin-Walled Structures*, 74, 155–165. <https://doi.org/10.1016/j.tws.2013.10.005>
- Alkhatib, S. E., Tarlochan, F., & Eyvazian, A. (2017). Collapse behavior of thin-walled corrugated tapered tubes. *Engineering Structures*, 150, 674–692. <https://doi.org/10.1016/j.engstruct.2017.07.081>
- Alkhatib, S. E., Tarlochan, F., Hashem, A., & Sadok, S. (2016). Collapse behavior of thin-walled corrugated tapered tubes under oblique impact. *Thin-Walled Structures*, 122, 510–528.
- Altin, M, Acar, E., & Güler, M. A. (2018). Foam filling options for crashworthiness optimization of thin-walled multi-tubular circular columns. *Thin Walled Structures*, 131(July), 309–323. <https://doi.org/10.1016/j.tws.2018.06.043>
- Altin, Murat, Güler, M. A., & Mert, S. K. (2017). The effect of percent foam fill ratio on the energy absorption capacity of axially compressed thin-walled multi-cell square and circular tubes. *International Journal of Mechanical Sciences*, 131–132(July), 368–379. <https://doi.org/10.1016/j.ijmecsci.2017.07.003>



- Amaro, A. M., Reis, P. N. B., De Moura, M. F. S. F., & Neto, M. A. (2013). Influence of multi-impacts on GFRP composites laminates. *Composites Part B: Engineering*, *52*, 93–99. <https://doi.org/10.1016/j.compositesb.2013.03.041>
- An, X., Gao, Y., Fang, J., Sun, G., & Li, Q. (2015). Crashworthiness design for foam-filled thin-walled structures with functionally lateral graded thickness sheets. *Thin Walled Structures*, *91*, 63–71. <https://doi.org/10.1016/j.tws.2015.01.011>
- Asanjarani, A., Dibajian, S. ., & Mahdiana, A. (2017). Multi-objective crashworthiness optimization of tapered thin-walled square tubes with indentations. *Thin Walled Structures*, *116*, 26–36.
- ASTM D1621-10, Standard Test Method for Compressive Properties of Rigid Cellular Plastics, ASTM International, West Conshohocken, 2010.
- ASTM D1622 / D1622M-10, Standard Test Method for Apparent Density of Rigid Cellular Plastics, ASTM International, West Conshohocken, PA, 2008
- ASTM E8/E8M Standard Test Methods for Tension Testing Of Metallic Materials 1. (2010). <https://doi.org/10.1520/E0008>
- ASTM E9-89a, Standard Test Methods of Compression Testing of Metallic Materials at Room Temperature, ASTM International, West Conshohocken, PA, 1989
- Attia, M. S., Meguid, S. A., & Nouraei, H. (2012). Nonlinear finite element analysis of the crush behaviour of functionally graded foam-filled columns. *Finite Elements in Analysis and Design*, *61*, 50–59. <https://doi.org/10.1016/j.finel.2012.06.004>
- Avalle, M., Belingardi, G., & Montanini, R. (2001). Characterization of polymeric structural foams under compressive impact loading by means of energy-absorption diagram. *International Journal of Impact Engineering*, *25*, 455–472.
- Azarakhsh, S., Rahi, A., Ghamarian, A., & Motamedi, H. (2015). Axial crushing analysis of empty and foam-filled brass bitubular cylinder tubes. *Thin-Walled Structures*, *95*, 60–72. <https://doi.org/10.1016/j.tws.2015.05.019>
- Balaji, G., & Annamalai, K. (2018). Crushing response of square aluminium column filled with carbon fibre tubes and aluminium honeycomb. *Thin-Walled Structures*, Vol. 132, pp. 667–681. <https://doi.org/10.1016/j.tws.2018.07.037>
- Balaji, G., & K. Annamalai. (2018). Crushing response of square aluminium column filled with carbon fibre tubes and aluminium honeycomb. *Thin-Walled Structures*, Vol. 132, pp. 667–681. <https://doi.org/10.1016/j.tws.2018.07.037>
- Baroutaji, A., Gilchrist, M. D., Smyth, D., & Olabi, A. G. (2015). Crush analysis and multi-objective optimization design for circular tube under quasi-static lateral loading. *Thin Walled Structures*, *86*, 121–131.
- Baroutaji, A., Sajjia, M., & Olabi, A. G. (2017). On the crashworthiness performance of thin-walled energy absorbers: Recent advances and future developments. *Thin-Walled Structures*, *118*(November 2016), 137–163. <https://doi.org/10.1016/j.tws.2017.05.018>

- Bezerra, M. A., Santelli, R. E., Oliveira, E. P., Villar, L. S., & Escalera, L. A. (2008). Response surface methodology (RSM) as a tool for optimization in analytical chemistry. *Talanta*, 76(5), 965–977. <https://doi.org/10.1016/j.talanta.2008.05.019>
- Bigdeli, A., & Nouri, M. D. (2019). A crushing analysis and multi-objective optimization of thin-walled fibre-cell structures. *Thin Walled Structures*, 137(July 2018), 1–18. <https://doi.org/10.1016/j.tws.2018.12.033>
- Boria, S. (2017). Crashworthiness Optimization of an Automotive Front Bumper in Composite Material. *International Journal of Mechanical and Mechatronics Engineering*, 11.
- Buku statistik kemalangan jalan raya tahun 2018 (Kemaskini 17.05.2019) (2019), Jabatan Keselamatan Jalanraya, Kementerian Pengangkutan Malaysia.
- Costas, M., Díaz, J., Romera, L. E., Hernández, S., & Tielas, A. (2013). Static and dynamic axial crushing analysis of car frontal impact hybrid absorbers. *International Journal of Impact Engineering*, 62, 166–181. <https://doi.org/10.1016/j.ijimpeng.2013.06.011>
- Costas, M., Morin, D., Langseth, M., Díaz, J., & Romera, L. (2017). Static crushing of aluminium tubes filled with PET foam and a GFRP skeleton. Numerical modelling and multiobjective optimization. *International Journal of Mechanical Sciences*, 131–132, 205–217. <https://doi.org/10.1016/j.ijmecsci.2017.07.004>
- Costas, M., Morin, D., Langseth, M., Romera, L., & Díaz, J. (2016). Axial crushing of aluminum extrusions filled with PET foam and GFRP. An experimental investigation. *Thin-Walled Structures*, 99, 45–57. <https://doi.org/10.1016/j.tws.2015.11.003>
- Cui, C., Huang, Q., Li, D., Chunri, Q., & Li, H. (2016). Stress–strain relationship in axial compression for EPS concrete. *Construction and Building Materials*, 105, 377–389.
- Darvizeh, A., Meshkinzar, A., Alitavoli, M., & Rajabiehfar, R. (2017). Low velocity impact of empty and foam filled circumferentially grooved thick-walled circular tubes. *Thin Walled Structures*, 110, 97–105. <https://doi.org/10.1016/j.tws.2016.09.002>
- De Vries, D. V. W. M. (2009). Characterization of polymeric foams. In *Eindhoven University of Technology*.
- Deb, A., Shivakumar, N., & Chou, C. (2015). An Alternative Approach for Formulation of a Crushable PU Foam Considering its Behavior under Compressive Loads. *SAE Technical Paper*, 7. <https://doi.org/10.4271/2015-01-1483>
- Demharter, A. (1998). Polyurethane rigid foam, a proven thermal insulating material for applications between +130°C and -196°C. *Cryogenics*, 38(1), 113–117. [https://doi.org/10.1016/S0011-2275\(97\)00120-3](https://doi.org/10.1016/S0011-2275(97)00120-3)
- Deng, X., & Liu, W. (2019). Multi-objective optimization of thin-walled sandwich tubes with lateral corrugated tubes in the middle for energy absorption. *Thin Walled Structures*, 137(August 2018), 303–317. <https://doi.org/10.1016/j.tws.2018.12.040>

- Dirgantara, T., Jusuf, A., Kurniati, E. O., & Gunawan, L. (2018a). Crashworthiness analysis of foam-filled square column considering strain rate effect of the foam. *Thin Walled Structures*, 129(May), 365–380. <https://doi.org/10.1016/j.tws.2018.04.004>
- Dirgantara, T., Jusuf, A., Kurniati, E. O., & Gunawan, L. (2018b). Crashworthiness analysis of foam – filled square column considering strain rate effect of the foam. *Thin Walled Structures*, 129(May), 365–380. <https://doi.org/10.1016/j.tws.2018.04.004>
- Djamaluddin, F. (2019). Review : deformation and optimisation crashworthiness method for foam filled structures. *Latin American Journal of Solids and Structures*, 16(7), 1–20.
- Dong, Z., Li, Y., Zhao, T., Wu, W., Xiao, D., & Liang, J. (2019). Experimental and numerical studies on the compressive mechanical properties of the metallic auxetic reentrant honeycomb. *Materials & Design*, 182, 108036. <https://doi.org/10.1016/j.matdes.2019.108036>
- Duarte, I., Krstulovi, L., & Vesenjak, M. (2018). Axial crush behaviour of the aluminium alloy in-situ foam filled tubes with very low wall thickness. 192(January), 184–192. <https://doi.org/10.1016/j.compstruct.2018.02.094>
- Duarte, I., Krstulović-opara, L., Dias-de-oliveira, J., & Vesenjak, M. (2019). Axial crush performance of polymer-aluminium alloy hybrid foam filled tubes. *Thin Walled Structures*, 138(October 2018), 124–136. <https://doi.org/10.1016/j.tws.2019.01.040>
- Elahi, S. A., Rouzegar, J., Niknejad, A., & Assae, H. (2017). Theoretical study of absorbed energy by empty and foam-filled composite tubes under lateral compression. *Thin-Walled Structures Journal*, 114(July 2016), 1–10.
- Enderich, T. (2007). *Advanced Simulation Techniques for Low Speed Vehicle Impacts*. Microsoft Word - LS-DYNA Anwenderforum 2007. 25–36.
- Estrada, Q., Szwedowicz, D., Silva-Aceves, J., Majewski, T., Vergara-Vazquez, J., & Rodriguez-Mendez, A. (2017). Crashworthiness behavior of aluminum profiles with holes considering damage criteria and damage evolution. *International Journal of Mechanical Sciences*, 131–132(December 2016), 776–791. <https://doi.org/10.1016/j.ijmecsci.2017.07.042>.
- Eyvazian, A., Mozafari, H., & Hamouda, A. M. (2016). Experimental study of corrugated metal-composite under axial loading. *11th International Symposium on Plasticity and Impact Mechanics, Implast 2016*, 1314–1321.
- Eyvazian, A., Tran, T. N., & Magid, A. (2018). Experimental and theoretical studies on axially crushed corrugated metal tubes. *International Journal of Non-Linear Mechanics*, 101(February), 86–94. <https://doi.org/10.1016/j.ijnonlinmec.2018.02.009>
- Fan, Z., Lu, G., & Liu, K. (2013). Quasi-static axial compression of thin-walled tubes with different cross-sectional shapes. 55, 80–89. <https://doi.org/10.1016/j.engstruct.2011.09.020>

- Fang, H., Rais-Rohani, M., Liu, Z., & Horstemeyer, M. F. (2005). A comparative study of metamodeling methods for multiobjective crashworthiness optimization. *Computers and Structures*, 83(25–26), 2121–2136. <https://doi.org/10.1016/j.compstruc.2005.02.025>
- Fang, J., Gao, Y., Sun, G., Zhang, Y., & Li, Q. (2014). Parametric analysis and multiobjective optimization for functionally graded foam-filled thin-wall tube under lateral impact. *Computational Materials Science*, 90, 265–275. <https://doi.org/10.1016/j.commatsci.2014.03.044>
- Fentahun, M. A., & Savas, M. A. (2018). Materials Used in Automotive Manufacture and Material Selection Using Ashby Charts. *International Journal of Materials Engineering*, 8(3), 40–54. <https://doi.org/10.5923/j.ijme.20180803.02>
- Galehdari, S. A., & Kadkhodayan, M. (2015). Analytical , experimental and numerical study of a graded honeycomb structure under in-plane impact load with low velocity. Analytical , experimental and numerical study of a graded honeycomb structure under in-plane impact load with low velocity. *International Journal of Crashworthiness*, 20(4), 387–400.
- Gameiro, C. P., & Cirne, J. (2007). Dynamic axial crushing of short to long circular aluminium tubes with agglomerate cork filler. *International Journal of Mechanical Sciences*, 49(9), 1029–1037. <https://doi.org/10.1016/j.ijmecsci.2007.01.004>
- Gan, Nianfei, Feng, Y., Yin, H., Wen, G., Wang, D., & Huang, X. (2016). Quasi-static axial crushing experiment study of foam-filled CFRP and aluminum alloy thin-walled structures. *Composite Structures*, 157, 303–319. <https://doi.org/10.1016/j.compstruct.2016.08.043>
- Gan, Ning, Yao, S., Dong, H., Xiong, Y., Liu, D., & Pu, D. (2018). Energy absorption characteristics of multi-frusta configurations under axial impact loading. *Thin-Walled Structures*, Vol. 122, pp. 147–157. <https://doi.org/10.1016/j.tws.2017.10.011>
- Gibson, L. J., & Ashby, M. F. (1999). *Cellular Solids: structure and properties* (Second Edi). Cambridge University Press.
- Gkritza, K., Pyrialakou, V., Maksimović, J., Krishnan, V., & Kastrouni, E. (2015). An optimization model of energy and transportation systems: Assessing the high-speed rail impacts in the United States. *Transportation Research Part C: Emerging Technologies*.
- Goel, M. D. (2015). Deformation , energy absorption and crushing behavior of single, double and multi-wall foam filled square and circular tubes. 90, 1–11. <https://doi.org/10.1016/j.tws.2015.01.004>
- Guden, M., Yüksel, S., Taşdemirci, A., & Tanoğlu, M. (2007). Effect of aluminum closed-cell foam filling on the quasi-static axial crush performance of glass fiber reinforced polyester composite and aluminum/composite hybrid tubes. *Composite Structures*, 81(4), 480–490. <https://doi.org/10.1016/j.compstruct.2006.09.005>



- Guillow, S. R., Lu, G., & Grzebieta, R. H. (2001). Quasi-static axial compression of thin-walled circular aluminium tubes. *International Journal of Mechanical Sciences*, 43, 2103–2123.
- Hangai, Y., Otazawa, S., & Utsunomiya, T. (2018). *Aluminum alloy foam-filled aluminum tube fabricated by friction stir*.
- Hanssen, A. G., Langseth, M., & Hopperstad, O. S. (2000). *Static and dynamic crushing of square aluminium extrusions with aluminium foam filler*. 24, 47–73.
- Holbery, J., & Houston, D. (2006). *Natural-Fiber-Reinforced Polymer Composites in Automotive Applications*. (November).
- Hou, S., Li, Q., Long, S., Yang, X., & Li, W. (2007). Design optimization of regular hexagonal thin-walled columns with crashworthiness criteria. *Finite Elements in Analysis and Design*, 43(6–7), 555–565. <https://doi.org/10.1016/j.finel.2006.12.008>
- Hou, S., Zhang, Z., Yang, X., Yin, H., & Li, Q. (2014). Crashworthiness optimization of new thin-walled cellular configurations. *Engineering Computations (Swansea, Wales)*, 31(5), 879–897. <https://doi.org/10.1108/EC-11-2012-0300>
- Hu, D., Wang, Y., Song, B., Dang, L., & Zhang, Z. (2019). Energy-absorption characteristics of a bionic honeycomb tubular nested structure inspired by bamboo under axial crushing. *Composites Part B*, 162(September 2018), 21–32. <https://doi.org/10.1016/j.compositesb.2018.10.095>
- Hussain, N. N. (2015). Automobile Crash Box Design Improvement Using HyperStudy. *Altair Technology Conference*, 1–7.
- Hussain, N. N., Regalla, S. P., & Rao, Y. V. D. (2017). Comparative Study of Trigger Configuration for Enhancement of Crashworthiness of Automobile Crash Box Subjected to Axial Impact Loading. *Procedia Engineering*, 173, 1390–1398. <https://doi.org/10.1016/j.proeng.2016.12.198>
- Hussain, Z., & Suffin, N. S. (2011). Microstructure and Mechanical Behaviour of Aluminium Foam Produced by Sintering Dissolution Process Using NaCl Space Holder. *Journal of Engineering Science*, 7, 37–49.
- Hussein, R. D., Ruan, D., Lu, G., Guillow, S., & Yoon, J. W. (2017). Crushing response of square aluminium tubes filled with polyurethane foam and aluminium honeycomb. *Thin-Walled Structures*, 110(November 2016), 140–154. <https://doi.org/10.1016/j.tws.2016.10.023>
- Jailani, A., & Othman, A. (2014). Axial Crushes Simulation of Thin-walled Square Aluminum Alloy 6061-T5 Foam-filled Section. *APCBEE Procedia*, 9(Icbee 2013), 388–394. <https://doi.org/10.1016/j.apcbee.2014.01.068>
- Jiang, H., Ren, Y., Gao, B., Xiang, J., & Yuan, F. G. (2017). Design of novel plug-type triggers for composite square tubes: enhancement of energy-absorption capacity and inducing failure mechanisms. *International Journal of Mechanical Sciences*, 131–132(June), 113–136. <https://doi.org/10.1016/j.ijmecsci.2017.06.050>

- John, B. (2013). Application of desirability function for optimizing the performance characteristics of carbonitrided bushes. *International Journal of Industrial Engineering Computations*, 4(3), 305–314. <https://doi.org/10.5267/j.ijiec.2013.04.003>
- Kenyon, D., Shu, Y., Fan, X., Reddy, S., Dong, G., & Lew, A. J. (2018). Parametric design of multi-cell thin-walled structures for improved crashworthiness with stable progressive buckling mode. *Thin Walled Structures*, 131(January), 76–87. <https://doi.org/10.1016/j.tws.2018.06.031>
- Khemani, K. C. (1997). *Polymeric Foams: An Overview*. ACS Symposium Series; American Chemical Society: Washington, DC, 1997.1–7.
- Kiliçaslan, C. (2015). Numerical crushing analysis of aluminum foam-filled corrugated single-and double-circular tubes subjected to axial impact loading. *Thin-Walled Structures*, 96, 82–94. <https://doi.org/10.1016/j.tws.2015.08.009>
- Kim, H. C., Shin, D. K., Lee, J. J., & Kwon, J. B. (2014). Crashworthiness of aluminum/CFRP square hollow section beam under axial impact loading for crash box application. *Composite Structures*, 112(1), 1–10. <https://doi.org/10.1016/j.compstruct.2014.01.042>
- Kirpluks, M., Cabulis, U., Zeltins, V., Stiebra, L., & Avots, A. (2014). Rigid polyurethane foam thermal insulation protected with mineral intumescent mat. *Autex Research Journal*, 14(4), 259–269. <https://doi.org/10.2478/aut-2014-0026>
- Kumar, D., Mahajan, N. N., & Linul, E. (2019). *Crashworthiness performance and microstructural characteristics of foam-filled thin-walled tubes under diverse strain rate*. 775. <https://doi.org/10.1016/j.jallcom.2018.10.160>
- Li, G., Zhang, Z., Sun, G., Xu, F., & Huang, X. (2014a). Crushing analysis and multiobjective optimization for functionally graded foam-filled tubes under multiple load cases. *International Journal of Mechanical Sciences*, 89, 439–452. <https://doi.org/10.1016/j.ijmecsci.2014.10.001>
- Li, G., Zhang, Z., Sun, G., Xu, F., & Huang, X. (2014b). Crushing analysis and multiobjective optimization for functionally graded foam-filled tubes under multiple load cases. *International Journal of Mechanical Sciences*, 89, 439–452. <https://doi.org/10.1016/j.ijmecsci.2014.10.001>
- Li, Z., Chen, R., & Lu, F. (2018). *Comparative analysis of crashworthiness of empty and foam-filled thin-walled tubes*. 124(December 2017), 343–349. <https://doi.org/10.1016/j.tws.2017.12.017>
- Linul, E., Şerban, D. A., Marsavina, L., & Sadowski, T. (2017). Assessment of collapse diagrams of rigid polyurethane foams under dynamic loading conditions. *Archives of Civil and Mechanical Engineering*, 17(3), 457–466. <https://doi.org/10.1016/j.acme.2016.12.009>



- Liu, Q., Shen, H., Wu, Y., Xia, Z., Fang, J., & Li, Q. (2018). Crash responses under multiple impacts and residual properties of CFRP and aluminum tubes. *Composite Structures*, 194(February), 87–103. <https://doi.org/10.1016/j.compstruct.2018.04.001>
- Liu, Q., Xu, X., Ma, J., Wang, J., Shi, Y., & Hui, D. (2017). Lateral crushing and bending responses of CFRP square tube filled with aluminum honeycomb. *Composites Part B: Engineering*, 118, 104–115. <https://doi.org/10.1016/j.compositesb.2017.03.021>
- Liu, Y. D., Yu, J. L., Zheng, Z. J., & Li, J. R. (2009). A numerical study on the rate sensitivity of cellular metals. *International Journal of Solids and Structures*, 46(22–23), 3988–3998. <https://doi.org/10.1016/j.ijsolstr.2009.07.024>
- Lu, G., & Yu, T. (2003). *Energy absorption of structures and materials*. Woodhead Publishing Limited.
- Ly, H. A., & Pham, T. T. (2016). *The Geometric Influence of the Tubular-Hat Tube on Its Energy Absorption Capacity in Axial Load Tubular-Hat*. 2, 12–17. <https://doi.org/10.11648/j.ijtet.s.2016020501.13>
- Mahbod, M., & Asgari, M. (2018). Energy absorption analysis of a novel foam-filled corrugated composite tube under axial and oblique loadings. *Thin Walled Structures*, 129(April), 58–73. <https://doi.org/10.1016/j.tws.2018.03.023>
- Mahdi, E., Mokhtar, A. S., Asari, N. A., Elfaki, F., & Abdullah, E. J. (2006). Nonlinear finite element analysis of axially crushed cotton fibre composite corrugated tubes. *Composite Structures*, 75, 39–48. <https://doi.org/10.1016/j.compstruct.2006.04.057>
- Marzougui, K., Brown, D., Park, H. ., Kan, C. ., & Opiela, K. . (2016). Development & Validation of a Finite Element Model for the 2012 Toyota Camry Passenger Sedan. <https://doi.org/10.13021/G8N88>
- Mat Rejab, M.R. (2004). Polymeric foam as core of side-door impact beam (Master's thesis).
- Mat Rejab, M. R. (2013). *The Mechanical Properties of Novel Lightweight Structures Based on Corrugated-Cores* (Doctoral dissertation).
- Mirfendereski, L., & Salimi, M. Ā. (2008). Parametric study and numerical analysis of empty and foam-filled thin-walled tubes under static and dynamic loadings. *International Journal of Mechanical Sciences*, 50, 1042–1057. <https://doi.org/10.1016/j.ijmecsci.2008.02.007>
- Mohammadiha, O., & Ghariblu, H. (2016). Crush behavior optimization of multi-tubes filled by functionally graded foam. *Thin-Walled Structures*, 98, 627–639. <https://doi.org/10.1016/j.tws.2015.10.025>
- Montazeri, S., Elyasi, M., & Moradpour, A. (2018). Investigating the energy absorption, SEA and crushing performance of holed and grooved thin-walled tubes under axial loading with different materials. *Thin Walled Structures*, 131(May), 646–653. <https://doi.org/10.1016/j.tws.2018.07.024>

- Mullur, A. A., & Messac, A. (2006). Metamodeling using Extended Radial Basis Functions: A Comparative Approach. *Engineering with Computers*, 21, 203–217. <https://doi.org/10.1007/s00366-005-0005-7>
- Myers, R., Montgomery, D., & Anderson-Cook, C. (2016). *Response surface methodology: process and product optimization using designed experiments* (Fourth ed.). New Jersey: John Wiley & Sons.
- Nakazawa, Y., Tamura, K., Yoshida, M., Takagi, K., & Kano, M. (2005). Development of crash-box for passenger car with high capability for energy absorption. *VIII International Conference on Computational Plasticity*.
- Nia, A. A., Ranjbarzadeh, H., & Kazemi, M. (2017). An empirical study on ballistic resistance of sandwich targets with aluminum facesheets and composite core. *Latin American Journal of Solids and Structures*, 14(6), 1085–1105. <https://doi.org/10.1590/1679-78253390>
- Nikkhah, H., Guo, F., Chew, Y., Bai, J., Song, J., & Wang, P. (2017). The effect of different shapes of holes on the crushing characteristics of aluminum square windowed tubes under dynamic axial loading. *Thin-Walled Structures*, 119(February), 412–420. <https://doi.org/10.1016/j.tws.2017.06.036>
- Niknejad, A., Abedi, M. M., Liaghat, G. H., & Nejad, M. Z. (2015). Absorbed energy by foam-filled quadrangle tubes during the crushing process by considering the interaction effects. *Archives of Civil and Mechanical Engineering*, 15(2), 376–391. <https://doi.org/10.1016/j.acme.2014.09.005>
- Niknejad, Abbas, Ali, S., & Hossein, G. (2012). Experimental investigation on the lateral compression in the foam-filled circular tubes. *Materials and Design*, 36, 24–34. <https://doi.org/10.1016/j.matdes.2011.10.047>
- Niknejad, Abbas, Mohammad, S., Ahmad, S., & Elahi, A. (2013). Theoretical and experimental study on the flattening deformation of the rectangular brazen and aluminum columns. *Archives of Civil and Mechanical Engineering*, 13(4), 449–464. <https://doi.org/10.1016/j.acme.2013.04.008>
- Niknejad, Abbas, & Orojloo, P. H. (2016). A novel nested system of tubes with special cross-section as the energy absorber. *Thin-Walled Structures*, 100, 113–123. <https://doi.org/10.1016/j.tws.2015.12.009>
- Niknejad, Abbas, Orojloo, P. H., & Johari, M. (2017). Flattening process on folded quadrangular columns under the lateral loading- a novel energy absorption method. *Thin-Walled Structures*, 119(April), 603–614. <https://doi.org/10.1016/j.tws.2017.04.028>
- Nurul Izzah, A., Salwani, M., Tan, S., Mas Ayu, H., & Rosdi, D. (2019). Effect of specimen geometry , quenching and trigger mechanism on crushing performance of single hat column. *IOP Conference Series: Materials Science and Engineering*. <https://doi.org/10.1088/1757-899X/469/1/012091>

- Onsalung, N., Thinvongpituk, C., & Pianthong, K. (2014). Impact Response of Circular Aluminum Tube Filled with Polyurethane Foam. *Materials Transactions*, 55(1), 207–215. <https://doi.org/10.2320/matertrans.M2013293>
- Patel, S., Vusa, V. R., & Guedes Soares, C. (2019). Crashworthiness analysis of polymer composites under axial and oblique impact loading. *International Journal of Mechanical Sciences*, 156(December 2018), 221–234. <https://doi.org/10.1016/j.ijmecsci.2019.03.038>
- Peraza-hernandez, E. A. (2016). Studies about the Behavior of the Crash Boxes of a Car Body Studies about the Behavior of the Crash Boxes of a Car Body. *IOP Conference Series: Materials Science and Engineering*. <https://doi.org/10.1088/1757-899X/160/1/012010>
- Prasad, Y., Shinde, A., Gangurde, Y., & Patel, P. (2016). Review on Weight Reduction in Automobile. *International Journal of Advanced Technology in Engineering Science*, 4(01), 478–483.
- Qiao, J., & Chen, C. (2016). In-plane crushing of a hierarchical honeycomb. *International Journal of Solids and Structures*, 85–86, 57–66. <https://doi.org/10.1016/j.ijsolstr.2016.02.003>
- Qiu, N., Gao, Y., Fang, J., Feng, Z., Sun, G., & Li, Q. (2015). Crashworthiness analysis and design of multi-cell hexagonal columns under multiple loading cases. *Finite Elements in Analysis and Design*, 104, 89–101. <https://doi.org/10.1016/j.finel.2015.06.004>
- Rameshchandra, C., Ajit, S., & Shelar, L. (2018). Strength Enhancement of Car Front Bumper for Slow Speed Impact by FEA Method as per IIHS Regulation. *Journal of The Institution of Engineers (India): Series C*, 99(5), 599–606. <https://doi.org/10.1007/s40032-017-0365-y>
- Reddy, T. Y., & Wall, R. J. (1988). Axial Compression Of Foam-Filled Circular Tubes. *International Journal of Impact Engineering*, 7(2), 151–166.
- Reinfried, M., Stephani, G., Luthardt, F., Adler, J., John, M., & Krombholz, A. (2011). Hybrid Foams – A New Approach for Multifunctional Applications. *Advanced Engineering Material*, 13(11), 1031–1036.
- Rezaei, B., Niknejad, A., Assaee, H., & Liaghat, G. H. (2015). Axial splitting of empty and foam-filled circular composite tubes – An experimental study. *Archives of Civil and Mechanical Engineering*, 15(3), 650–662. <https://doi.org/10.1016/j.acme.2014.09.003>
- Rouzegar, J., Assaee, H., Niknejad, A., & Elahi, S. A. (2015). Geometrical discontinuities effects on lateral crushing and energy absorption of tubular structures. *Materials and Design*, 65, 343–359. <https://doi.org/10.1016/j.matdes.2014.09.041>
- Ryberg, B. (2013). *Metamodel-Based Design Optimization – A Multidisciplinary Approach for Automotive Structures*. Linköping University, Sweden.

- Safety Bumper Test and Rating Protocol ( Version VIII )*. (2010). (September), 2.
- Sebaey, T. A., & Mahdi, E. (2017). Filler strengthening of foam-filled energy absorption devices using CFRP beams. *Composite Structures*, 160, 1–7. <https://doi.org/10.1016/j.compstruct.2016.10.049>
- Shahbeyk, S., Vafai, A., & Petrinic, N. (2005). Axial crushing of metal foam-filled square columns: Foam density distribution and impactor inclination effects. *Thin-Walled Structures*, 43(12), 1818–1830. <https://doi.org/10.1016/j.tws.2005.09.002>
- Shen, Z., Qiao, X., & Chen, H. (2012). BIW Safety Performance Research Based on Vehicle Frontal Crash. *Proceedings of the FISITA 2012 World Automotive Congress*, 13–27. <https://doi.org/10.1007/978-3-642-33805-2>
- Song, H. W., Fan, Z. J., Yu, G., Wang, Q. C., & Tobota, A. (2005). Partition energy absorption of axially crushed aluminum foam-filled hat sections. *International Journal of Solids and Structures*, 42(9–10), 2575–2600. <https://doi.org/10.1016/j.ijsolstr.2004.09.050>
- Song, J., Chen, Y., & Lu, G. (2012). Axial crushing of thin-walled structures with origami patterns. *Thin-Walled Structures*, Vol. 54, pp. 65–71. <https://doi.org/10.1016/j.tws.2012.02.007>
- Souza, F. De, Ferreira, G., Carlos, A., Jr, A., Simões, S., José, A., ... Morais, D. (2018). Experimental dynamic analysis of composite sandwich beams with magnetorheological honeycomb core. *Engineering Structures*, 176(May), 231–242. <https://doi.org/10.1016/j.engstruct.2018.08.101>
- Su, P., Han, B., Yang, M., Wei, Z., Zhao, Z., Zhang, Q., & Zhang, Q. (2018). Axial compressive collapse of ultralight corrugated sandwich cylindrical shells. *Materials & Design*, 160, 325–337. <https://doi.org/10.1016/j.matdes.2018.09.034>
- Subramaniyan, S. K., Mahzan, S., Ghazali, M. Imran, Ahmad Zaidi, A. M., & Prabagaransd, P. K. (2013). Energy Absorption Characteristics of Polyurethane Composite Foam-Filled Tubes Subjected to Quasi-Static Axial Loading. *Applied Mechanics and Materials*, 315, 872–878. <https://doi.org/10.4028/www.scientz>
- Sun, G., Li, G., Hou, S., Zhou, S., Li, W., & Li, Q. (2010). Crashworthiness design for functionally graded foam-filled thin-walled structures. *Thin Walled Structures*, 527, 1911–1919. <https://doi.org/10.1016/j.msea.2009.11.022>
- Sun, G., Li, S., Li, G., & Li, Q. (2018). On crashing behaviors of aluminium / CFRP tubes subjected to axial and oblique loading : An experimental study. *Composites Part B*, 145(August 2017), 47–56. <https://doi.org/10.1016/j.compositesb.2018.02.001>
- Sun, G., Li, S., Liu, Q., Li, G., & Li, Q. (2016). Experimental study on crashworthiness of empty/aluminum foam/honeycomb-filled CFRP tubes. *Composite Structures*, 152, 969–993. <https://doi.org/10.1016/j.compstruct.2016.06.019>
- Sun, G., Pang, T., Xu, C., Zheng, G., & Song, J. (2017). Energy absorption mechanics for variable thickness thin-walled structures. *Thin-Walled Structures*, 118(April), 214–228. <https://doi.org/10.1016/j.tws.2017.04.004>



- Sun, G., Wang, Z., Yu, H., Gong, Z., & Li, Q. (2019a). Experimental and numerical investigation into the crashworthiness of metal- foam-composite hybrid structures. *Composite Structures*, 209(September 2018), 535–547. <https://doi.org/10.1016/j.compstruct.2018.10.051>
- Sun, G., Wang, Z., Yu, H., Gong, Z., & Li, Q. (2019b). Experimental and numerical investigation into the crashworthiness of metal- foam-composite hybrid structures. *Composite Structures*, 209(October 2018), 535–547. <https://doi.org/10.1016/j.compstruct.2018.10.051>
- Sun, G., Yu, H., Wang, Z., Xiao, Z., & Li, Q. (2019). Energy absorption mechanics and design optimization of CFRP / aluminium hybrid structures for transverse loading. *International Journal of Mechanical Sciences*, 150(October 2018), 767–783. <https://doi.org/10.1016/j.ijmecsci.2018.10.043>
- Tabacu, S. (2015). Axial crushing of circular structures with rectangular multi-cell insert. *Thin Walled Structures*, 95, 297–309. <https://doi.org/10.1016/j.tws.2015.07.011>
- Thinwongpituk, C., Onsalong, N. and Poonaya, S. (2016). Crush Characteristic of Foam-Filled Circular Steel and Aluminum Tubes under Axial Loading. *Proceedings of the World Congress on Engineering 2016, II*. London,UK.
- Tiuc, A. E., Vermeşan, H., Gabor, T., & Vasile, O. (2016). Improved Sound Absorption Properties of Polyurethane Foam Mixed with Textile Waste. *Energy Procedia*, 85(January), 559–565. <https://doi.org/10.1016/j.egypro.2015.12.245>
- Toksoy, A. K., & Güden, M. (2005). The strengthening effect of polystyrene foam filling in aluminum thin-walled cylindrical tubes. *Thin-Walled Structures*, 43(2), 333–350. <https://doi.org/10.1016/j.tws.2004.07.007>
- Tran, T. (2017). Crushing and theoretical analysis of multi-cell thin-walled triangular tubes under lateral loading. *Thin Walled Structures*, 115(February), 205–214. <https://doi.org/10.1016/j.tws.2017.02.027>
- Tran, T., & Baroutaji, A. (2018). Crashworthiness optimal design of multi-cell triangular tubes under axial and oblique impact loading. *Engineering Failure Analysis*, 93(May), 241–256. <https://doi.org/10.1016/j.engfailanal.2018.07.003>
- Uma Devi, B., Vamsi Krishna, C., & Mohan Swaroop, P. (2014). Design Simulation of Crash Box in Car. *International Journal of Engineering Research & Technology*, 3(1). Retrieved from issn: 2278-0181
- Wadley, H. (2002). Cellular Metal Manufacturing. In *Advanced Engineering Material* (pp. 726–733). [https://doi.org/10.1002/1527-2648\(20021014\)4:10<726::AID-ADEM726>3.0.CO;2-Y](https://doi.org/10.1002/1527-2648(20021014)4:10<726::AID-ADEM726>3.0.CO;2-Y)
- Wang, Y., Zhai, X., & Wang, W. (2017). Numerical studies of aluminum foam filled energy absorption connectors under quasi-static compression loading. *Thin-Walled Structures*, 116(December 2016), 225–233. <https://doi.org/10.1016/j.tws.2017.03.032>

- Wang, Z. (2019). Recent advances in novel metallic honeycomb structure. *Composites Part B, 166*(January), 731–741. <https://doi.org/10.1016/j.compositesb.2019.02.011>
- Wang, Z., & Liu, J. (2019). Numerical and theoretical analysis of honeycomb structure filled with circular aluminum tubes subjected to axial compression. *Composites Part B: Engineering, 165*(December 2018), 626–635. <https://doi.org/10.1016/j.compositesb.2019.01.070>
- Wang, Z., Yao, S., Lu, Z., Hui, D., & Feo, L. (2016). Matching effect of honeycomb-filled thin-walled square tube—Experiment and simulation. *Composite Structures, 157*, 494–505. <https://doi.org/10.1016/j.compstruct.2016.03.045>
- Wangyu, L., Jiale, H., Xiaolin, D., Zhenqiong, L., & Ling, Z. (2018). Crashworthiness analysis of cylindrical tubes filled with conventional and negative Poisson's ratio foams. *Thin Walled Structures, 131*, 297–308.
- Weager, B. (2010). *High-performance biocomposites: novel aligned natural fibre reinforcements*.
- Wei, Z., Hou, H., Gao, N., Huang, Y., & Yang, J. (2020). Sound absorption coefficient measurement by extracting the first reflected wave in a short tube. *Applied Acoustics, 159*, 107087. <https://doi.org/10.1016/j.apacoust.2019.107087>
- Wu, S., Zheng, G., Sun, G., Liu, Q., Li, G., & Li, Q. (2016). On design of multi-cell thin-wall structures for crashworthiness. *International Journal of Impact Engineering, 88*, 102–117. <https://doi.org/10.1016/j.ijimpeng.2015.09.003>
- Xiao, D., Dong, Z., Li, Y., Wu, W., & Fang, D. (2019). Compression behavior of the graded metallic auxetic reentrant honeycomb: Experiment and finite element analysis. *Materials Science & Engineering A, 758*(May), 163–171. <https://doi.org/10.1016/j.msea.2019.04.116>
- Xiao, Y., Hu, Y., Zhang, J., Song, C., Liu, Z., & Yu, J. (2018). Dynamic bending responses of CFRP thin-walled square beams filled with aluminum honeycomb. *Thin-Walled Structures, 132*(April), 494–503. <https://doi.org/10.1016/j.tws.2018.09.023>
- Xie, S., & Wang, N. (2017). Crashworthiness analysis of multi-cell square tubes under axial loads. *International Journal of Mechanical Sciences, 121*(September 2016), 106–118. <https://doi.org/10.1016/j.ijmecsci.2016.12.005>
- Xiong, F., Wang, D., & Yin, S. (2018). Optimization analysis of novel foam-filled elliptical columns under multiple oblique impact loading. *Materials and Design, 156*, 198–214. <https://doi.org/10.1016/j.matdes.2018.06.057>
- Yan, L., Chouw, N., & Jayaraman, K. (2014a). Effect of triggering and polyurethane foam-filler on axial crushing of natural flax/epoxy composite tubes. *Materials and Design, 56*, 528–541. <https://doi.org/10.1016/j.matdes.2013.11.068>
- Yan, L., Chouw, N., & Jayaraman, K. (2014b). Lateral crushing of empty and polyurethane-foam filled natural flax fabric reinforced epoxy composite tubes. *Composites Part B: Engineering, 63*, 15–26.



<https://doi.org/10.1016/j.compositesb.2014.03.013>

- Yan, L. L., Han, B., Yu, B., Chen, C. Q., Zhang, Q. C., & Lu, T. J. (2014). Three-point bending of sandwich beams with aluminum foam-filled corrugated cores. *Materials and Design*, 60, 510–519. <https://doi.org/10.1016/j.matdes.2014.04.014>
- Yan, L. L., Yu, B., Han, B., Chen, C. Q., Zhang, Q. C., & Lu, T. J. (2013). Compressive strength and energy absorption of sandwich panels with aluminum foam-filled corrugated cores. *Composites Science and Technology*, 86, 142–148. <https://doi.org/10.1016/j.compscitech.2013.07.011>
- Yang, F., Fan, H., & Meguid, S. A. (2019). Effect of foam-filling on collapse mode transition of thin-walled circular columns under axial compression: Analytical, numerical and experimental studies. *International Journal of Mechanical Sciences*, 150(July 2018), 665–676. <https://doi.org/10.1016/j.ijmecsci.2018.10.047>
- Yang, M., Han, B., Su, P., Wei, Z., Zhang, Q., & Zhang, Q. (2019). Axial crushing of ultralight all-metallic truncated conical sandwich shells with corrugated cores. *Thin Walled Structures*, 140 (December 2018), 318–330. <https://doi.org/10.1016/j.tws.2019.03.048>
- Yang, X., Ma, J., Sun, Y., & Yang, J. (2018). Ripplecomb: A novel triangular tube reinforced corrugated honeycomb for energy absorption. *Composite Structures*, 202(May), 988–999. <https://doi.org/10.1016/j.compstruct.2018.05.019>
- Yin, H., Wen, G., Fang, H., Qing, Q., Kong, X., Xiao, J., & Liu, Z. (2014). Multiobjective crashworthiness optimization design of functionally graded foam-filled tapered tube based on dynamic ensemble metamodel. *Journal Of Materials & Design*, 55, 747–757. <https://doi.org/10.1016/j.matdes.2013.10.054>
- Yin, H., Wen, G., Wu, X., Qing, Q., & Hou, S. (2014). Crashworthiness design of functionally graded foam-filled multi-cell thin-walled structures. *Thin Walled Structures*, 85, 142–155. <https://doi.org/10.1016/j.tws.2014.08.019>
- Yin, H., Wena, G., Hou, S., & Qing, Q. (2013). Multiobjective crashworthiness optimization of functionally lateral graded foam-filled tubes. *Materials and Design*, 44, 414–428. <https://doi.org/10.1016/j.matdes.2012.08.033>
- Ying Liu, & Zhang, X.-C. (2009). The influence of cell micro-topology on the in-plane dynamic crushing of honeycombs. *International Journal of Impact Engineering*, 36(1), 98–109.
- Yu, X., Qin, Q., Zhang, J., He, S., Xiang, C., Wang, M., & Wang, T. J. (2018). Crushing and energy absorption of density-graded foam-filled square columns: Experimental and theoretical investigations. *Composite Structures*, 201(May), 423–433.
- Yunus A. Cengel, & Boles, M. A. (n.d.). *Thermodynamics: An Engineering Approach* (Fifth Edit). McGraw-Hill Book Company.

- Zarei, H. R., & Kröger, M. (2008). Optimization of the foam-filled aluminum tubes for crush box application. *Thin-Walled Structures*, 46(2), 214–221. <https://doi.org/10.1016/j.tws.2007.07.016>
- Zarei Mahmoudabadi, M., & Sadighi, M. (2011). A study on the static and dynamic loading of the foam filled metal hexagonal honeycomb - Theoretical and experimental. *Materials Science and Engineering A*, 530(1), 333–343. <https://doi.org/10.1016/j.msea.2011.09.093>
- Zhang, L., Bai, Z., & Bai, F. (2018). Crashworthiness design for bio-inspired multi-cell tubes with quadrilateral, hexagonal and octagonal sections. *Thin Walled Structures*, 122(June 2017), 42–51. <https://doi.org/10.1016/j.tws.2017.10.010>
- Zhang, Q., Yang, X., Li, P., JianLu, G. H., Feng, S., Cheng Shen, Feng Xu. (2015). Bioinspired engineering of honeycomb structure – Using nature to inspire human innovation. *Progress in Materials Science*, 74, 332–400.
- Zhang, X., Wen, Z., & Zhang, H. (2014). Axial crushing and optimal design of square tubes with graded thickness. *Thin-Walled Structures*, 84, 263–274. <https://doi.org/10.1016/j.tws.2014.07.004>
- Zhang, X., & Zhang, H. (2013). Theoretical and numerical investigation on the crush resistance of rhombic and kagome honeycombs. *Composite Structures*, 96, 143–152. <https://doi.org/10.1016/j.compstruct.2012.09.028>
- Zhang, X., & Zhang, H. (2014). Axial crushing of circular multi-cell columns. *International Journal of Impact Engineering*, 65, 110–125. <https://doi.org/10.1016/j.ijimpeng.2013.12.002>
- Zhang, Yanqin, Liu, Q., He, Z., Zong, Z., & Fang, J. (2019). Dynamic impact response of aluminum honeycombs filled with Expanded Polypropylene foam. *Composites Part B: Engineering*, Vol. 156, pp. 17–27. <https://doi.org/10.1016/j.compositesb.2018.08.043>
- Zhang, Yong, Sun, G., Li, G., Luo, Z., & Li, Q. (2012). Optimization of foam-filled bitubal structures for crashworthiness criteria. *Journal Of Materials & Design*, 38, 99–109. <https://doi.org/10.1016/j.matdes.2012.01.028>
- Zhaokai, L., Qiang, Y., Xuan, Z., Man, Y., Peilong, S., & Cilei, Y. (2017). Crashworthiness and lightweight optimization to applied multiple materials and foam-filled front end structure of auto-body. *Advances in Mechanical Engineering*, 9(8), 1–21. <https://doi.org/10.1177/168784017702806>
- Zheng, G., Pang, T., Sun, G., Wu, S., & Li, Q. (2016). Theoretical, numerical, and experimental study on laterally variable thickness (LVT) multi-cell tubes for crashworthiness. *International Journal of Mechanical Sciences*, 118(June), 283–297. <https://doi.org/10.1016/j.ijmecsci.2016.09.015>
- Zhi, J. (2018). Application of thin polyurethane plastering thermal insulation system in building energy conservation. *Chemical Engineering Transactions*, 66, 349–354. <https://doi.org/10.3303/CET1866059>

- Zhou, P., Beeh, E., Kriescher, M., Friedrich, H. E., & Kopp, G. (2016). Experimental comparison of energy absorption characteristics of polyurethane foam-filled magnesium and steel beams in bending. *International Journal of Impact Engineering*, 93, 76–87. <https://doi.org/10.1016/j.ijimpeng.2016.02.006>
- Zhu, G., Sun, G., Yu, H., Li, S., & Li, Q. (2018). Energy absorption of metal, composite and metal/composite hybrid structures under oblique crushing loading. *International Journal of Mechanical Sciences*, 135(November 2017), 458–483. <https://doi.org/10.1016/j.ijmecsci.2017.11.017>
- Zhu, G., Wang, Z., Huo, X., Cheng, A., Li, G., & Zhou, C. (2017). Experimental and numerical investigation into axial compressive behaviour of thin-walled structures filled with foams and composite skeleton. *International Journal of Mechanical Sciences*, 122(January), 104–119. <https://doi.org/10.1016/j.ijmecsci.2016.12.019>
- Zuhri, M. Y. M., Guan, Z. W., & Cantwell, W. J. (2014). The mechanical properties of natural fibre based honeycomb core materials. *Composites : Part B*, 58, 1–9. <https://doi.org/10.1016/j.compositesb.2013.10.016>



اونيورسيتي ملايسيا قهق

UNIVERSITI MALAYSIA PAHANG

## APPENDIX A OPTIMIZATION METHOD USING DESIGN EXPERT SOFTWARE

### Historical data design

Under historical data design menu, the number of input whether numerical or categoric data should be inserted. Then name, unit, min value and max value of the input factor is filled in the table as in Figure 1

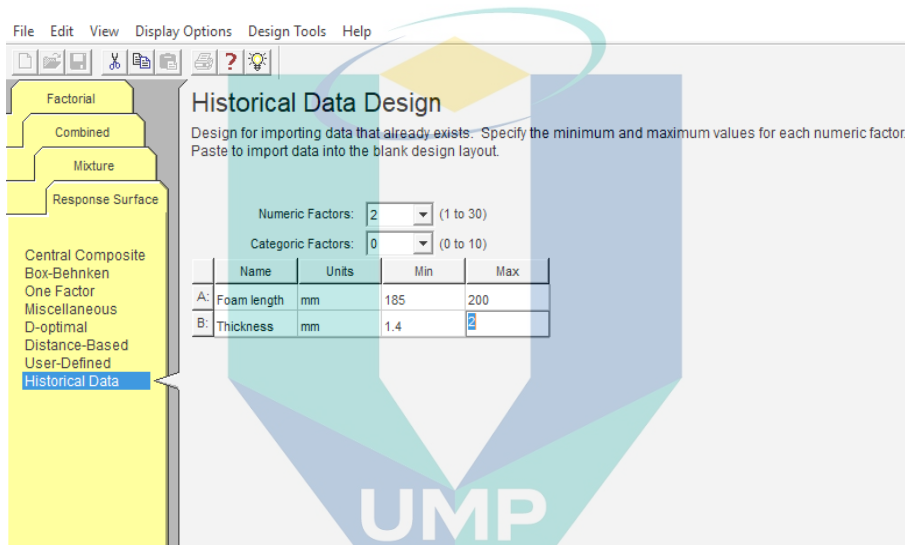


Figure 1 : Input data table in Design Expert software

Next, the output data table as in Figure 2 is filled with the output name and unit.

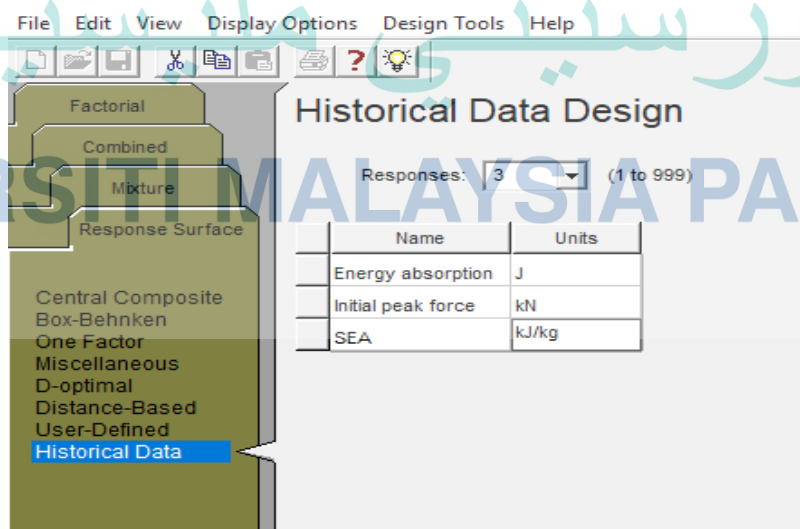


Figure 2 : Output data table in Design Expert software

Historical data obtain from experiment was filled in the table as in Figure 3

Std	Run	Block	Factor 1 A: Foam length mm	Factor 2 B: Thickness mm	Response 1 Energy absorp J	Response 2 Initial peak forc kN	Response 3 SEA kJ/kg
1	1	Block 1	185.00	1.40	464.5	32.9	1325.41
2	2	Block 1	190.00	1.40	502.7	32.1	1421.77
3	3	Block 1	195.00	1.40	541.5	35.2	1519.12
4	4	Block 1	200.00	1.40	547.1	45.5	1524.2
5	5	Block 1	185.00	2.00	606.5	85.9	1403.94
6	6	Block 1	190.00	2.00	702.5	91.6	1614.94
7	7	Block 1	195.00	2.00	840.8	97.3	1919.63
8	8	Block 1	200.00	2.00	944.8	100.1	2142.4

Figure 3: Table to be fill-in with the data from experiment

### 5.3.1 Analysis

For analysis process, choose transformation and select response node in the ‘transform’ tab (refers Figure 4). Then evaluate model for RSM using ‘Fit summary’ tab. Under ‘Model’ tab, choose model order and desired term from the list. Click on the ‘ANOVA’ tab to analyse the model and view results. ‘Diagnostic’ tab is used to evaluate model fit and transformation in graph form. The needed graph can be selected from the list. Finally, in ‘Model graphs’, the model can be evaluated and interpreted. Each output response has to be analysed individually.

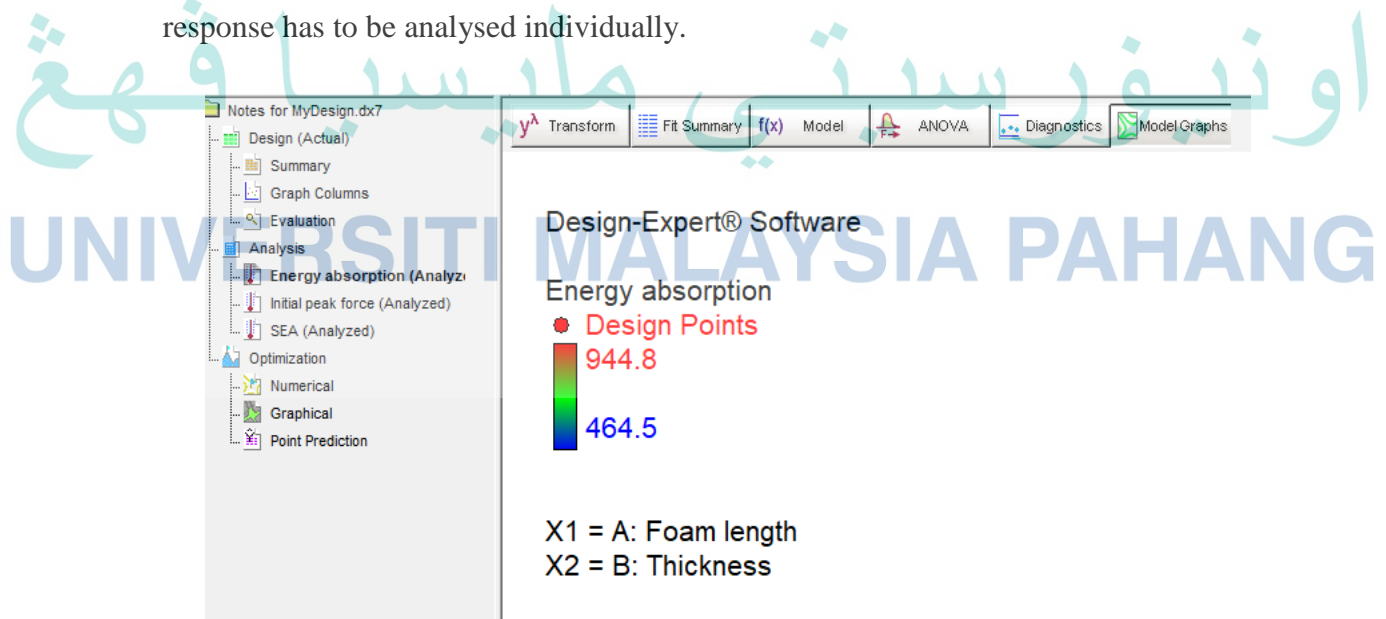


Figure 4 : Tab in the Analysis menu



### 5.3.2 Optimization

Under optimization menu, there are three choices that can be selected which is numerical, graphical and point prediction. First, the goal for each the input factor and output response were selected in criteria tab. For example, in initial peak force, the chosen goal is to be minimised

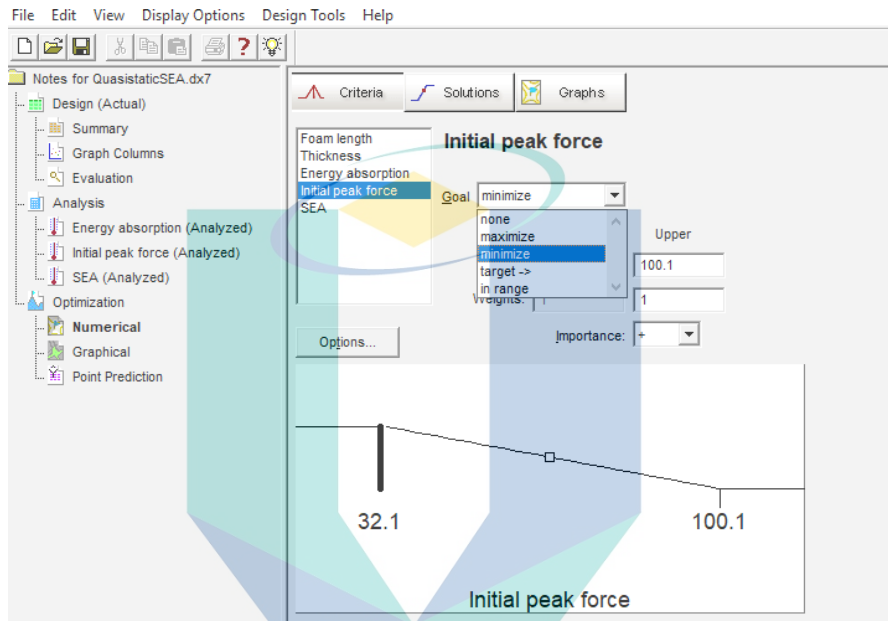


Figure 5 : Goal for each input and output response were chosen in ‘Criteria’ tab

Then, when the solution tab is activated, interface in Figure 6 was displayed

Constraints		Lower	Upper	Lower	Upper		
Name	Goal	Limit	Limit	Weight	Weight	Importance	
Foam length	is in range	185	200	1	1	3	
Thickness	is in range	1.4	2	1	1	3	
Energy absorpti	maximize	464.5	944.8	1	1	5	
Initial peak force	minimize	32.1	100.1	1	1	1	
SEA	maximize	1325.41	2142.4	1	1	5	

Solutions							
Number	Foam length	Thickness	Energy absorp	Initial peak for	SEA	Desirability	
1	200.00	1.93	898.56	93.3469	2074.66	0.744	Selected
2	200.00	1.93	899.985	93.5563	2076.84	0.744	

Figure 6 : Data displayed under ‘solution’ tab



The suggested solution for the inserted data was displayed in this tab. Importance of each input and output response can be edited to increase the desirability value of the solution. Besides, data of each output response can be viewed in the form of graph for perturbation, one-factor, interaction, contour or 3D surface. The aforementioned types of graph can be viewed under 'Graphs' tab. For example, graph for energy absorption in 3D surface is shown in Figure 7.

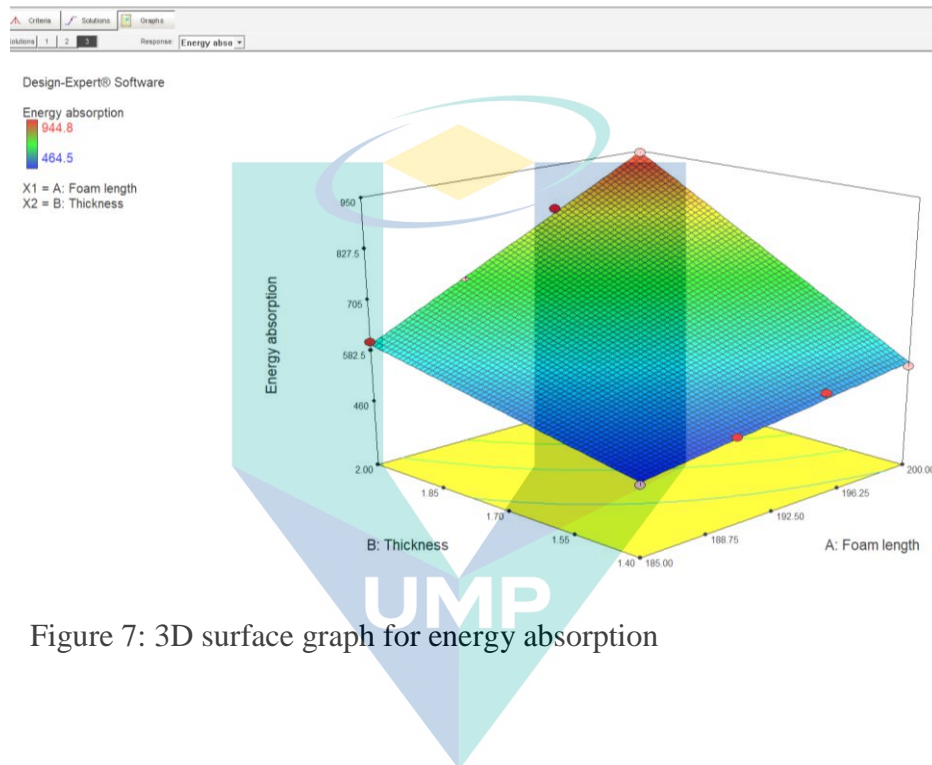


Figure 7: 3D surface graph for energy absorption